5-2011

Novel Nanofiber Structures and Advanced Tissue Engineering Applications

Vince Beachley
Clemson University, vbeachle@gmail.com

NOVEL NANOFIBER STRUCTURES AND ADVANCED TISSUE ENGINEERING APPLICATIONS

A Dissertation
Presented to
the Graduate School of
Clemson University

In Partial Fulfillment
of the Requirements for the Degree
Doctor of Philosophy
Bioengineering

---

by
Vincent Beachley
May 2011

Accepted by:
Xuejun Wen, PhD, Committee Chair
Karen Burg, PhD
Martine LaBerge, PhD
Hai Yao, PhD

ABSTRACT

Extracellular matrix (ECM) nanofibers such as collagen and elastin make up an important component of natural tissues. These structural components serve to impart mechanical strength and provide locations for cell attachment and biomolecule storage. Cells respond to their structural environment in a wide variety of ways beyond physical support, and it has been demonstrated that this environment directly modulates cell behaviors such as, morphology, differentiation, ECM production, attachment, and migration. ECM nanofibers also play an important role as a template for tissue formation during development, remodeling, and regeneration. Nanofiber based tissue engineering strategies aim to mimic the geometry of the natural fibrous component of the ECM to promote tissue regeneration. Nanofiber based approaches are of special interest in regeneration of aligned tissues such as, nerve, blood vessel, muscle, and connective tissue because they are able to promote aligned morphologies in resident cells.

While there are many different nanofiber fabrication methods available, the electrospinning method may be the most promising due its simplicity, versatility and scalability. Many different types of materials can be easily electrospun into nanofibers with a wide variety of morphologies, sizes, and structural arrangements. However, the potential of the electrospinning method in tissue engineering applications is limited by the available assembly techniques. It was our goal to investigate new technologies that allow more precise assembly of electrospun nanofibers into useful complex structures.

First, the parallel plate technique for collecting aligned nanofiber arrays was investigated systematically. Results of this study provided valuable insights into the relationships of fiber length to collection rate and collecting plate size, which were used in

designing novel loose fiber collection technologies. One of our technologies utilizes parallel mobile tracks to collect and distribute aligned electrospun nanofibers into loose 3D arrays. Advantages of this technology include indefinitely continuous steady state nanofiber collection, and the capability to simultaneously collect nanofibers from an electrospinning jet in one location and assemble them into complex structures at another. In addition, nanofibers are allowed an indefinite amount of time to dry between collection and assembly, thus eliminating complications related to fiber-to-fiber adhesions. This technology demonstrates potential in complex nanofiber structure assembly, and in industrial scale up.

Precision assembly, facilitated by the mobile track technology, led to the development of technologies to fabricate composite nanofiber/protein matrix thin films. These composites combined the strengths of each component as a scaffold for regenerating different types of tissues. Precision assembly technologies also facilitated the development of hybrid two components fibrous structures with finely tuned biomimetic microstructures. The mechanical properties of these structures were similar to those of natural tissues. It was demonstrated that the biomimetic mechanical properties of the hybrid materials were derived from precise nanofiber arrangement at the mechanical properties were highly responsive to subtle changes nanofiber arrangement.

Nanofibrous structures were evaluated as tissue engineering scaffolds in vitro and in vitro. C2C12 myoblasts seeded on aligned nanofibers scaffolds attached, aligned, and grew to confluence to form thin cell/nanofiber sheets and cell/nanofiber/protein matrix films. Three dimensional skeletal muscle scaffolds were further assembled by stacking these constructs layer-by-layer or by assembling them into 3D bundled structures. Integration of multilayered grafts with natural muscle was evaluated in vivo. Tubular vascular grafts were also fabricated

with biomimetic wavy stiff nanofibers and straight elastic fibers. These grafts demonstrated a remarkably similar mechanical profile to natural blood vessels when the microstructure was optimized. In vivo evaluation of vascular grafts was conducted in a rabbit carotid artery replacement model.

Our studies indicate that advances in nanofiber assembly allow for the design of tissue engineering scaffolds with improved control over fiber density, placement, and microstructure. These advances offer the potential for the design of better tissue engineering scaffolds for regeneration of many tissues such as skeletal muscle, blood vessels, nerve, tendon, skin, and so on.

ACKNOWLEDGEMENTS

My years studying for my PhD have been unbelievably rewarding both in career development and personal enjoyment. This would not have been possible without the help of many people. First and foremost I want to thank my advisor Dr. Xuejun Wen. Dr. Wen worked hard to teach me not only what I needed to know to complete my research and graduate, but every aspect of independent research and running a laboratory. Throughout the course of my studies, Dr. Wen has continually motivated me with his support and confidence. As an advisor Dr. Wen offered me abundant experience, resources, and creativity, but most important to me is knowing that his foremost goal has always been my success. I would also like to thank my committee members; Dr. Martine LaBerge, Dr. Hai Yao, and Dr. Karen Burg for their support and advice during all stages of my work. I greatly appreciate their efforts.

In addition to my committee I would like to thank several other faculty members who helped me along the way. This includes Dr. Richard Swaja, Dr. Ning Zhang, Dr. Thomas Brothers, Dr. Vladimir Mironov, and Dr. Kay Kang who spend so much time helping me with surgeries and teaching me techniques. I would also like to thank Margaret Romano, Carol Moskos, and Johnny Mole for their advice and contributions to my work.

The Wen lab has always worked together as a team and I could not have made it to this point without the support of that team. The people around me made my time here more productive and more enjoyable. I appreciate all of the help that I received from everyone over the years, and at the moment I recall specifically substantial contributions from Lin Cui, Yong Qiu, Wendy Vanden Berg-Foels, Xiaowei Li, Ben Whatley, Eleni Katsanevakis, and Glenn Hepfer. I would also like to thank Jon Kuo of Dr. Yao's lab for his contributions in

ideas and technical support.

My acknowledgements could not be complete without thanking all of my friends outside of the lab who helped me have an amazing stay in Charleston, and especially my girlfriend Becky who has given me so much encouragement and happiness.

Finally I would like to thank my family. I would like to thank my brother for his support and advice, and for always leading the way for me. To my Mom and Dad, I thank you for your guidance throughout all aspects of my life and for your encouragement and support throughout all of the ups and downs.

TABLE OF CONTENTS

LIST OF FIGURES

LIST OF TABLES

CHAPTER 1

1. INTRODUCTION

1.1 Role of the fibrous component in regenerating aligned tissues

Natural tissues have a fibrous extracellular matrix (ECM) component made up of collagen, elastin, keratin, or other similar types or natural nanofibers. This nanofibrous ECM provides mechanical strength, storage locations for biomolecules, and structural support for cell attachment, and organization. It also serves as a template for tissue formation in development, regeneration, and remodeling. For example, ECM deposition precedes cell migration in embryonic branching morphogenesis, nerve cells grow along aligned ECM tubes in peripheral nerve regeneration, and hydroxyapatite calcifies on collagen nanofibers to form bone during remodeling. Polymeric nanofibers have received a great amount of attention in recent years due to their potential to fill some of the roles of ECM nanofibers in tissue engineering. Polymeric nanofibers have proven to be excellent substrates for cell attachment and growth, and the microstructure of polymeric nanofiber grafts can predictably modulate cell behaviors such as morphology, differentiation, ECM deposition, and migration. In addition, the bioactivity of polymer nanofibers can be easily optimized due to a wide variety of available molecular compositions, methods of biomolecule incorporation, and surface modification techniques.

Many types of tissues such as muscle, nerve, and connective tissue, require a well aligned cellular and ECM organization for proper tissue function. Nerves are able to transmit signals throughout the body quickly through long well aligned axons, and muscles, blood vessels, and tendons are able to apply and resist loads efficiently due to the aligned organization of cells and ECM fibers. Cells that are cultured in vitro on aligned nanofibrous

scaffolds adopt an aligned elongated morphology that mimics the natural morphology of cells in aligned tissues in vivo. In addition to cell shape and organization, aligned nanofiber substrates have shown the ability to modulate cell behaviors such as differentiation, migration, and ECM assembly. It is of the highest importance that a tissue engineering scaffold used to mimic aligned tissues is able to impart uniaxial alignment in its resident cells to induce biomimetic organization and desired cellular responses. Challenges in tissue engineering applications of aligned nanofiber scaffolds include optimizing substrate topographical cues to promote desired cell responses and designing scaffolds with architecture conductive to the formation of tissue-like structures in vitro and in vivo.

1.2 Nanofiber scaffold fabrication with Electrospinning

Methods associated with many different fiber fabrication techniques are available for production of aligned nanofibers. However, the vast majority of research in this field is focused of aligned nanofiber fabrication using electrospinning. Electrospinning is an electrostatic method of fabricating polymer nanofibers that has generated widespread interest in the tissue engineering field due to its simplicity and immense versatility. Electrospinning utilizes an electric field to eject a polymer solution or melt from a needle or small orifice as a thin liquid jet. The electric field generates forces on the polymer solution that overcome surface tension forces in the needle resulting in the ejection of a jet that is accelerated toward a grounded target. Violent whipping motions thin the jet as it travels toward the target and thus increasing its surface area. A very high surface area to volume ratio promotes evaporation of the solvent, or cooling of a melt, resulting in the formation of solid polymer fibers at the target. When a flat target is used as the collecting area, a random fibrous mesh is formed, but many different variations of the electrospinning setup have been employed to

allow fabrication of nanofibers with uniaxial alignment. There are two basic methods that are most commonly used to fabricate aligned nanofiber structures: (1) Mechanical alignment using a high speed target, and (2) electrostatic alignment by a manipulated electric field. The preferred method of high speed target collection is the rotating mandrel technique and the preferred method of electric field manipulation is the parallel plate technique.

1.3 Limitations and approaches

Electrospun polymer nanofibers have demonstrated a great amount of promise in a variety of disciplines, but their application to actual products has been severely limited due to limitations in structural assembly techniques. The electrospinning jet is highly charged and subject to violent whipping instabilities that make it very difficult to assemble complex structures directly from the jet. Nanofiber structures fabricated from an electrospinning jet are most commonly randomly aligned non-woven meshes, aligned fiber meshes with very high fiber packing densities, or aligned fiber meshes with very low fiber packing densities.

Our goal was to develop new technologies that will allow greater control over fiber assembly and thus greater versatility in structure fabrication. We hypothesized that better tissue engineering scaffolds could be designed if a more suitable system of electrospun nanofiber collection were available. This work presents a way to continuously collect and deliver stable arrays of loose aligned individual nanofibers. The described technology allows for precise control of parameters such as drying time, charge dissipation and fiber placement that cannot be attained by any other electrospinning method. Two additional technologies were developed that extended the capabilities of our first technology to make composite and hybrid nanofiber scaffolds with architectures and mechanical properties that are well suited for tissue engineering applications. Several specific tissue engineering scaffolds were

fabricated and evaluated.

1.3 Specific Aims

Aim 1: To develop a novel technology for fabricating electrospun nanofibers that allows more precise control over structural assembly.

Rationale: The major factors which make it difficult to fabricate complex structures from an electrospinning jet are the high charge, high velocity, and random whipping instabilities associated with it. Current approaches to nanofiber scaffold fabrication are limited because they are assembled directly from the jet. It is our hypothesis that more precise structures could be assembled if an intermediate step is added between fiber collection and structure assembly.

***Aim 2*:** To fabricate aligned nanofiber arrays with precise structural arrangements

Rationale: We hope to use our electrospinning approach to fabricate structures with precise nanofiber placement and orientation. It is our hypothesis that our new approach will facilitate fabrication of aligned nanofiber arrays with precise fiber densities and geometries and allow assembly of complex composite structures.

Aim 3: Assemble nanofiber based structures for aligned tissue regeneration applications

Rationale: Complex aligned nanofiber structures may be optimized for tissue engineering applications. We hypothesis that aligned sheets, cylinders and tubes can be fabricated with fiber densities and geometries that optimize structural and mechanical properties useful in aligned tissue engineering applications.

Aim 4: Evaluate nanofiber based tissue engineering structures

Rationale: Aligned nanofiber scaffolds will be evaluated in vitro and in vivo to test their potential as tissue engineering scaffolds. It is our hypothesis that our new tools can be used to design several nanofiber structures that demonstrate potential as functional tissue engineering scaffolds.

1.4 Dissertation arrangement

The following manuscript is arranged in chapters that highlight individual studies that relate to the overall aims of the project. In Chapter 2 we present a detailed literature review of nanofiber based tissue engineering. This chapter explores different methods of nanofiber fabrication and methods of functionalizing nanofiber for biological applications. Cell interactions, organized by specific cell processes that are affected by culture on nanofiber substrates, are described in detail. Finally, current strategies to make better tissue engineering scaffolds using the electrospinning fabrication method are reviewed. Chapter 3 describes an investigation of the parameters and limitations of the parallel plate electrospinning method. The results of this experiment were used in designing the novel electrospinning technology described in Chapter 4. The new technology utilizes mobile tracks to collect and stabilize aligned nanofibers, while simultaneously assembling them into secondary structures. This device facilitated fabrication of large area ultra thin aligned nanofiber arrays that could be used to make nanofiber/protein matrix composite films as described in Chapter 5. These composites effectively combined the strengths of each component as a tissue engineering scaffold, while addressing their individual weaknesses. Chapter 6 described a method of fabricating hybrid straight-wavy nanofiber scaffolds with precisely arranged microstructure that mimics the arrangement of natural fibers in tissue. It was demonstrated that this

biomimetic microstructure resulted in mechanical properties that mimicked natural tissues such as blood vessels. In Chapter 7 a vascular graft with straight-wavy composite nanofiber based microstructure as described in Chapter 6 was tested in a rabbit carotid replacement model. Straight-wavy nanofiber based grafts demonstrate mechanical behavior that is remarkably similar to that of natural blood vessels before implantation and after retrieval. In Chapter 8 skeletal muscle tissue engineering scaffolds were fabricated by seeding C2C12 myoblast cells on aligned nanofiber scaffolds. C2C12 cells were able to align, grow to confluence, and differentiate on free suspended aligned nanofiber/cell sheets and aligned nanofiber/cell/fibrin gel films. Three dimensional skeletal muscle tissue engineering constructs were fabricated by stacking sheets and films layer-by-layer, and by bundling them. Fabricated structures were implanted into the paravertebral muscle of the mouse to evaluate their integration with natural muscle. Chapter 9 summarizes overall conclusions drawn from the body of work and discusses challenges and future developments related to the presented research.

CHAPTER 2

2. POLYMER NANOFIBROUS STRUCTURES: FABRICATION, BIOFUNCTIONALIZATION, AND CELL INTERACTIONS

2.1 Introduction

The fibrous component of the extracellular matrix (ECM) in the tissue is made up of protein fibers such as collagens, elastin, keratin, laminins, fibronectin and vitronectin. These protein fibers provide structural support to tissues and regulate many aspects of cell behavior. The building blocks of protein nanofibers are synthesized intracellularly by cells, and then secreted into the extracellular space by exocytosis. Soluble precursors are enzymatically modified within the ECM for formation into fibers. ECM fibers provide structural support and mechanical integrity to tissues as well as locations for cell adhesion and regulation of cell functions such as proliferation, shape, migration, and differentiation [1]. Tissues requiring high levels of mechanical strength such as tendons, ligaments, and bone, have high levels of organized fibers to impart mechanical strength, while some soft tissues have much higher levels of unorganized fibers. Composition and arrangement of ECM fibers in a tissue can impart fine tuned mechanical properties. For example, arteries exhibit precise mechanical behavior characterized by highly elastic behavior at low levels of distension and stiffer behaviors at high levels of distention due to a highly organized microstructure of elastin and collagen fibers [2]. ECM fibers also offer locations for cell adhesion and can regulate cell shape and migration patterns based on composition and arrangement. Structural fibrous proteins can also act as storage locations for the release of small bioactive peptides and growth factors upon release by proteolytic cleavage. The ECM in natural tissue is constantly being remodeled by proteolytic cleavage and cellular reassembly, and accelerated ECM remodeling is critical during embryonic development and during tissue regeneration. For

example, assembly of a fibrillar matrix from fibronectin is crucial for embryonic development and wound healing [3] and multiple ECM fibrous proteins, such as fibronectin and laminin are required for the process of branching morphogenesis evident in the development of organs such as the kidney, lung, and prostate [4,5]. Remodeling in adult bone tissue involves an initial assembly of collagen fibers with entrapped cells, followed by calcium salt precipitation on the collagen fibers to form bone. In the peripheral nervous system after axonal degeneration following injury, regenerating axons grow back to their targets by following the laminin and fibronectin containing basal lamina tube that surrounded the original nerve fiber [6]. Tissue engineering strategies utilizing fibrous components attempt to fill the role of fibrous components in natural tissue. Fibrous components of tissue engineering scaffolds can impart mechanical strength, structure for cell attachment, and act as reservoirs for biomolecule delivery in much the same way as the natural fibrous components of the ECM. For example, in many bone tissue engineering strategies a fibrous mesh is used as a template for subsequent mineralization in a similar way to collagen fibers in natural remodeling. The fabricated matrix forms a bonelike structure and provides an attractive microenvironment for osteogenic function in resident cells. Blood vessel tissue engineering with nanofibrous scaffolds benefits from its properties of high tensile strength, good cell attachment properties for endothelium formation, and directional alignment for smooth muscle cells in the vessel wall. In vivo, injectable self-assembling nanofibrous networks introduced to injury sites have been used to provide a 3-dimensional structural environment that has been shown to increase the infiltration and retention of endogenous cells [7,8].

2.2 Methods of polymer nanofiber scaffold fabrication

Polymer nanofibers have been fabricated using a number of different techniques. The methods of nanofiber fabrication are varied and utilize physical, chemical, thermal, and electrostatic fabrication techniques. The methods of polymer nanofiber fabrication most commonly associated with tissue engineering scaffolds in the literature are electrospinning, self assembling peptide reactions, and phase separation [9–11]. There are however several other ways to fabricate polymer nanofibers as well. Several of these fabrication methods are briefly described in the following section and some of the advantages and disadvantages of each method are listed in Table 2.1.

2.2.1 Electrospinning

Electrospinning is an electrostatically driven method of fabricating polymer nanofibers. Nanofibers are formed from a liquid polymer solution or melt that is feed through a capillary tube into a region of high electric field. The electric field is most commonly generated by connecting a high voltage power source in the kilovolt range to the capillary tip (Figure 2.1). As electrostatic forces overcome the surface tension of the liquid, a Taylor cone is formed and a thin jet is rapidly accelerated to a grounded or oppositely charged collecting target. Instabilities in this jet cause violent whipping motions that elongate and thin the jet allowing the evaporation of some of the solvent or cooling of melts to form solid nanofibers on the target site. Nanofiber size and microstructure can be controlled by several processing parameters including: solution viscosity, voltage, feed rate, solution conductivity, capillary-to-collector distance, and orifice size [12]. The electrospinning technique is very versatile and a wide range of polymer and copolymer materials with a wide range of fiber diameters

Table 2.1: Comparison of methods for fabricating polymer nanofiber scaffolds

	Advantages	Disadvantages
Electrospinning	• Easy to setup • Cost effective • High level of versatility allows control over fiber diameter, microstructure and arrangement • Vast materials selection	• Poor cell infiltration into the core of the scaffolds • 2-Dimensional pore or microstructure arrangement • Toxic solvents often used
Self Assembly	• Easy incorporation of cells during fiber formation • 3-Dimensional pore arrangement • Injectable for in vivo assembly	• Complex procedure • Lack of control of fiber orientation and arrangement • Limited fiber diameter ~2-30 nm and length ~10 μm
Phase Separation	• 3-Dimensional pore arrangement	• Complex procedures • Lack of control of fiber arrangement
Bacterial Cellulose	• Low cost • High yield	• Limited material selection • Lack of versatility for functionalization
Templating	• Vast materials selection • Control over fiber diameter and length	• Sacrificial materials • Limitation on fiber dimensions and arrangement
Drawing	• Vast materials selection • Simple procedure	• Low productivity (One single fiber at a time) • Difficult to form fibers with consistent diameter
Extraction	• Natural materials	• Limited material selection • Limited control of fiber diameter and length (a few microns)
Vapor-Phase Polymerization	• Polymer synthesized directly into nanofibers	• Limited control of fiber diameter and length (hundreds of microns) • Limited material selection • Complicated procedures
Kinetically controlled solution synthesis	• Polymers synthesized directly into nanofibers	• Limited control of fiber diameter and length (60 μm) • Limited material selection • Complicated procedures
Chemical Polymerization of Aniline	• Polymers synthesized directly into nanofibers	• Limited control of fiber diameter and length • Limited material selection • Complicated procedures

(several nanometers to several microns) can be fabricated using this technique. Many different types of molecules can be easily incorporated during the electrospinning fabrication process to produce functionalized nanofibers. Electrospun nanofibers are usually collected from an electrospinning jet as non-woven randomly or uniaxially aligned sheets or arrays.

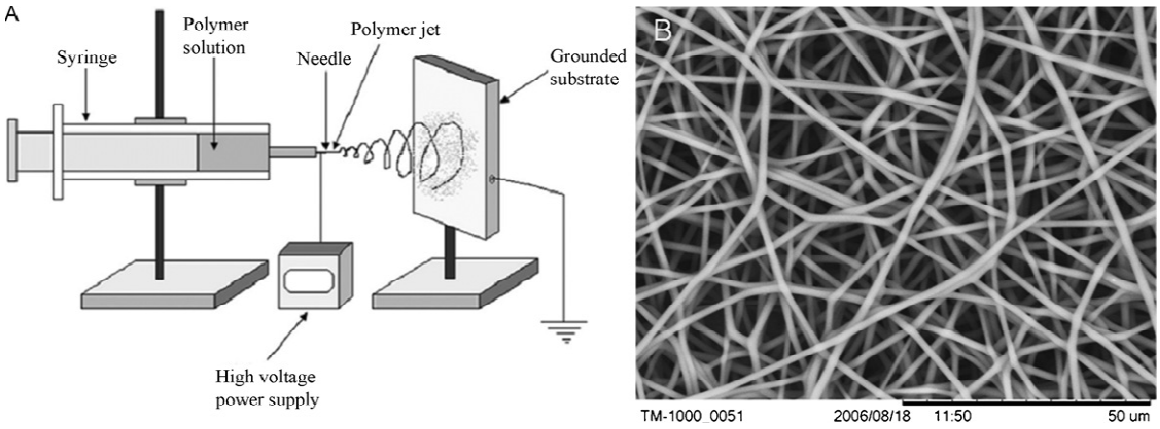

Figure 2.1: (A) schematic of a standard electrospinning setup (reproduced with permission from Year 2006 Dove Medical Press Ltd. [11]) and a scanning electron microscope (SEM) image (B) of electrospun polyurethane nanofibers.

2.2.2 Self assembly

Self assembly is a process by which molecules organize and arrange themselves into patterns or structures through non-covalent forces such as hydrogen bonding, hydrophobic forces, and electrostatic reactions. Dialkyl chain amphiphiles containing peptides were developed to mimic the ECM. These peptide amphiphiles (PA), derived from a collagen ligand, allow for a self assembling system that consists of a hydrophobic tail group and a hydrophilic head group (Figure 2.2) [13]. The specific composition of amino acid chains in peptide amphiphile systems determines the assembly, chemical, and biological properties of the system, and therefore PA systems can be tailored to specific applications [14,15]. Nanofibers with diameters around 5–25nm can be formed by the self assembly process, and systems have been developed where nanofiber assembly can be induced by appropriate pH values [16,17]. Cells can be encapsulated in a nanofibrous PA structure if they are added during the self assembly process and PAs can also be injected in vivo where they subsequently self assemble into a nanofibrous network. It has been demonstrated that self assembled peptide nanofibers can spontaneously undergo reassembly back to a nanofiber scaffold after destruction by

sonication, and after multiple cycles of destruction and reassembly, the peptide nanofiber scaffolds were still indistiquishable from their original structures [18]. While peptides are most commonly used in self assembly of tissue engineering structures, synthetic polymer nanofibers have also been fabricated by self assembly [19,20].

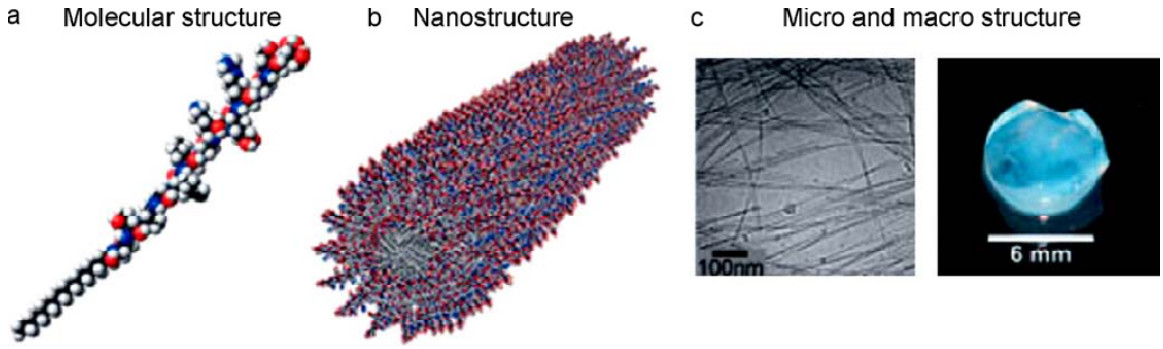

Figure 2.2: Schematics of the (A) molecular structure and (B) nanostructure, and images of the (C) micro and macro structure of a self assembling peptide amphiphile nanofiber network (reproduced with permission from Year 2005 Wiley-VCH Verlag GmbH & Co. KGaA [21]).

2.2.3 Phase separation

Nanofibrous foam materials have been fabricated by a technique called thermally induced liquid-liquid phase separation [22]. This fabrication procedure involves (a) the dissolution of polymer in solvent (b) phase separation and polymer gelatination in low temperature (c) solvent exchange by immersion in water and (d) freezing and freeze-drying (Figure 2.3). The morphology of these structures can be controlled by fabrication parameters such as gelatination temperature and polymer concentration. Interconnected porous nanofiber networks have been formed from polymers such as, poly-L-lactide acid (PLLA), poly-lactic-co-glycolic acid (PLGA), and poly-DL-lactic acid (PDLLA) with fiber diameters from 50–500 nm, and porosities up to 98.5%.

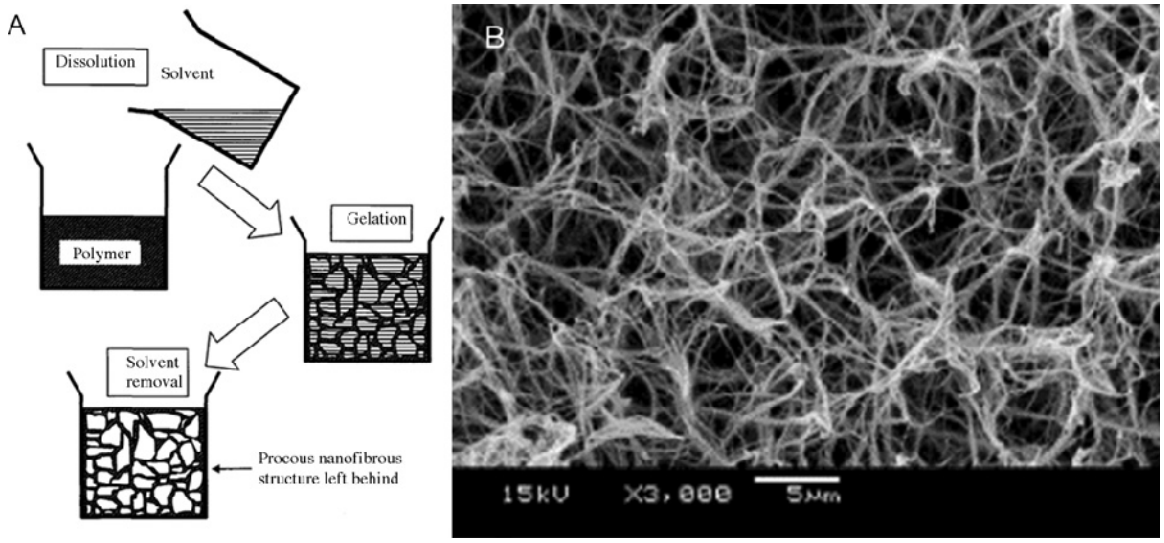

Figure 2.3: A schematic (A) of nanofiber formation by phase separation (reproduced with permission from Year 2005 World Scientific Publishing [23]), and an SEM image (B) of nanofibrous structure fabricated by this technique [22].

2.2.4 Bacterial cellulose

Cellulose nanofibers produced by bacteria have been long used in a variety of applications, including biomedical applications [24]. Cellulose synthesis by Acetobacter involves the polymerization of glucose residues into chains, followed by the extracellullar secretion, assembly and crystallization of the chains into hierarchically composed ribbons (Figure 2.4). Networks of cellulose nanofibers with diameters less than 100nm are readily produced, and fibers with different characteristics may be produced by different strains of bacteria [24]. Copolymers have been produced by adding polymers to the growth media of the cellulose producing bacteria [25,26].

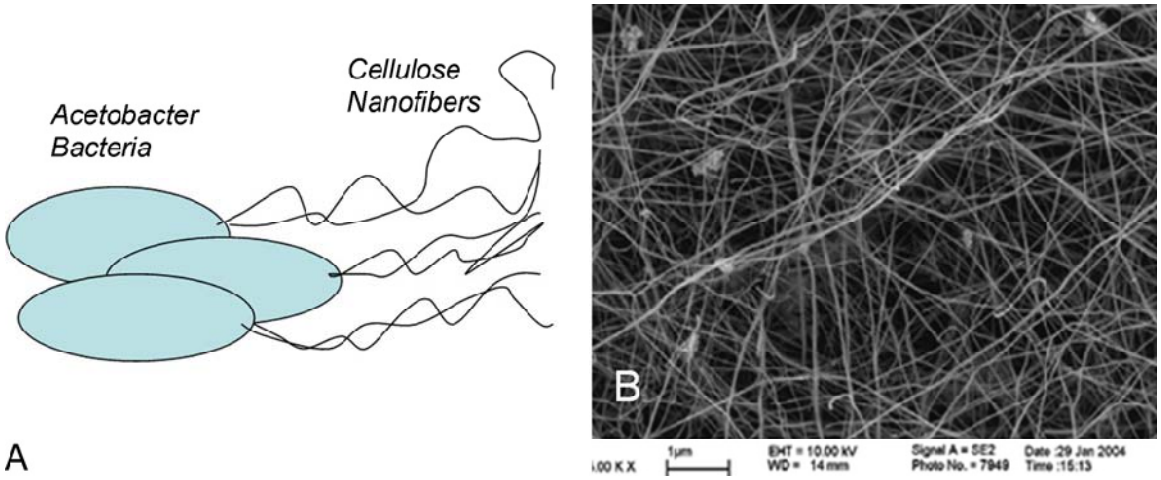

Figure 2.4: Schematic of Acetobacter cells depositing cellulose nanofibers (A), and an SEM image of a cellulose nanofiber mesh produced by bacteria (B) (reproduced with permission from Year 2007 American Chemical Society [24]).

2.2.5 Templating

Polymer nanofibers can be fabricated using templates such as self-ordered porous alumina. Alumina network templates with pore diameters from 25 to 400 nm, and pore depths from around 100nm to several 100µm have been be fabricated. Polymer nanofiber arrays can be released from these molds by destruction of the molds or mechanical detachment (Figure 2.5) [27,28]. The length of polycaprolactone (PCL) nanofibers fabricated from alumina templates can be controlled as a function of parameters such as melt time and temperature [29].

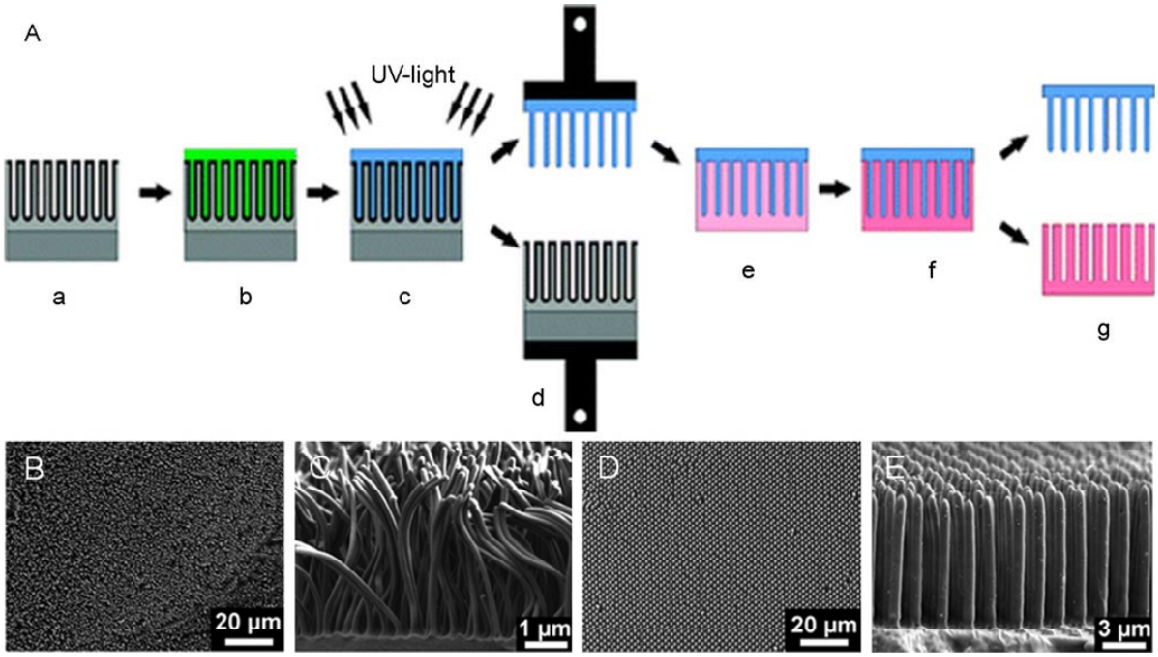

Figure 2.5: (A) Schematic of the fabrication of polymer nanofibers using a nondestructive templating technique (grey: alumina template, green: resin, blue: polymer nanofibers, pink: silica replica template. (B) SEM images of 120nm (B&C) and 1 µm (D&E) polymer fibers fabricated by the above technique (reproduced with permission from Year 2008 American Chemical Society [27]).

2.2.6 Drawing

Nanofibers can be mechanically drawn from viscous polymer liquids directly [30]. In one example, nanofibers were drawn directly when a rod was placed in a polymer melt and moved up forming a thin filament that cooled to form a nanofiber (Figure 2.6). This method was used to fabricate poly(trimethylene terephthalate) nanofibers with diameters as low as 60 nm, and lengths up to 500mm [31]. An automated drawing technique utilized a pipette dispensing liquid polymer solution while intermittently contacting a substrate and moving the x-y direction across the substrate [32]. This process allowed the formation of thin suspended nanofibers connecting droplet shaped dots on the substrate. This technique was used to fabricate polystyrene nanofibers with diameters ranging from tens nanometers to several microns in highly ordered patterns.

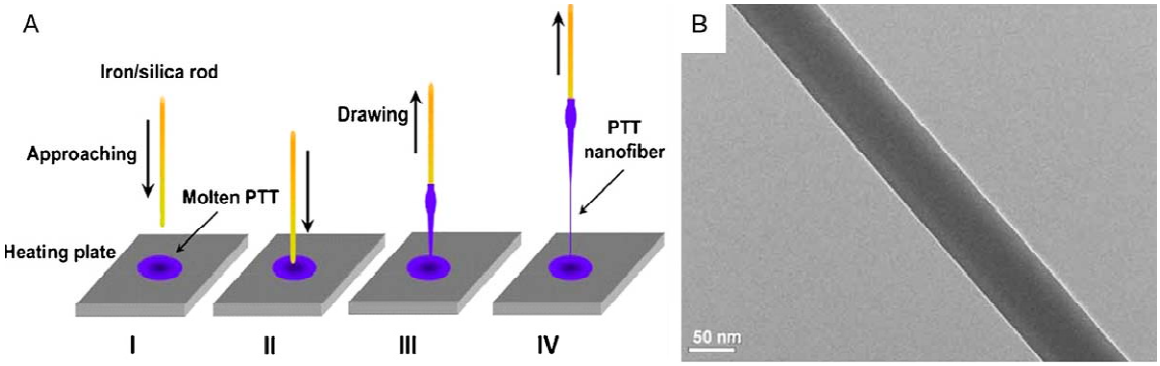

Figure 2.6: (A) Schematic of nanofiber fabrication by the drawing technique. (B) Transmission electron microscope (TEM) image of a polymer nanofiber fabricated using the drawing technique (reproduced with permission from Year 2008 The Optical Society [31]).

2.2.7 Extraction

Nanofibers can be extracted from natural materials using chemical and mechanical treatments. Cellulose fibrils can be disintegrated from plant cell walls. In one example, cellulose nanofibers were extracted from wheat straw and soy hull with diameters ranging from 10 to 120nm and lengths up to a few thousand nanometers (Figure 2.7) [33]. Invertebrates have also been used as a source for the extraction of nanofibers. Chitin nanofibers 3-4nm in diameter and a few micrometers in length were extracted from squid pen and Poly-N-acetyl glucosamine nanofibers isolated from a marine diatom demonstrated prothrombotic interactions with red blood cells [34,35].

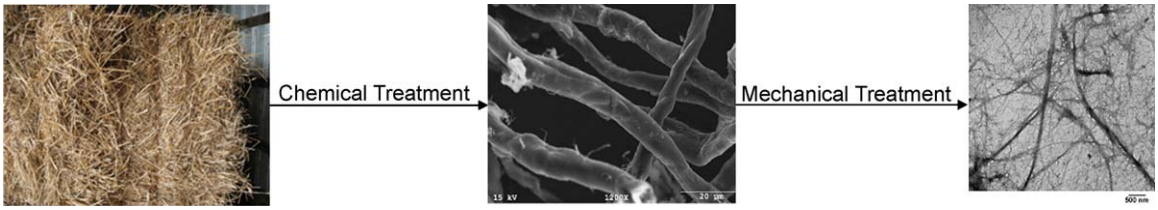

Figure 2.7: Images of natural wheat straw [36], wheat straw microfibers [33] after chemical treatment and wheat straw nanofibers [33] after chemical treatment.

2.2.8 Vapor-phase polymerization

Polymer nanofibers have also been fabricated from vapor-phase polymerization. Plasma-induced polymerization of vapor phase vinyltrichlorosilane produced organosiloxane fibers with diameters around 25nm and typical lengths of 400–600nm and cyanoacrylate fibers with diameters from 100 to 400nm and lengths of hundreds of microns (Figure 2.8) [37,38].

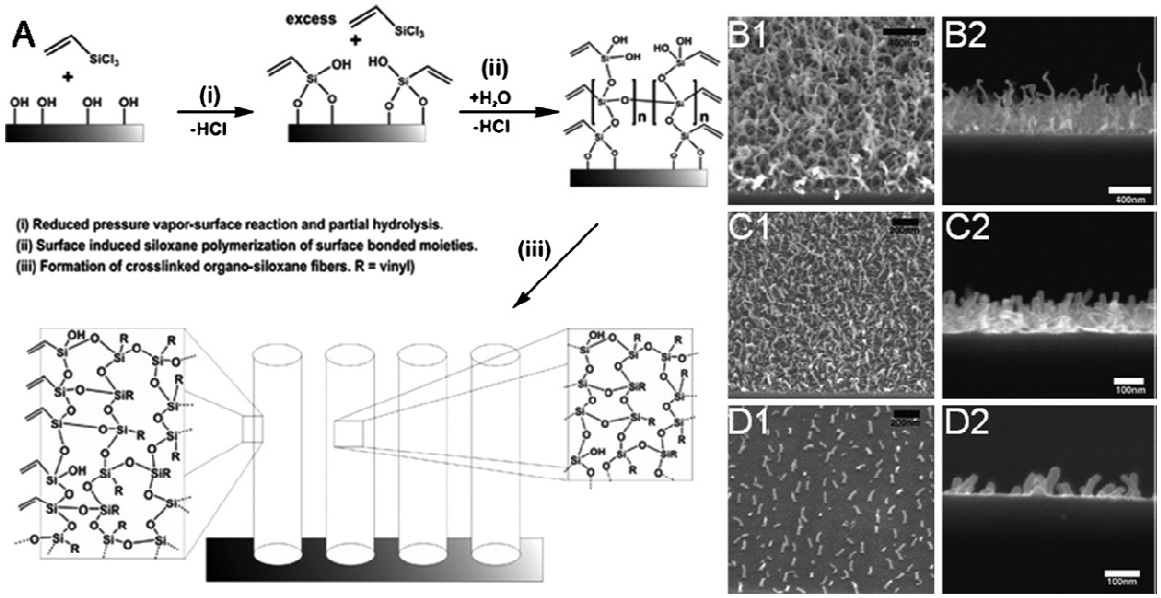

Figure 2.8: (A) Schematic describing a proposed mechanism for nanofiber formation by vapor-phase polymerization (B) Arial (1) and side views (2) of polymer nanofibers fabricated from vapor-phase polymerization at high (B), intermediate (C) and low (D) packing densities [37]. (Reproduced with permission from Year 2007 American Chemical Society [37]).

2.2.9 Kinetically controlled solution synthesis

Nanofibers and nanowires have been fabricated in solution using linear aligned substrates as templating agents such as iron-cation absorbed reverse cylindrical micelles and silver nanoparticles [39]. Poly(vinyl alcohol)-poly(methyl methacrylate) nanofibers were fabricated using silver nanoparticle that were linearly aligned in solution by vigorous magnetic stirring (Figure 2.9) [40]. These nanoparticle chain assemblies acted as a template for further polymerization of nanofibers with diameters from 10 to 30nm and lengths up to 60μm.

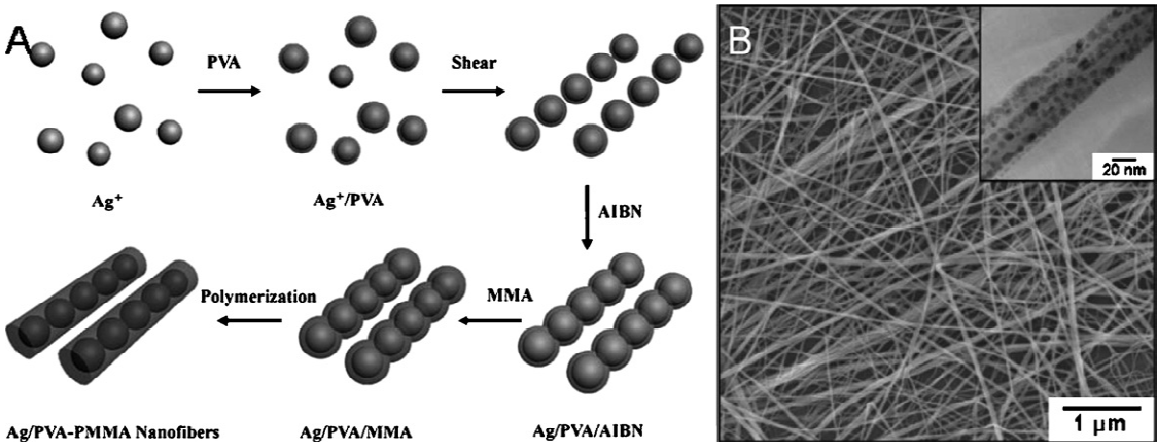

Figure 2.9: (A) Schematic of silver nanoparticle embedded polymer nanofibers fabrication (B) SEM and TEM images of silver nanoparticle embedded polymer nanofibers (reproduced with permission from Year 2006 Royal Society of Chemistry [40]).

2.2.10 Conventional chemical oxidative polymerization of aniline

Chemical oxidative polymerization of aniline is a traditional method for synthesizing polyaniline and during the early stages of this synthesis process polyaniline nanofibers are formed (Figure 2.10). Optimization of polymerization conditions such as temperature, mixing speed, and mechanical agitation allows the end stage formation of polyaniline nanofibers with diameters in the range of 30–120nm [41,42].

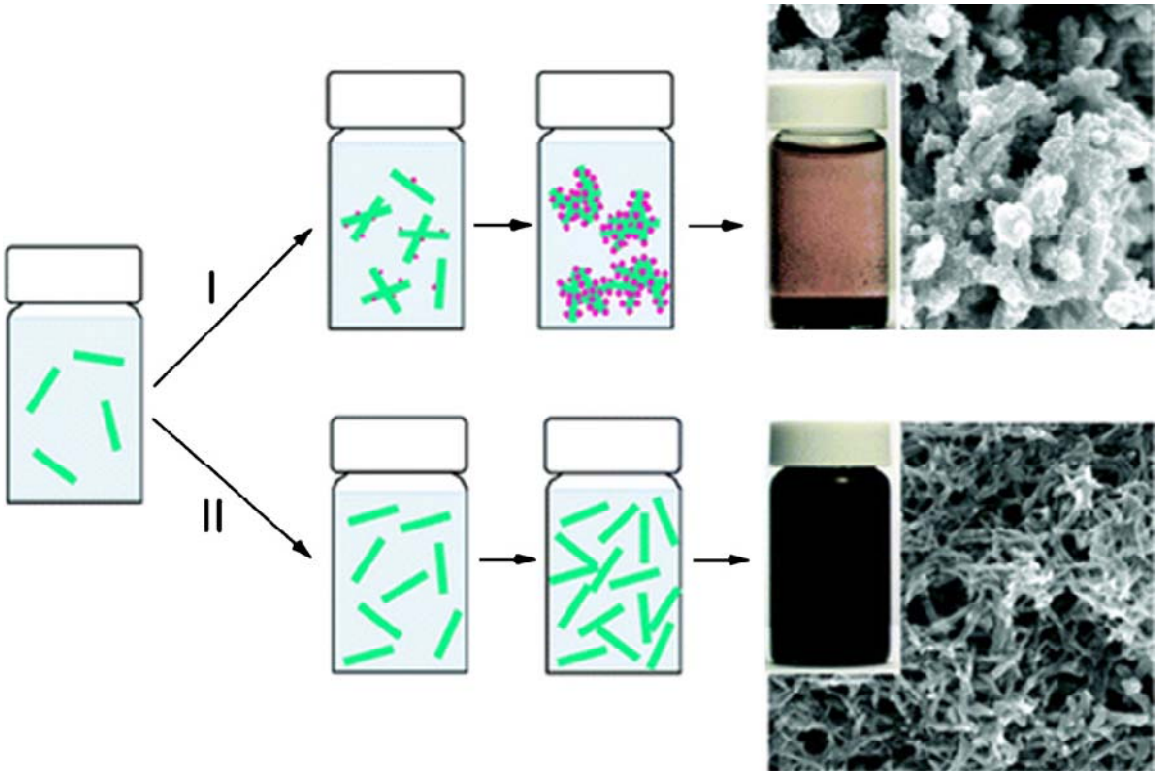

***Figure 2.10:** Schematic showing the nucleation of polyaniline nanofibers. (I) Under non-ideal nucleation conditions aggregate formation is present. (II) When ideal nucleation conditions are predominant, well-dispersed polyaniline nanofibers are formed. Typical images of the reaction vials and microstructure are displayed next to the schematic (reproduced with permission from Year 2009 American Chemical Society [42]).*

2.3 Biofunctionalization of polymer nanofibers

Polymer nanofibers are excellent structures for the design of tissue engineering scaffolds because of the wide variety of biocompatible polymer materials that can be formed into nanofibrous structures. Different types of biocompatible polymers demonstrate a variety of mechanical properties, degradation rates, and cell-material interactions, and new types of polymers are continuously being synthesized. In addition to the vast material selection available, one of the most favorable characteristics of polymer materials in tissue engineering scaffolds are their suitability for biofunctionalization. Biofunctional polymer nanofibers can be fabricated entirely from materials found in the ECM, and a variety of biomolecules and

drugs can be incorporated into polymer nanofibers during the fabrication process or by using post processing surface modification techniques. Biofunctionalization techniques can be utilized to fabricate tissue engineering scaffolds that guide cells toward desired behavior and function.

2.3.1 Natural ECM molecule nanofibers

Molecules that are naturally occurring in the extracellular matrix are ideal materials for cell attachment, survival, proliferation, and differentiation. In addition, substrate interactions between cells and ECM molecules may modulate certain cell functions. Biofunctional nanofibers can be directly fabricated from natural ECM materials or synthetic polymers can be blended with natural ECM molecules to form copolymer fibers. Blended nanofibers generally benefit from improved physical properties due to the synthetic polymer component and improved bioactivity due to the natural ECM component [43,44].

2.3.1.1 Collagen

Pure collagen nanofibers are commonly electrospun from solutions of soluble type I collagen dissolved in organic solvents such as 1,1,1,3,3,3-hexafluoro-2- propanol (HFIP) or aqueous acids. Bead free pure collagen nanofibers have been fabricated with diameters ranging from 100 to 500nm [45,46]. Water soluble collagen nanofibers must be crosslinked before use in cell culture with crosslinking agents, such as glutaraldehyde vapor, 1,6-diisocyanatohexane, genipin, 1-ethyl-3-(3-dimethylaminopropyl) carbodiimide hydrochloride (EDC), and so on [45,47,48]. Nanofiber blends containing collagen and synthetic polymers such as PCL are also easily fabricated by electrospinning when both materials are dissolved in the same solvents [49]. In nanofibers electrospun from single solvent solutions containing collagen and PCL, collagen was well dispersed as small spherical aggregates at low concentrations (10

wt%) and as much larger irregular shapes at higher concentrations (50 wt%) [50]. Cells cultured on synthetic nanofibers blended with collagen have shown better attachment, growth, and ECM production than fibers without collagen incorporation [51,52]. Blends allow for the fabrication of collagen containing nanofibers with a greater range of mechanical properties and fiber diameters. It has been shown that electrospinning collagen from organic solvents causes extensive denaturation and it was suggested that similar bioactivity may be obtained using gelatin in these cases [53]. However, several studies directly comparing electrospun collagen and gelatin nanofibers indicate that electrospun collagen nanofibers may retain some favorable bioactivity when compared to gelatin nanofibers despite solvent denaturation [51,54,55].

2.3.1.2 Gelatin

Gelatin nanofibers have been electrospun by dissolution in organic solvents such as HFIP and 2,2,2-trifluoroethanol (TFE) or aqueous acids. Pure gelatin nanofibers have been electrospun with fiber diameters around 50 to 500nm [45,56]. Gelatin nanofibers are crosslinked before use in cell culture with crosslinking agents, such as glutaraldehyde vapor, 1,6-diisocyanatohexane, genipin, EDC, and so on [45,48]. Gelatin nanofiber blends can also be electrospun by combination of gelatin and other polymers in one solution with a variety of fiber diameters. Cells attached and proliferated better on synthetic fibers when they were blended with gelatin [51,57–59]. Increases in cell attachment and proliferation have been shown to be a function of the ratio of gelatin in the fiber blends [44]. PCL fibers blended with gelatin also enhanced nerve differentiation as compared to plain PCL nanofibrous scaffolds [57].

2.3.1.3 Elastin

Alpha-elastin and tropoelastin fibers have been electrospun from HFIP solutions and aqueous acids with diameters ranging from 1 to several microns [45,46,48]. Electrospun elastin fibers have been observed to possess a ribbon like morphology as opposed to the uniform cross-section filament shape most common in other electrospun fibers. Elastin nanofibers must be crosslinked before use in cell culture with various crosslinking agents such as glutaraldehyde vapor, 1,6-diisocyanatohexane, EDC, and so on [45,46,48]. Elastin fiber blends with collagen and synthetic materials have also been successfully electrospun [45,60].

2.3.1.4 Chitosan

Pure chitosan nanofibers are difficult to electrospin due to limited solubility, ionic character and three-dimensional networks of strong hydrogen bonds [61]. High molecular weight chitosan nanofibers have however been successfully electrospun using high concentration acid solutions (diameter = 130 nm) and organic solvents (diameter = 60–330 nm) [61–63]. Chitosan can be mixed with other polymers in organic solvent solutions such as HFIP or acid solutions to more easily form blended nanofibers [43]. Chitosan nanofibers have been electrospun as blends with very low concentrations of polyethylene oxide (PEO) (10%) with diameters from 150 to 200 nm [64]. Chitosan/cellulose blends have also been produced by bacteria fabrication with chitosan concentrations of 7–10% dry weight [26]. Nanofiber scaffolds containing chitosan have demonstrated favorable properties as tissue engineering constructs [64].

2.3.1.5 Dextran

Dextran fibers with a wide range of fiber diameters have been electrospun from aqueous solutions and organic solvents such as dimethylformamide (DMF) and dimethyl sulfoxide

(DMSO) mixtures [65]. Dextran is highly soluble in an aqueous environment, but methacrylated dextran nanofibers photocrosslinked after electrospinning formed stable hydrogels in the aqueous environment [65]. Blended PLGA/dextran nanofibers have also been fabricated and have demonstrated favorable tissue engineering properties [66].

2.3.1.6 Fibrinogen

Fibrinogen nanofibers with diameters from 80 to 700 nm have been electrospun from solutions of fibrinogen dissolved in HFIP and 10× minimal essential medium (9:1) [67]. Fibrinogen nanofiber scaffolds were able to maintain their structure when hydrated without crosslinking and demonstrated good interactions with cells in vitro culture conditions [68,69]. The protease inhibitor, aprotinin can be added to cell culture media to slow down the degradation rate of fibrinogen nanofibers [68,69].

2.3.1.7 Laminin

Laminin purified from Engelbreth–Holm–Swarm (EHS) tumor was solubilized in HFIP and electrospun into 90 to 300 nm fibers with various amounts of bead composition [70]. Bioactivity of laminin nanofibers was confirmed by the in vitro behavior of PC12 and human adipose stem cells. Laminin nanofibers were able retain their structure under hydrated conditions without crosslinking.

2.3.1.8 Hyaluronic acid

Hyaluronic acid nanofibers are very difficult to fabricate, but a combination procedure involving electrospinning from an acidic solution with heated air blown around the electrospining jet was developed to obtain uniform fibers [71]. Pure hyaluronic acid nanofibers (diameter = 110 nm) were also fabricated by electrospinning hyaluronic acid:PEO blended nanofibers followed by extraction of the PEO component of the fibers [72,73].

Scaffolds assembled from these hyaluronic acid nanofibers demonstrated good cell interaction properties in vitro.

2.3.2 Surface functionalization

One of the major advantages of polymeric materials in tissue engineering scaffold design is vast versatility for surface modifications. Biomolecules can be absorbed or chemically bonded to the surface of polymer nanofibers in order to modulate specific cell functions in tissue engineering. In this review only surface functionalization techniques that have previously been carried out with polymer nanofiber structures are included, but in theory any method of polymer surface modification may be applicable to polymer nanofibers as long as some part of the process does not destroy the sometimes fragile nanofiber structures.

2.3.2.1 Physical absorption

The simplest method for surface biofunctionalization of polymer nanofibers with biomolecules is to incubate nanofiber meshes with solutions containing solubilized biomolecules to allow for physical absorption of the biomolecules onto the nanofiber surfaces. Biomolecules may adhere to the surface of the nanofibers because of interactions such as Van der Waals force, electrostatic forces, hydrophobic interactions, and hydrogen bonding. The efficiency of physical adsorption onto hydrophobic nanofiber scaffolds can be increased by treatment with air plasma to make them more hydrophilic and allow greater infiltration of aqueous solutions containing water soluble biomolecules. Plasma treatment can also be used to improve the hydrophilicity of nanofiber meshes for improved covalent grafting modifications explained in the following section [74]. The efficiency of plasma treatment may be improved by placing a sample a distance downstream of the plasma source to allow surface modification while minimizing damages due to etching and ablation [75].

2.3.2.2 Covalent surface bonding

Covalent surface bonding can be used to chemically bond biomolecules to exposed functional groups directly on the nanofiber surface. Covalent surface bonding provides a much more efficient coating and greater long term retention of biomolecules [76]. Covalent coating of biomolecules on nanofibers usually involves at least two requirements: (1) exposed functional groups on the fiber surface, (2) covalent bonding of biomolecules to these functional groups.

2.3.2.2.1 Exposing functional groups

Depending on the molecular configuration of the specific polymer requiring modification, functional groups may already be present, or can be added to the surface by various chemical treatments. The functional groups most commonly used in polymer nanofiber surface modification reactions in the literature are carboxyl and amine groups. Carboxyl groups can be exposed on the surface of nanofibers made from materials, such as PLLA and PCL, by treatment with chemicals such as sodium hydroxide (NaOH) [77,78]. Amine groups were grafted on the surface of degradable polyester nanofibers by treatment with 1,6-hexanediamine/propanol solution or ethylenediamine (ED) [79,80]. When the desired functional groups cannot be easily grafted directly on the polymer nanofiber surface then a linker molecule with the desired exposed functional groups can be tethered to the fiber surface. Acrylic acid in the gas phase was grafted to various polymer nanofibers as a plasma treatment to add carboxyl groups [81]. An additional di-aminopoly(ethylene glycol) (di-NH2-PEG) was used as a linker molecule to add functional amine groups to polyester nanofibers that had previously been soaked in NaOH to expose carboxylic acid groups [82]. Exposed carboxyl groups were added to polyethersulfone (PES) nanofibers by photo polymerization grafting of

poly (acrylic acid) as a linker molecule [83]. When adding linker molecules to the surface of polymer nanofibers it may be important to consider the properties of the specific linker molecules used because several research groups have shown that linker properties such as length have an effect on the cell response to functionalized polymer nanofibers [83–85]. Polymer blends and modified polymers can also be synthesized to include desired exposed functional groups on their structure. A PCL-PEG block copolymer was synthesized with functional amine groups on the surface via PEG linkers and electrospun into nanofibers that were further functionalized [86]. A copolymer of methyl methacrylate (MMA) and acrylic acid (AA) was synthesized and electrospun into nanofibers with different carboxyl group contents by varying the ratio of MMA to AA [87]. In another case PLGAb-PEG-NH2 di-block copolymer was directly blended with PLGA in organic solvents and electrospun to form PLGA nanofibers with exposed functional amino groups [88].

2.3.2.2.2 Covalently attaching biomolecules to functional groups.

Covalently attaching biomolecules to polymer nanofiber surfaces may require the activation of exposed functional groups on the polymer surface, the biomolecules or both. Carboxyl groups can be activated for reaction with primary amines by treatment with 1-ethyl-3-(3-dimethylaminopropyl) carbodiimide hydrochloride (EDC). This method of activation is commonly referenced in the literature for bonding biomolecules to polymer nanofibers [55,74,75]. The efficiency of EDC initiated bonding can be improved by adding N-hydroxysuccinimide (NHS), which converts an unstable amine-reactive intermediate formed by the EDC reaction into an amine-reactive NHS ester [55,74]. Glutaraldehyde, and 1-hydroxybenzole (HOBt) with EDC have been used to attach biomolecules to exposed amine groups on polymer nanofibers [79,86].

2.3.2.3 Examples of biomolecule surface functionalized nanofibers

A variety of biomolecules have been attached to polymer nanofibers to increase their bioactivities. Many research groups have used the physical absorption method to coat nanofibers with nanocrystalline apatites by immersion in simulated body fluid (SBF), which is an aqueous solution that contains ions in concentrations similar to those of human body plasma [89]. The degree of coating can be controlled by incubation time and SBF solution composition [77,78]. Hydroxyapatite coatings stimulate the expression of osteogenic genes by osteoblastic cells when compared to uncoated scaffolds [78]. The physical absorption method has also been used to coat synthetic nanofibers with biomolecules such as collagen, laminin, E-selection, and many others and successful biomolecule incorporation is reflected in enhanced cell spreading, viability, attachment, and phenotype preservation [76,90,91]. The physical absorption method has the advantage of being a very simple and gentle procedure. Modifications preformed by this method limit damage to fragile nanofiber structures and biomolecules, but binding can be relatively weak.

Many biomolecules have been covalently bonded to the surface of polymer nanofiber scaffolds as well. Covalent attachment of collagen and laminin to polymer nanofibers enhanced the suitability of the nanofibers as neural tissue engineering scaffolds [76,87]. Collagen synthesis by esophageal epithelial cells was increased by covalent bonding of fibronectin to nanofibers, and covalent attachment of an RGD peptide enhanced the attachment and proliferation of fibroblasts [79,88]. When compared to physical absorption, covalent bonding provides a more efficient and stable surface attachment of biomolecules. The major disadvantages of covalent bonding are more complex procedures and the potential use of harsh conditions that may limit the types of biomolecules that can be incorporated. For

example, the organic solvents used in some covalent binding procedures may deactivate biomolecules such as growth factors.

Combinational techniques to utilize both covalent bonding and physical absorption can also be used to biofunctionalize polymer nanofiber surfaces. The physical absorption of hydroxyapatite coatings with SBF can be made more efficient if carboxyl groups are exposed by NaOH prior to incubation [77,78]. Growth factors can be bound to polymer nanofibers using a combinational technique where molecules such as heparin are covalently bonded to act as reservoirs that stabilize, store, and protect growth factors introduced by physical absorption [55,82]. This technique allows for strong, stable covalent binding of heparin to the nanofiber surface, without exposing the growth factors to harsh conditions that could reduce their biofunctionality.

2.3.3 Bulk biomolecule incorporation

In addition to surface functionalization, biomolecules can also be incorporated into the bulk material of nanofibers during the fabrication process. The three most common methods of bulk biomolecule incorporation into polymer nanofibers are direct mixing into a polymer solution, co-axial electrospinning, and insertion of biofunctional peptide sequences into peptide amphiphile molecules for self assembly. It has been shown that the direct incorporation technique can allow for greater amounts of biomolecule incorporation and improved bioactivity when compared to surface modification techniques [76]. In addition, biomolecules incorporated by this technique are embedded into the bulk material of the fibers and can facilitate extended release of biomolecules by diffusion through the nanofibers or release by degradation of the nanofibers in the case of biodegradable materials. The release kinetics of biomolecules contained in polymer nanofibers commonly involves an initial burst

followed by steady extended release.

2.3.3.1 Mixing biomolecules directly into a polymer solution

Many biomolecules can be directly incorporated into a polymer solution during fabrication. This method of biomolecule incorporation can be employed for nanofiber fabrication techniques that utilize a polymer solution such as electrospinning, phase separation, templating, drawing, and so on, most notably electrospinning. Biomolecules may be directly dissolved in a polymer solution if a common solvent is available [92], dissolved in a miscible solvent and incorporated as a suspension [92–94], or dissolved in an immiscible solvent and incorporated as an emulsion with agitation [95–97]. When two miscible solvents for a particular polymer and biomolecule solution are not available, a multi-component system may be used. For example a three component solution containing dichloromethane (DCM), methanol, and water was used to incorporate water soluble heparin into DCM soluble PCL nanofibers [98]. Heparin was dissolved in water, which is miscible in methanol, which is miscible in DCM. Electrospinning of emulsions formed by stirring, vortexing, or sonication resulted in beadlike pockets containing an aqueous phase or even a core-shell structure [99–101]. Inclusion of miscible solvents and emulsions may however disturb the electrospinning process and make fiber formation more difficult due to inclusion of multiple phases in the jet [95]. Distribution of a biomolecule in a single phase solution was found to be even thoughout the nanofiber, while biomolecule distribution was aggregated for a two phase system [92,97]. However, even biomolecule distribution has also been observed in nanofibers electrospun from miscible solvent suspensions [98]. Reported efficiency of direct biomolecule incorporation in electrospun nanofibers varies greatly. This should be expected due to the high level of variations in material selection and electrospinning parameters reported in the

literature. Heparin electrospun as a miscible suspension had an efficiency of around 100% [98], laminin directly blended in organic solvent with PLLA had an efficiency of around 75% [76], and nerve growth factor (NGF) electrospun into nanofibers from an emulsion had a reported efficiency of just 2.5% [95]. Incorporation of biomolecules can have an effect on the morphology of electrospun nanofibers because biomolecule incorporation can change the solution properties such as viscosity and charge density [92,93,98]. For example, fiber diameter decreased with increasing loading levels of retinoic acid, while fiber diameter increased with increased loading levels of bovine serum albumin (BSA) [92]. Incorporation of biomolecules can also have an effect on the mechanical properties of nanofibers because of the inclusion of aggregates. Increased loading levels of BSA were observed to decrease the ductility of PCL and ethyl ethylene phosphate nanofibers, while the presence of retinoic acid increased the strength of the nanofibers independent of the fiber diameter [92]. A variety of biomolecules have been directly incorporated into electrospun nanofibers. NGF was mixed with BSA as a carrier protein and electrospun from an emulsion with sustained release up to 3 months after a 20% burst effect and retention of at least some degree of bioactivity [95]. Antibiotics have also been incorporated into electrospun polymer nanofibers with sustained release and bioactivity retention [93]. DNA has also been successfully incorporated into electrospun nanofibers with a sustained release of intact DNA capable to cellular transfection and protein encoding [94]. Vitamins were also loaded into electropsun polymer nanofibers with expended release [102]. Nanoparticles have also been loaded directly into polymer solutions and electrospun as dispersions [103]. A special extruder (Figure 2.11) used to feed polymer solution/nanoparticle dispersions into an electrospinning capillary helped to break up particle aggregates and maintain a uniform solution composition [103].

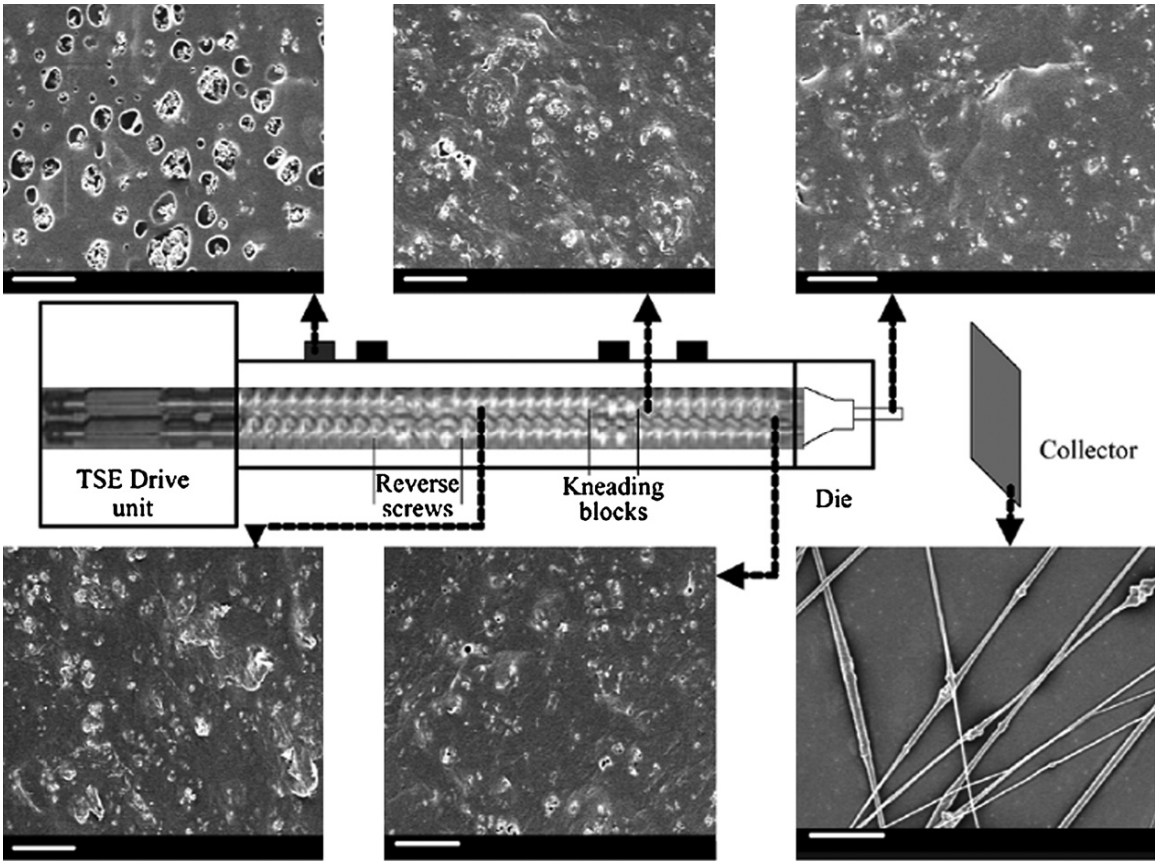

Figure 2.11: Deagglomeration of nanoparticles during stages of continuous processing in twin screw extrusion electrospinning apparatus (scale bar is 20 µm [103].

2.3.3.2 *Co-axial incorporation (electrospinning)*

An alternative approach to directly mixing biomolecules in an electrospinning solution is to use a special co-axial nozzle, which allows the formation of core-shell nanofibers where one material makes up a core filament that is surrounded by another material in a concentric geometry [104]. Multiple solutions are feed though a special nozzle in a concentric geometry to form a two phase liquid electrospun jet where a solution at the center is surrounded by an outer solution, forming solid core shell nanofibers upon solvent evaporation. Hollow tube nanofibers have also been electrospun using the co-axial technique [105]. Core shell nanofibers offer many attractive properties in tissue engineering applications, especially in

biomolecule incorporation. Biomolecules incorporated inside of core shell nanofiber are not affected by initial burst and they do not require extended contact with any toxic solvents used in the formation of the shell materials [106]. The flow rate of each component of the nanofiber can be independently controlled to vary the overall diameter of the fibers and the core to shell volume ratio. Coaxial electrospinning can also be used to electrospin materials that cannot be electrospun using conventional methods. For example, nanofibers were formed from poly(glycerol sebacate), a material that cannot be electrospun directly, by encapsulating its precursors in a constraining shell material that was removed after curing [107].

2.3.3.3 Incorporation of biofunctional peptide sequences (self assembly)

Biofunctional peptide sequences can be directly incorporated into peptide amphiphile nanofiber scaffolds. Biofunctional sequences are inserted into peptide amphiphile molecules and these biofunctional sequences are presented to cells on the nanofiber surface after self assembly. In one example, a peptide sequence called RADA16 was mixed with modified RADA16 sequences directly coupled with various bioactive motifs to promote cell adhesion and osteogenic functions [108]. Compared to pure RADA16 scaffolds, scaffolds containing bioactive motifs increased cell proliferation and markers of osteogenic differentiation. Incorporation of a designed chemokine similar to stromal cell-derived factor-1 improved cardiac function after myocardial infarction [109], and cell adhesion, differentiation and bone marrow homing motifs added to RADA16 sequences improved neural cell survival in nanofiber scaffolds [110]. A peptide amphiphile nanofiber scaffold with the incorporation of the pentapeptide epitope isolucinelysine-valine-alanine-valine (IKVAV), known to promote neurite sprouting and to direct neurite growth was designed as a tissue engineering scaffold specifically for neuronal cells [15]. The effect of IKVAV incorporation in the peptide

nanofibers was demonstrated by the superior bioactive properties of these scaffolds versus controls without the IKVAV sequence. The arrangement of biofunctional peptide sequences can have an effect on their bioactivity in nanofibrous scaffolds. RGD peptide sequences incorporated into self assembling peptide scaffolds had better cell attachment properties when the motif was displayed at a branched site than with linear incorporations of RDG because of increased motif availability at the nanofiber surface [111].

2.4 Cell behavior on polymeric nanofibers

Cells in their natural in vivo surroundings are exposed to a complex chemical and structural environment. The natural extracellular matrix is made up of structural components that are of nanoscale dimensions. Major fibrous extracellular molecules such as collagen fibers, elastin fibers, keratin fibers, etc. have nano-scale diameters. It is highly important to mimic the natural environment when culturing cells in vitro because cell behavior is determined by both genetic makeup and the surrounding environmental cues. Cellular behaviors such as proliferation, differentiation, morphology, and migration are commonly controlled in culture by modulation of the chemical environment. Cells also respond to different morphological cues that can be determined by the growth substrate in vitro and in vivo. Four components may be involved in the growth, differentiation, functions and morphology of cells on bio-material surfaces: (1) adsorption of serum components (2) extracellular matrix components secreted by the cell (3) cell adhesion molecules and (4) cytoskeleton mechanics [112]. It has been shown that the structural substrate property of surface roughness can cause selective protein absorption, and that higher surface roughness increases total protein absorption [113]. In this case, increased protein adsorption could be attributed to an increase in surface area for rough surfaces and thus could be important in relation to nanotopographical materials

because these exhibit extremely high surface area. In relation to nanostructure and cell interactions, the cytoskeletal mechanics is of importance because cells cultured on substrates with nanoscale features can take on different shapes in response to the specific features that are encountered.

Nanotopography can affect cellular behavior through known mechanisms such as the regulation of cell shape and surface protein absorption properties, but it is possible that there are unknown effects associated with nanotopographies as well. Cells can react to objects as small as 5nm [114] and it is possible that nanostructures, especially those with similar dimensions to the natural ECM, can influence cell behavior through unknown mechanisms. It has been shown that cell behavior can be highly dependent on the substrate that they are cultured on, and the understanding of cell substrate interactions with nanostructures could provide valuable information that would allow for the design of better tissue engineering scaffolds. Nanofibrous scaffolds present nanostructured features, mimic the fibrous components of natural tissue, allow three-dimensional configurations, and provide a unique mode of presentation of chemical and biological cues to cells. In order to gain a better understanding of the effect that nanofibrous architecture has on cell behavior, experimental results have been summarized according cell morphology, alignment, attachment, viability, ECM production, differentiation, and migration.

2.4.1 Cell morphology

Cell morphology can be influenced by the substrate that a cell is attached to. Cells many times adopt a different morphology on nanofibrous substrates compared to flat substrates, and cell morphology on nanofibrous substrates can be influenced by the fiber diameter. Cell morphology is commonly described by the projected area/degree of spreading or the aspect

ratio (ratio of the long and short axis). Cell morphology is an important characteristic in tissue engineering scaffold design because of its significance in controlling cell arrangement and the translational effects that cell morphology have on other cell functions.

Cells may adopt a more rounded shape with a smaller projected area when cultured on nanofibers as opposed to flat surfaces. Osteoprogenitor cells cultured on electrospun polymer fiber meshes with diameters of 140 and 2100 nm displayed significantly smaller projected areas than cells cultured on smooth surfaces [115], and fetal bovine chondrocytes cultured on nanofibrous scaffolds maintained a round or spindle-like shape in contrast to a flat well spread morphology observed on tissue culture plate [116]. Rounded morphologies may correspond with lack of organized actin fibers compared to cells with more well spread morphologies [116]. Chondrocytes grown on polymer nanofibers (500–900 nm) also adopted a rounded shape with a disorganized actin cytoskeleton in contrast to cells grown on 15 μm microfibers, which adopted a well spread shape [117]. Because fifteen microns approaches the size of a cell, they may react to these fibers in a manner similar to a flat substrate in the previous example.

Cells also may adopt a more elongated shape on nanofibers of certain diameters. Osteoprogenitor cells cultured on 140 nm fibers adopted a similar aspect ratio to those on smooth surfaces, but cells on 2100 nm fibers had a statistically higher aspect ratio [115]. In agreement with this result, dermal fibroblasts had statistically significant increase in aspect ratio for fiber diameters of 8640 and 970 nm versus flat controls, but not for fiber diameters of 160 and 650 nm [118]. Human umbilical vein endothelial cells also showed enhanced elongated cell morphology on larger fibers (1–5 μm) than smaller nanofiber scaffolds (200–1000 nm and 10–200 nm) [119]. This elongating effect could be due to cells growing along

single fibers, as it would be logical that cells would be more likely to grow along single fibers in nanofiber meshes with larger diameter fibers.

2.4.2 Cell alignment

One of the most important cell morphologies associated with tissue engineering is elongated unidirectional cell alignment. Many tissues such as nerve, skeletal and cardiac muscle, tendon, ligament, and blood vessels contain cells oriented in a highly aligned arrangement, thus it is desirable that scaffolds designed for these tissue types are able to induce aligned cell arrangements. It is well documented that cells adopt a linear orientation on aligned substrates such as grooves and fibers. Aligned nanofibers arrays can be easily fabricated using the electrospinning method [120,121] and many studies have shown that cells align with the direction of the fibers in these scaffolds. Primary cardiac ventricular cells and smooth muscle cells aligned in the direction of 1.8 μm and 550 nm aligned nanofiber meshes respectively [122,123]. Neuron elongation and outgrowth was parallel to the direction of aligned 113 and 431 nm nanofibers and neuronal stem cells seeded on random and aligned 300 nm and 1.5 μm nanofibers turned through large angles in order to grow parallel to the fiber alignment independent of fiber diameter [57,124]. Human skeletal muscle cells grown on 300 nm nanofiber scaffolds aligned on aligned fibers scaffolds in contrast to a random orientation adopted on randomly oriented scaffolds [125]. The effect of nanofiber alignment on neurite alignment of dorsal root ganglion (DRG) was measured quantitatively for nanofibrous scaffolds with different degrees of alignment using Fourier image analysis. Neurite alignment corresponded to the degree of fiber alignment as demonstrated by full-width-half max of the intensities of the fast Fourier transform images of 38, 69, and 84% ($p < 0.0001$) for highly aligned, intermediate, and randomly oriented samples respectively [126].

In addition to the influence on fiber arrangement, cell alignment can have positive effects on cell growth within tissue engineering scaffolds. Myotubes formed on aligned nanofiber scaffolds were more than twice the length of myotubes grown on randomly oriented fibers ($p < 0.05$) and neurites extending from DRG explants on highly aligned scaffolds were 16 and 20% longer than those grown on intermediate and randomly aligned scaffolds respectively [125,126].

2.4.3 Attachment

When designing tissue engineering scaffolds it is critically important that cells readily attach to the constructs. Many studies have confirmed that nanofibrous architectures have cell attachment properties superior to flat surfaces. Two factors that may lead to improved cell attachment on nanofibers could be the physical entrapment of cells penetrating inside of nanofiber meshes or improved focal adhesions. Many more filopia have been observed projecting from the edges of cells cultured on small diameter fibers compared to flat surfaces [118] and uniform focal adhesion distribution has been observed in cells cultured on nanofibers as compared to a distribution around the cell perimeter for cells cultured on flat surfaces [118]. An extreme example of physical entrapment was demonstrated when large hepatocyte spheroids completely enveloped nanofibers and demonstrated improved adhesion to flat controls upon agitation [127].

Relatively consistent results have been reported on the improved attachment of various cell types on nanofibers as opposed to flat surfaces. Fibroblasts, adipose stem cells, and smooth muscle cells that were allowed 15 min to 8 h to attach, adhered to nanofibers (100–500 nm) at rates 50–150% higher than cells on flat substrate controls [70,123,128]. Bone marrow-derived hematopoietic stem cells attached to nanofibrous scaffolds fabricated

from various materials at levels at least four times that of tissue culture plate at time points from 10 to 60 min [91]. After long term cell culture of 10 days, 40% of total hematopoietic stem cells grown on polymer nanofiber meshes were adherent after washing, while only 25% of total cells stayed on flat substrates [129]. Fiber diameter can have an effect on the cell attachment properties of nanofibrous scaffolds, however optimum fiber size seems to vary for different types of cells and conditions. The attachment of human mesenchymal stem cells was found to be around 40% greater on 1 μm diameter fibers as compared to 500 nm fibers [130], but in contrast, attachment of 3T3 fibroblasts on nanofiber scaffolds was greatest on 425 nm diameter scaffolds and decreased with increasing fiber diameter for 641 and 900 nm scaffolds [131]. On a smaller size scale, astrocytes seeded on 60, 100, 120, and 200 nm carbon fiber disks attached best to the largest fiber diameter disks [132].

2.4.4 Viability: survival/proliferation

Cell survival and proliferation must be well controlled in tissue engineering scaffolds. In most cases, maximum survival and proliferation are desired, but in some applications reductions in cell survival and proliferation are required. For example, astrocyte proliferation at an implant/tissue interface in the central nervous system causes the formation of an undesirable glial scar. It is well documented that nanofibrous architecture can have a significant effect on the survival and proliferation of cells, however the specific effects may vary for different cell types and conditions. Nanofibers have been shown to both increase and decrease cell proliferation for various cell types and conditions when compared to flat control. Fiber diameter effects on cell proliferation also vary for different cell types and conditions.

Self assembling peptide nanofiber scaffolds were found to improve the viability of

transplanted islet cells after 7 days of standard culture and in hypoxia injury model [133]. Cell viability as confirmed by MTT assay was increased from 58.6% to 81.0% in standard culture and from 29.2% to 60.6% in injury model. Viable fibroblast cell numbers after 8–13 days of culture were increased up to 3 times on 300–500 nm fibers vs. flat control [128]. It was further confirmed by transwell culture that nanofibrous architecture caused cells to release soluble factors that could stimulate increased cell numbers. In contrast, hematopoietic stem cells cultured on three different types of 500 nm fibers had 10–50% fewer cells than those cultured on flat films after 10 days [129], and Schwann cells cultured on five different polymer materials for 3–5 days had decreased MTT viabilities on four types of polymer fibers (1–4 μm) compared to films and similar viability on one type of nanofiber (130 nm) when compared to film [134].

Specific fiber diameter also has a variable effect on the proliferation of cultured cells. 3T3 fibroblasts cultured on polymer nanofibers with 6 diameters from 117 to 1051 nm had similar cell counts on day 1, but on days 3-7 cell number was greatest on 428 nm scaffolds and decreased towards the ends of the range up to 40% for the smallest and largest fiber diameters [131]. In contrast, human umbilical vein endothelial cells demonstrated higher viability and cell densities on 1000 to 1500 nm fibers as compared to 10–200 nm and 200–1000 nm fibers [119]. Carbon nanofibers with diameters of 60 and 100 nm resulted in osteoblast numbers nearly 3 times that of 125 and 200 nm fibers after 7 days of culture, but astrocyte cell counts were up to 66% higher on 125 and 200 nm fibers as compared to 60 and 100 nm fibers after 5 days of culture [132,135].

2.4.5 ECM production

The goal of many tissue engineering approaches is to provide a framework for the assembly of natural ECM secreted by resident cells in vitro or in vivo. For example, biodegradable tissue engineering scaffolds are designed to provide initial structural support that is intended to be replaced by naturally produced ECM as the original scaffold materials degrade. Thus it is important that a well designed tissue engineering scaffold promotes ECM production from resident cells. Several studies have shown that nanofibrous architecture can elicit increased ECM production from resident cells and that deposited ECM may be more highly organized. Chondrocytes seeded on 700 nm nanofiber scaffolds produced more sulfated proteoglycan rich, cartilaginous matrix than those seeded on tissue culture plate [116] and chondrocytes grown on nanofiber (500–900 nm) meshes showed a nearly 2 fold increase in glycosaminoglycan (GAG) production at 28 days as compared to microfiber (15 μm) culture [117]. Cartilage ECM markers, such as collagen II and IV, aggrecan, and cartilage proteoglycan link protein were also greater in chondrocyte cultures grown on nanofibers than microfibers as confirmed by immunostaining [117].

Fiber diameter and orientation can affect the ECM production of cells residing in nanofibrous scaffolds. Calcium production in osteoblasts from 7 to 21 days was significantly higher in cells cultured on 60 and 100 nm carbon fibers compared to cells cultured on 125 and 200 nm fibers [135]. Lee et al. found that human ligament fibroblasts cultured on 650 nm nanofibers synthesized significantly more collagen on aligned fibers than on randomly oriented fibers as confirmed by collagen assay normalized by DNA content at 3 and 7 days [136].

In addition to stimulating increased ECM production, nanofibrous structure can also result in organized deposition of ECM products. Immunohistochemistry at 7 and 14 days revealed that rotator cuff fibroblasts deposited collagen matrix in an aligned orientation on aligned nanofiber scaffolds but not on randomly oriented scaffolds [137]. Baker et al. linked [138] an increase in scaffold strength after in vitro culture of mesenchymal stem cells (MSCs) and meniscal fibrochondrocytes on aligned fiber scaffolds to organized collagen arrangement independently of collagen production. Collagen produced by both cell types oriented parallel to aligned nanofibers, and despite similar overall collagen content, aligned fiber scaffolds showed a >7 MPa increase in modulus over 10 weeks in culture as compared to an ~1 MPa increase in modulus for randomly oriented fiber scaffolds.

2.4.6. Differentiation

Many tissue engineering strategies require the selective differentiation of stem or progenitor cells into a specific lineage. It is well established that various soluble cues can be applied to certain cell types to induce them to differentiate to a specific fate. There is also evidence that the physical environment can affect cell differentiation. Nanofibrous architecture can have strong effects on cell fate versus flat culture surfaces and fiber properties, such as diameter and arrangement can affect cell differentiation. The effect of nanofibers on cell differentiation can be quite strong, but varies for different cell types and conditions. Nanofibrous architecture has also been shown to promote, prevent, and have no effect on differentiation when compared to flat surfaces.

Mouse embryonic fibroblasts cultured in self assembling peptide scaffolds were observed to undergo strong osteogenic differentiation after osteogenic induction while cells cultured on flat culture plate did not differentiate [139]. Furthermore, mouse embryonic stem

cells cultured in nanofibers without osteogenic induction expressed enhanced early stage markers of osteoblast differentiation compared to tissue plate culture [139]. Primary cardiac ventricular cells cultured on 2 μm diameter fiber scaffolds also shifted to a more mature phenotype than those grown on tissue culture plate [122]. In another study, differentiated chondrocyte phenotype was maintained on 700 nm nanofiber scaffolds for 21 days of culture while chondrocyte cells seeded on flat tissue culture plate de-differentiated [116]. In contrast MSCs cultured on 50-1000 nm nanofibers showed no differences in osteogenic phenotype markers compared to tissue culture plate after 12 days of osteogenic differentiation induction [140].

Nanofibrous scaffolds have also been observed to prevent differentiation and allow for the proliferation and maintenance of a pluripotent niche, which is important in vitro stem cell expansion. Hematopoietic stem cells cultured in 529 nm polymer nanofiber meshes for 10 days mediated a greater percentage of primitive progenitor cells when compared to the flat surface [129] and proliferation and self-renewal of pluripotent mouse embryonic stem cells were greatly enhanced in nanofibrillar meshes when compared to smooth culture surface [141]. While proliferation with self-renewal was allowed to continue in nanofiber topography, the cells were observed to maintain their ability to differentiate when exposed to differentiation factors [141]. In another study, a small fraction of mouse embryonic stem cells appeared to develop into small embryo body like colonies [139]. It was found that the frequency of these colonies was remarkably higher in self assembling peptide nanofiber cultures than in flat tissue plate culture.

In addition to possessing the capability to support both stem cell differentiation and self renewal, nanofibrous topography can selectively influence differentiation based on fiber

diameter and alignment. Differentiation of neural stem cells cultured on aligned and random nanofiber meshes with fiber diameters of 300 and 1500 nm was observed to be highly dependent on fiber diameter [124]. The quantitative differentiation rates evaluated on the basis of shape change were approximately 80% and 40% for 300 and 1500 nm fibers respectively. Expression of ligament markers by bone marrow stromal cells was effected by both fiber diameter and alignment [142]. While expression of Col-1e1, decorin, and tenomodulin in cells cultured on 270 nm fibers was greater than on films, expression of all three markers was significantly repressed in cells cultured on 820 and 2300 nm fibers. In contrast, expression of the ligament marker Scleraxis increased with increasing fiber diameter and fiber alignment. Primary cardiac ventricular cells cultured on aligned fiber scaffolds also expressed more markers of a mature phenotype than those grown on randomly oriented fibers [122].

2.4.7 Cell migration

Cell migration is a critical process in determining the success of tissue regeneration. In many designs, tissue scaffolds are populated by cells due to cell migration, either from cells seeded on the scaffold surface in vitro or endogenous cell migration in vivo. Tissue engineering scaffolds designed with controlled conduction of cell migration are desirable, and nanofibrous architecture can have a significant effect on cell migration properties in vitro and in vivo.

Traditional agarose droplet spreading experiment confirmed that nanofibrous surface topography can have an effect on the specific migration patterns of adult human dermal fibroblasts [118]. Migration and aggregation of hepotocyte cells appeared to be

restricted by nanofibrous architecture and this resulted in the formation of smaller more uniform aggregates as compared to flat films [127]. MSCs also had reduced migration distances on three different ranges of collagen nanofibers (50–200, 200–500, and 500–1000 nm) that were quantified and found to be 37–56% of those observed on TCPS control [140].

Endogenous cell migration in vivo was increased with the addition of nanofibrous architecture. A 3D peptide nanofiber mesh assembled in the in vivo myocardium was able to recruit endothelial progenitor cells, smooth muscle cells, and myocyte progentitor cells and promote vascularization and tissue regeneration. Implantation of matrigel without fibers as control resulted in few numbers of endothelial cells and no myocyte progenitors [7]. In this case nanofibrous structure may facilitate cell migration by providing structure in 3-dimensional space for them to move along and attach to.

In addition to the structural roles of nanofibers, they may also elicit functional responses in cells to migratory and remodeling behaviors. Nanofibrous structure induced fibroblasts to increase production of collagenase that degrades the adhesive collagen between the scaffold surface and cell membrane, and this led to the hypothesis that the nanofibrous architecture may have been encouraging migratory or remodeling behavior in comparison to a smooth surface [128].

2.4.8 Potential mechanisms of cell–nanostructure interactions

It is clear that nanofibrous architecture has major effects on modulating a wide variety of cell behaviors. It is not surprising that nanofibrous architecture has such an effect on cell behavior when considering the differences in local environmental conditions experienced

by a cell in a nanofibrous substrate as compared to a flat culture surface. It is theorized that nutrient infiltration, surface molecule presentation, and cell shape many be mechanisms by which nanofibrous architecture modulate cell behavior. It is intuitive that cells in a 3D nanofibrous structure would be able to exchange nutrients and utilize receptors throughout their surface, while cells in flat culture conditions are limited to nutrient exchange on only one side. By limiting the useable surface area of cells, flat culture conditions may also limit their function.

The surface molecule presentation of nanofibers may be another mechanism by which nanofibers modulate cell behavior. Interest in nanofibrous architecture in biology is many times credited to mimicking the fibers of the natural ECM, but the more general property that has fuelled the study of nanofibers is their extremely high surface area to volume ratio. It has been shown that this property results in higher protein absorption and more efficient presentation of biomolecules to cells in nanofibrous architectures and that this translates to modulation of cell behavior. Leong et al. [143] found that solid poly(D,L-lactide) fibers (850 nm) absorbed 16 times as much protein as films, and they fabricated porous nanofibers that absorbed 80% more protein than the solid fibers. Cell attachment on the three scaffolds increased in agreement with the observed increases in protein absorption. Baker et al. [144] found that polystyrene nanofiber scaffolds (200 nm) also absorbed 16 fold more serum than the equivalent flask area and hypothesized that stromal cell differentiation into smooth muscle cells was inhibited by non-specific serum protein absorption. Observed increases in myoblastic mouse cell attachment, proliferation and differentiation on fibrous pressed carbon nanotubes as compared to flat pressed

graphite were amplified by pre-culture incubation with 50% fetal bovine serum to increase the effect of surface protein absorption on cell behavior [145]. It has also been shown that biomolecules incorporated into nanofibers are much more efficient at modulating cell behavior than flat coated surfaces or soluble factors due to the high surface area to volume ratio of nanofibers. Three dimensional and two dimensional self-assembling peptide nanofiber meshes incorporating the IKVAV motif of laminin induced neural stem cell (NSC) differentiation into neurons at a rate of 35% after 1 day, as compared to 15% after 7 days on flat laminin coated substrates [15]. Neuronal differentiation was not increased in non-bioactive fiber meshes with the addition of soluble IKVAV and it was hypothesized that improved differentiation rates were caused by an increased efficiency in the presentation of the motif to the cells, which was estimated to be amplified by 1000 times compared to flat laminin coated surfaces.

Another pathway for modulation of cell behavior by nanofibrous architecture may be through cell shape. One proposed mechanism for the transduction of cell shape information into gene expression is by the transmission of mechanic forces directly from the actin cytoskeleton to the nucleus [146]. It has been shown that regulation of cell shape can influence the differentiation of multipotent human mesenchymal stem cells (hMSCs) into adiogenic or osteoblastic fate [147]. Human mesenchymal stem cells allowed to flatten and spread expressed osteoblastic markers, such as alkaline phosphatase, while constrained cells that remained unspread and rounded expressed adiogenic lipid production. While cytoskeletal organization is related to cell shape, the cytoskeleton can influence gene expression independently of cell shape. The inhibition of myosin-

generated cytoskeletal tension in hMSCs caused decreased alkaline phosphatase activity and increased lipid production without changing cell shape [147]. In a similar study, Spiegelman and Ginty [148] found that differentiation of an adipogenic cell line could be inhibited when it was allowed to attach and spread on fibronectin coated surfaces and that the inhibitory effect on cell differentiation could be reversed by keeping the cells rounded and by chemically disrupting the actin cytoskeleton.

Nuclear shape has also been measured directly and correlated to gene expression and protein synthesis [149,150]. Intermediate values of nuclear distention promoted maximum collagen I synthesis in primary osteogenic cells [149]. Two to nine fold increases in gene expression above baseline accompanied significant rounding of nuclei in mesenchymal stem cells [150].

Nanofibrous architecture is able to influence a variety of cell behaviors through a variety of mechanisms, therefore smart design of nanofibrous components in tissue engineering scaffolds can allow for increased control over resident cell behavior and thus improved overall function. It is however important to consider that the effect of nanofibers on cell behavior varies widely with specific cell types, fiber type and environmental conditions. For example, osteoprogenitor cells cultured on electrospun polymer fiber meshes exhibited a lower cell density than those on smooth surfaces in the absence of osteogenic factors, but when osteogenic factors were added the cell density of fiber surfaces was equal to or greater than that on smooth surfaces [115].

2.5 Tissue engineering applications of polymer nanofiber scaffolds

Many different applications for nanofibers in tissue engineering have been explored. Because polymer nanofibers can provide three-dimensional architecture, modulate cell behavior, and have the potential to deliver biomolecules, they are a good candidate for a wide variety of tissue engineering applications. Some of the other properties of polymer nanofiber scaffolds lead them to be well suited for more specific applications. For example, nanofibers may offer good mechanical properties for load bearing applications, directional alignment to tissues with aligned structures, and nanofiber meshes with fine pores act as membranes that allow transport of nutrients and waste, but limit cellular infiltration. Table 2.2 organizes several references to experiments where polymer nanofibers have been used as scaffolds for specific tissue regeneration applications. Each of these experiments is related to a specific tissue or application based on (1) The incorporation of tissue specific biomolecues (2) eliciting a desirable response from tissue specific cells in vitro (3) sharing a similar microstucture or mechanical properties to a natural tissue and (4) in vivo applications. The mechanical integrity of polymer nanofibers has lead to a vast amount of research for bone tissue engineering scaffolds. Many of these studies concentrated on the functionalization of nanofibers with bone specific biomolecules such as hydroxyapatite. It has been demonstrated that nanofibrous scaffolds can support osteogenic differentiation in vitro and promote in vivo bone growth into nanofibrous scaffolds in subcutaneous and bone defect models. The mechanical properties of nanofibrous structures also make them an attractive scaffold for use in cartilage tissue engineering where chondrocytic function and differentiation has been

demonstrated in nanofibrous scaffolds. Polymer nanofibers are a suitable material choice for vascular grafts because of their tensile strength and directional guidance properties. Polymer nanofiber vascular grafts have been tested in vitro under static and pulsatile conditions and in vivo. In skeletal muscle, tendon, and ligament tissue engineering, the tensile strength and directional alignment of polymer nanofibers are also attractive properties. Nerve tissue engineering benefits from the directional guidance offered by aligned nanofibers as well. Polymer nanofiber scaffolds can improve the viability, growth, alignment, and differentiation of neural cells in vitro and they have been applied to injuries in the peripheral and central nervous system to promote regeneration in vivo. Many in vivo studies have been conducted using nanofiber scaffolds in wound healing applications, including clinical trials [151]. Nanofiber scaffolds can provide structure for the ingrowth of cells around a wound site and provide a barrier to outside infection.

Table 2.2: Nanofibrous scaffolds for tissue engineering applications.

Tissue Type	Functionalization with tissue specific biomolecules	Promotion of desired behaviors from tissue specific cells in vitro	Favorable Structural properties for tissue specific application	In vivo models
Bone	Secondary surface mineralization [14,77,78,89,152,153] Bioactive peptide incorporation [108] Hydroxyapatite particle incorporation [154–158] BMP-2 incorporation [157]	Osteoblastic and pre-osteoblastic cells [159–161] Mesenchymal stem cells [28,162,163]	Selective pore size [164]	Subcutaneous implantation [165–167] Bone Defect-Skull [167–169] Bone defect- Femur [170]
Cartilage		Chondrocytes [116,117,171,172] Meniscal fibrochondrocytes [138] Mesenchymal stem cells [138,173]	Physiological shape [174] Suitable mechanical properties [175]	
Vascular	Elastin/collagen blend [176]	Endothelial cells [90,177] Smooth muscle & endothelial cells [178,179]	Shape & mechanical properties [180,181]	Epigastric vein graft [182] Abdominal aortic graft [183]
Ligament/Tendon		Ligament/tendon derived fibroblasts[136,137,184]		
Muscle		Skeletal muscle derived cells/myobasts [125,185]		
Neural	Bioactive peptide incorporation [15,186] Laminin surface modification [82]	Brain derived neural stem cells [57,80,187] Dorsal root ganglion (DRG) [126] DRG & perineural membrane derived primary neurons [188]	Shape [189]	Severed optic tract [8] Spinal cord transaction [190] Tubular sciatic nerve bridging device [191,192]
Wound Healing	Antibiotic incorporation [193]	Hair follicular cells [51] Dermal fibroblasts [66,194,195] Dermal fibroblasts & keratinocytes [196,197] Human skin equivalent tissue model [198]		Surgical wound model [47,199,200] Burn wound model [86,201] Subcutaneous implantation [202]
Intervertebral Disc			Mechanical properties [203] Shape & Structure [204]	
Islet/Hepotocyte Transplantation		Islets [133] Hepatocytes [205,206] Stem cell derived hepatic cells[207]		Islet transplantation [208]

2.6 Cell incorporation into nanofibrous electrospun scaffolds

The success of a tissue engineering scaffold is determined by its ability to incorporate desired cell types and to promote the desired functionality of the incorporated cells. Despite great promise and widespread investigation there have been few clinically relevant successes for nanofibers as tissue engineering scaffolds. One of the main reasons for this limited success is the difficulty of incorporating cells into electrospun nanofibrous scaffolds. Electrospinning is the most versatile and widely studied method of nanofibrous scaffold fabrication, but it still remains a major challenge to fabricate electrospun

scaffolds with antiquate cell incorporation or permeability. Cells can be easily incorporated into self assembling peptide nanofiber scaffolds, which is one of the major reasons for the success of this technique. There are however some major limitations to the self assembling peptide method such as, complex procedures, and limited control over fiber material, size, and arrangement. In contrast, the electrospinning technique is a very simple and versatile process that allows the fabrication of nanofibers from many types of materials and offers control over fiber size and arrangement. A feasible and practical method of quickly advancing the field of nanofibrous tissue engineering scaffolds is through the development of better methods to incorporate cells into electrospun scaffolds. Several creative approaches have been explored to address this major challenge in polymer nanofiber scaffold fabrication. Cell incorporation into nanofibrous scaffolds may be achieved in two ways: (1) Cell incorporation inside of the scaffold during fabrication (2) Migration of cells into the scaffold in vitro or by host tissue cells after in vivo implantation. Some of the strategies for improving cell incorporation into electrospun nanofiber scaffolds include cell incorporation during fabrication, physically assisted seeding methods and the design of cell permeable scaffolds using composite techniques, layer by layer assembly, and incorporation of sacrificial materials.

2.6.1 Cell incorporation during fabrication

Several techniques for direct incorporation of cells into electrospun nanofiber scaffolds have been developed. Cell nanofiber constructs were fabricated by directly pipetting cell suspension into an electrospun nanofiber scaffold during collection. Nanofibers were electrospun onto a charged ring on the surface of culture media and intermittent pipetting

of cells during the fabrication process resulted in nanofibrous constructs with uniform cell incorporation [101]. No significant toxicity was caused by residual solvent left on the electrospun nanofibers. A similar approach incorporated cells into an electrospun nanofiber scaffold by electrospraying a cell containing solution onto a grounded target while nanofibers were simultaneously electrospun onto the same target [209]. Cells integrated into the nanofiber constructs and no significant decrease in cell viability from the fabrication process was apparent. Fibroblast and adipose-derived adult stem cells were directly added into an aqueous PVA solution and electrospun to form nanofibers that encapsulated the cells [210]. Fibroblasts incorporated into PVA nanofibers retained viability, proliferation, and function.

2.6.2 Cell population by migration

When cells are not directly incorporated into a nanofiber scaffold, the scaffold may be populated by cells that migrate into the interior of the scaffold from the outer surface. The extent of cell migration into nanofiber scaffolds can be affected by both the architecture of the scaffolds and the biological or chemical cues incorporated into the scaffold.

2.6.2.1 Perfusion

Cells infiltration into nanofibrous scaffolds can be enhanced by physical forces, such vacuum, flow perfusion, or centrifuge [172,211]. These types of techniques can be utilized to increase the speed at which cells infiltrate nanofibrous scaffolds during in vitro seeding. Flow perfusion speeds up cell infiltration by moving cells with hydrodynamic forces and increases nutrient transport improving cell viability deeper inside the scaffolds [211].

2.6.2.2 Scaffold permeability

In order for cell migration into a nanofibrous scaffold to occur there must be adequate void space for cells to occupy and move around. In the case of randomly aligned electrospun mats, pore size is generally related to fiber diameter, where scaffolds fabricated from larger fibers have larger pores and thus greater permeability to cell infiltration [212]. Pham et al. [211] fabricated electrospun microfiber scaffolds with fiber diameters ranging from 2 to 10 μm. The pore size of these scaffolds increased with increasing fiber diameter from a value of around 10 μm for 2 μm diameter fibers, to around 40 μm for 10 μm diameter fibers. In contrast, overall porosity ranged from around 85–89% with the greatest porosity in smaller diameter fiber scaffolds. Cell infiltration into 5 μm diameter nanofiber scaffolds was severely limited by the inclusion of a thin layer of electrospun 600 nm fiber on its surface under both static and flow perfusion culture conditions [211]. Migration of human venous myofibroblasts into nanofiber scaffolds with diameters ranging from 3.4 to 12.1 μm increased with fiber diameter during 3 days of culture [213]. Even the relatively large 3.4 μm diameter fiber significantly impeded cell migration when compared to the 12.1 μm fiber scaffolds. Optimal pore size may be dependent on the specific cell type or application, but the minimum pore size necessary for infiltration must not be significantly smaller than that of the migrating cells. Small diameter nanofibers can be desirable because of the effects that fiber diameter has on cell behaviors as discussed in section 2.4, but pore size requirements limit the use of small diameter nanofibers in tissue engineering scaffolds. The tradeoff between scaffold porosity and fiber diameter in electrospun scaffolds is a limiting factor of this technology in tissue engineering.

2.6.2.3 Strategies to increase cell permeability

Several strategies have been developed to fabricate nanofiber scaffolds that combine both small diameter nanofibers and adequate permeability for cell infiltration. Several groups have fabricated composite fiber scaffolds that combine microfibers for large pore size and structural stability and nanofibers for improved cell interactions and increased area for attachment. A starch based scaffold made by fiber bonding with 160 μm microfibers was electrospun with 400 nm nanofibers that allowed endothelial cells to span the spaces between microfibers, migrate, and organize into capillary-like structures while maintaining structural integrity and a porosity of 70% [214,215]. A composite scaffold made from direct polymer melt deposition of microfibers that included electrospun PCL/collagen nanofibers showed improved cell adhesion and proliferation [216]. Multilayered micro/nanofiber structures have also been fabricated by modifying electrospinning conditions to include layers of 5 μm and 600 nm fibers [211]. Nanofibers with diameters of 400–500 nm were even directly electrospun onto 30 μm microfibers, which were subsequently formed into a highly porous scaffold containing nanofibers [217].

Another method to produce nanofiber scaffolds with improved cell infiltration properties is by addition of large pores within a nanofibrous structure. One hundred micron holes etched into 500 nm fiber scaffolds by UV lithography allowed the migration of smooth muscle cells into the scaffolds [218]. Porogen leaching has also been used as a method of fabricating structures with large interconnected pores within a nanofibrous network. Silk fibroin electrospun nanofiber scaffolds were soaked in a salt containing solution and lyophilized to create a porous structure. This process formed 600–900 μm

pores in a scaffolds with fiber diameters of 400 nm, in contrast to an initial pore size of 1–2 μm [219]. Salt particles have also been incorporated into nanofiber meshes by mechanical addition of solid salt particles directly to an electrospun jet during fabrication [164]. Salt particles were deposited in intervals during electrospinning to form a layered structure containing regions of salt particles. Cell infiltration of depths up to 4 mm was reported in these scaffolds after 3 weeks of in vitro culture.

Similar techniques have utilized other types of sacrificial materials to create an evenly distributed enhanced porous structure within electrospun nanofibrous scaffolds. Ice crystals were introduced to nanofiber scaffolds during fabrication by cooling a collecting mandrel to –30 $^{\circ}$C while electrospinning at room temperature [220]. Ice crystals simultaneously deposited on the mandrel during electrospinning and were distributed throughout the mesh. Freeze drying resulted in a nanofiber mesh with pores around 100 times larger than in control meshes and pore size changed with the level of humidity. Larger pore size resulted in nanofiber meshes that allowed cell penetration up to 50 μm, while control meshes allowed only surface cell growth. A similar technique involves simultaneously electrospinning water soluble sacrificial fibers into a nanofibrous scaffolds to create void space after sacrificial fiber dissolution. In randomly oriented PCL nanofiber (diameter ~1 μm) scaffolds, the depth of cell penetration after 7 days was increased from 48 to 114 μm with the addition of soluble gelatin nanofibers (diameter ~1μm) [7]. Cell penetration into PCL scaffolds containing water soluble PEO fibers increased with increasing percentage of PEO fibers [144]. In contrast, it has also been reported that nanofiber meshes with sacrificial PEO and gelatin fibers offered very limited

improvement versus control meshes in an infiltration experiment due to the collapse of the structure after sacrificial fiber leaching [221].

Cell permeable materials can be added as a filler material within a nanofibrous scaffold to add space for cell penetration. Ekaputra et al. fabricated a hybrid fibrous PCL/Col mesh with regions of hydrogel matrix by simultaneously electrospinning nanofibers and electrospraying hydrogel onto a collection mandrel [221]. The depth of cell infiltration into nanofiber meshes containing electrosprayed hydrogel was increased from around 60 to 225 μm when compared to control after 10 days of culture. Composite films containing a protein matrix and nanofibers were fabricated by adding fixed nanofiber arrays to an aqueous gelatin solution [12]. After gelatination, the gelatin matrix provided structural support to fragile aligned nanofiber arrays with significant void space between individual fibers.

Porous 3D nanofibrous networks have been fabricated by suspending electrospun nanofibers in liquids. A unique method of dispersing hydrophobic nanofibers in aqueous solutions was developed that utilized the attachment of lipase onto the surface of electrospun polystyrene nanofibers [222]. Alcohol pretreatment of the surface modified fibers caused the tightly aggregated nanofibers to be dispersed into a loosely entangled structure with greatly increased volume, and this dispersed geometry remained when the fibers were immersed DI water as long as the fibers remained hydrated throughout the washing step. Silk fibroin nanofibers collected directly in a methanol bath formed a three dimensional structure that was retained after hydration and freeze drying [223]. Cells were able to penetrate into the porous structure of these scaffolds, while control scaffolds

collected on a rotating mandrel did not allow cell penetration. Three dimensional networks of PCL nanofiber yarns were fabricated as suspensions in water by electrospinning into a novel dynamic flow collecting system [224]. These nanofiber yarn networks also retained their porous microstructure after freeze drying. It is hypothesized that these loosely dispersed nanofibers would allow improved cell penetration.

2.6.2.4 Layer by layer assembly of pre-seeded nanofiber sheets

Three-dimensional nanofibrous constructs with uniform cell distributions have been fabricated with layer-by-layer stacking of thin cell containing nanofibrous sheets. A cylinder with an 8 mm diameter and a height of 3 mm was constructed by stacking thirty 100 μm thick cell seeded nanofiber disks, and nourished with a perfusion bioreactor [225]. Thin sheets of nanofibers with a thickness of 10 μm were collected on a wire ring with a diameter of about 15 mm and seeded with cardiomyocytes [226]. Individual layers adhered immediately when these thin cell-nanofiber sheets were stacked, and constructs of up to 5 layers were formed without incidence of core ischemia. Multilayer cell-nanofiber structures have also been formed by stacking additional layers of cell containing fiber sheets every few days during cell culture [184].

2.7 Concluding remarks

Many damaged or degenerated tissues cannot be treated by conventional methods. Tissue engineering presents a promising alternative to regenerate damaged and degenerated tissues by guiding the formation of new healthy tissue. An ideal matrix for promoting the formation of such tissue requires a supporting structure for cell attachment within three dimensions as well as adequate void space for cell infiltration and vascularization.

Polymer nanofibers are an ideal material for assembling structures that address both of these requirements. In addition polymer nanofibers posses many other advantages as tissue engineering scaffolds, such as versatility for biofunctionalization, and the promotion of specific desired cell behaviors that are elicited by the nanofibrous architecture. Despite a variety of techniques employed to fabricate polymer nanofibers and to assemble them into structures, no optimal method has emerged that combines the potential advantages of polymer nanofibers and a truly 3-dimensional structure. The future clinical success of polymer nanofiber tissue engineering scaffolds will depend on whether new techniques are developed that allow for the fabrication of polymer nanofiber scaffolds with control over structural arrangement, material composition, and biofunctionalization, while maintaining reasonable cost and yield.

2.8 References

[1] Daley WP, Peters SB, Larsen M. Extracellular matrix dynamics in development and regenerative medicine. J Cell Sci 2008;121:255–64.

[2] Roach MR, Burton AC. The reason for the shape of the distensibility curves of arteries. Can J Biochem Physiol 1957;35:681–90.

[3] George EL, Georges-Labouesse EN, Patel-King RS, Rayburn H, Hynes RO. Defects in mesoderm, neural tube and vascular development in mouse embryos lacking fibronectin. Development 1993;119:1079–91.

[4] Rebustini IT, Patel VN, Stewart JS, Layvey A, Georges-Labouesse E, Miner JH, Hoffman MP. Laminin alpha5 is necessary for submandibular gland epithelial morphogenesis and influences FGFR expression through beta1 integrin signaling. Dev Biol 2007;308:15–29.

[5] Sakai T, Larsen M, Yamada KM. Fibronectin requirement in branching morphogenesis. Nature 2003;423:876–81.

[6] Fawcett JW, Keynes RJ. Peripheral nerve regeneration. Annu Rev Neurosci 1990;13:43–60.

[7] Zhang Y, Ouyang H, Lim CT, Ramakrishna S, Huang ZM. Electrospinning of gelatin fibers and gelatin/PCL composite fibrous scaffolds. J Biomed Mater Res B Appl Biomater 2005;72:156–65.

[8] Ellis-Behnke RG, Liang YX, You SW, Tay DK, Zhang S, So KF, Schneider GE. Nano neuro knitting: peptide nanofiber scaffold for brain repair and axon regeneration with functional return of vision. Proc Natl Acad Sci U S A 2006;103:5054–9.

[9] Venugopal J, Low S, Choon AT, Ramakrishna S. Interaction of cells and nanofiber scaffolds in tissue engineering. J Biomed Mater Res B Appl Biomater 2008;84:34–48.

[10] Ma Z, Kotaki M, Inai R, Ramakrishna S. Potential of nanofiber matrix as tissue-engineering scaffolds. Tissue Eng 2005;11:101–9.

[11] Vasita R, Katti DS. Nanofibers and their applications in tissue engineering.
Int J Nanomed 2006;1:15–30.

[12] Beachley V, Wen X. Fabrication of nanofiber reinforced protein structures for tissue engineering. Mater Sci Eng C 2009;29:2448–53.

[13] Berndt P, Fields G, Tirrell M. Synthetic lipidation of peptides and amino acids: monolayer structure and properties. J Am Chem Soc 1995;117:9515–22.

[14] Hartgerink JD, Beniash E, Stupp SI. Self-assembly and mineralization of peptide-amphiphile nanofibers. Science 2001;294:1684–8.

[15] Silva GA, Czeisler C, Niece KL, Beniash E, Harrington DA, Kessler JA, Stupp SI. Selective differentiation of neural progenitor cells by high-epitope density nanofibers. Science 2004;303:1352–5.

[16] Zhang S. Fabrication of novel biomaterials through molecular self assembly. Nat Biotechnol 2003;21:1171–8.

[17] HongY, Legge RL, Zhang S, Chen P. Effect of amino acid sequence and pH on nanofiber formation of self-assembling peptides EAK16-II and EAK16-IV. Biomacromolecules 2003;4:1433–42.

[18] Yokoi H, Kinoshita T, Zhang S. Dynamic reassembly of peptide RADA16 nanofiber scaffold. Proc Natl Acad Sci U S A 2005;102:8414–9.

[19] Liu G. Nanofibers. Adv Mater 1997;9:437–9.

[20] Liu D, De Feyter S, Cotlet M, Wiesler U-M,Weil T, Herrmann A, et al. Flourescent self-assembled polyphenylene dendrimer nanofibers. Macromolecules 2003;36:8489–98.

[21] Jun HW, Yuwono V, Paramonov SE, Hartgerink JD. Enzymemediated degradation of peptide-amphiphile nanofiber network. Adv Mater 2005;17:2612–7.

[22] Ma PX, Zhang R. Synthetic nano-scale fibrous extracellular matrix. J Biomed Mater Res 1999;46:60–72.

[23] Ramakrishna S, Fujuhara K, Teo WE, Lim TC, Ma Z. An introduction to electrospinning and nanofibers. Singapore: World Scientific Publishing Company; 2005, 396 pp.

[24] Czaja WK, Young DJ, Kawecki M, Brown Jr RM. The future prospects of microbial cellulose in biomedical applications. Biomacromolecules 2007;8:1–12.

[25] Brown EE, Laborie MP. Bioengineering bacterial cellulose/ poly(ethylene oxide) nanocomposites. Biomacromolecules 2007;8:3074–81.

[26] Ciechanska D. Multifunctional bacterial cellulose/chitosan composite materials for medical applications. Fibres Textiles Eastern Europe 2004;12:69–72.

[27] Grimm S, Giesa R, Sklarek K, Langner A, Gosele U, Schmidt HW, Steinhart M. Nondestructive replication of self-ordered nanoporous alumina membranes via cross-linked polyacrylate nanofiber arrays. Nano Lett 2008;8:1954–9.

[28] Porter JR, Henson A, Popat KC. Biodegradable poly(epsiloncaprolactone) nanowires for bone tissue engineering applications. Biomaterials 2009;30:780–8.

[29] Tao SL, Desai TA. Aligned arrays of biodegradable poly(epsiloncaprolactone) nanowires and nanofibers by template synthesis. Nano Lett 2007;7:1463–8.

[30] Jeong HE, Lee SH, Kim P, Suh KY. Stretched polymer nanohairs by nanodrawing. Nano Lett 2006;6:1508–13.

[31] Xing X, Wang Y, Li B. Nanofibers drawing and nanodevices assembly in poly(trimethylene terephthalate). Opt Express 2008;16:10815–22.

[32] Nain A, Wong J, Amon C, Sitti M. Drawing suspended polymer micro-/nanofibers using glass micropipettes. Appl Phys Lett 2006;89:1831051–3.

[33] Alemdar A, Sain M. Isolation and characterization of nanofibers from agricultural residues: wheat straw and soy hulls. Bioresour Technol 2008;99:1664–71.

[34] Fischer TH, Valeri CR, Smith CJ, Scull CM, Merricks EP, Nichols TC, et al. Non-classical processes in surface hemostasis: mechanisms for the poly-N-acetyl glucosamine-induced alteration of red blood cell morphology and surface prothrombogenicity. Biomed Mater 2008;3, 015009/1-9.

[35] Fan Y, Saito T, Isogai A. Preparation of chitin nanofibers from squid pen beta-chitin by simple mechanical treatment under acid conditions. Biomacromolecules 2008;9:1919–23.

[36] Aden Brook Farms Website. Large 3x3 bales of bright wheat straw; 2009 http://adenbrookfarms.com/order/index.php?main page=index&cPath=2.

[37] Rollings DA, Tsoi S, Sit JC, Veinot JG. Formation and aqueous surface wettability of polysiloxane nanofibers prepared via surface initiated, vapor-phase polymerization of organotrichlorosilanes. Langmuir 2007;23:5275–8.

[38] Mankidy P, Rajagopalan R, Foley H. Facile catalytic growth of cyanoacrylate nanofibers. Chem Commun 2006:1139–41.

[39] Jang J, Chang M, Yoon H. Chemical sensors based on highly conductive Poly(3,4-ethylene-dioxythiophene) Nanorods. Adv Mater 2005;17:1616–20.

[40] Kong H, Jang J. One-step fabrication of silver nanoparticle embedded polymer nanofibers by radical-mediated dispersion polymerization. Chem Commun 2006:3010–2.

[41] Jing X, Wang Y, Wu D, Qiang J. Sonochemical synthesis of polyaniline nanofibers. Ultrason Sonochem 2007;14:75–80.

[42] Li D, Huang J, Kaner RB. Polyaniline nanofibers: a unique polymer nanostructure for versatile applications. Acc Chem Res 2009;42:135–45.

[43] Chen F, Li X, Mo X, He C, Wang H, Ikada Y. Electrospun chitosan-P(LLA-CL) nanofibers for biomimetic extracellular matrix. J Biomater Sci Polym Ed 2008;19:677–91.

[44] Jeong SI, Lee AY, Lee YM, Shin H. Electrospun gelatin/poly(Llactide- co-epsilon-caprolactone) nanofibers for mechanically functional tissue-engineering scaffolds. J Biomater Sci Polym Ed 2008;19:339–57.

[45] Li M, Mondrinos MJ, Gandhi MR, Ko FK, Weiss AS, Lelkes PI. Electrospun protein fibers as matrices for tissue engineering. Biomaterials 2005;26:5999–6008.

[46] Boland ED, Matthews JA, Pawlowski KJ, Simpson DG, Wnek GE, Bowlin GL. Electrospinning collagen and elastin: preliminary vascular tissue engineering. Front Biosci 2004;9:1422–32.

[47] Rho KS, Jeong L, Lee G, Seo BM, Park YJ, Hong SD, et al. Electrospinning of collagen nanofibers: effects on the behavior of normal human keratinocytes and early-stage wound healing. Biomaterials 2006;27:1452–61.

[48] Zhang YZ, Venugopal J, Huang ZM, Lim CT, Ramakrishna S. Crosslinking of the electrospun gelatin nanofibers. Polymer 2006;47:2911–7.

[49] Chen ZC, Ekaputra AK, Gauthaman K, Adaikan PG, Yu H, Hutmacher DW. In vitro and in vivo analysis of co-electrospun scaffolds made of medical grade poly(epsilon-caprolactone) and porcine collagen. J Biomater Sci Polym Ed 2008;19:693–707.

[50] Kwon IK, Matsuda T. Co-electrospun nanofiber fabrics of poly(Llactide-co-epsilon-caprolactone) with type I collagen or heparin. Biomacromolecules 2005;6:2096–105.

[51] Han I, Shim KJ, Kim JY, Im SU, Sung YK, Kim M, et al. Effect of poly(3-hydroxybutyrate-co-3-hydroxyvalerate) nanofiber matrices cocultured with hair follicular epithelial and dermal cells for biological wound dressing. Artif Organs 2007;31:801–8.

[52] Meng W, Kim SY, Yuan J, Kim JC, Kwon OH, Kawazoe N, et al. Electrospun PHBV/collagen composite nanofibrous scaffolds for tissue engineering. J Biomater Sci Polym Ed 2007;18:81–94.

[53] Zeugolis DI, Khew ST, Yew ES, Ekaputra AK, Tong YW, Yung LY, et al. Electro-spinning of pure collagen nano-fibres—just an expensive way to make gelatin? Biomaterials 2008;29:2293–305.

[54] Gauthaman K, Venugopal JR, Yee FC, Peh GS, Ramakrishna S, Bongso A. Nanofibrous substrates support colony formation and maintain stemness of human embryonic stem cells. J Cell MolMed; in press.

[55] Casper CL, Yang W, Farach-Carson MC, Rabolt JF. Coating electrospun collagen and gelatin fibers with perlecan domain I for increased growth factor binding. Miomacromolecules 2007;8:1116–23.

[56] Song JH, Kim HE, Kim HW. Production of electrospun gelatin nanofiber by water-based co-solvent approach. J Mater Sci Mater Med 2008;19:95–102.

[57] Ghasemi-Mobarakeh L, Prabhakaran MP, Morshed M, Nasr-Esfahani MH, Ramakrishna S. Electrospun poly(epsiloncaprolactone)/ gelatin nanofibrous scaffolds for nerve tissue engineering. Biomaterials 2008;29:4532–9.

[58] Kim HW, Yu HS, Lee HH. Nanofibrous matrices of poly(lactic acid) and gelatin polymeric blends for the improvement of cellular responses. J Biomed Mater Res A 2008;87:25–32.

[59] Meng W, Xing ZC, Jung KH, Kim SY, Yuan J, Kang IK, et al. Synthesis of gelatin-containing PHBV nanofiber mats for biomedical application. J Mater Sci Mater Med 2008;19:2799–807.

[60] Stitzel J, Liu J, Lee SJ, Komura M, Berry J, Soker S, et al. Controlled fabrication of a biological vascular substitute. Biomaterials 2006;27:1088–94.

[61] Geng X, Kwon OH, Jang J. Electrospinning of chitosan dissolved in concentrated acetic acid solution. Biomaterials 2005;26:5427–32.

[62] Ohkawa K, Cha D, Kim H, Nishida A, Yamamoto H. Electrospinning of chitosan. Macromol Rapid Commun 2004;25:1600–5.

[63] Ohkawa K, Minato K, Kumagai G, Hayashi S, Yamamoto H. Chitosan nanofiber. Biomacromolecules 2006;7:3291–4.

[64] Chu XH, Shi XL, Feng ZQ, Gu ZZ, Ding YT. Chitosan nanofiber scaffold enhances hepatocyte adhesion and function. Biotechnol Lett 2009;31:347–52.

[65] Jiang H, Fang D, Hsiao BS, Chu B, Chen W. Optimization and characterization of dextran membranes prepared by electrospinning. Biomacromolecules 2004;5:326–33.

[66] Pan H, Jiang H, Chen W. Interaction of dermal fibroblasts with electrospun composite polymer scaffolds prepared from dextran and poly lactide-co-glycolide. Biomaterials 2006;27:3209–20.

[67] Wnek G, Carr M, Simpson D, Bowlin G. Electrospinning of nanofiber fibrinogen structrures. Nano Lett 2003;3:213–6.

[68] McManus MC, Boland ED, Simpson DG, Barnes CP, Bowlin GL. Electrospun fibrinogen: feasibility as a tissue engineering scaffold in a rat cell culture model. J Biomed Mater Res A 2007;81:299– 309.

[69] McManus M, Boland E, Sell S, Bowen W, Koo H, Simpson D, Bowlin G. Electrospun nanofibre fibrinogen for urinary tract tissue reconstruction. Biomed Mater 2007;2:257–62.

[70] Neal RA, McClugage SG, Link MC, Sefcik LS, Ogle RC, Botchwey EA. Laminin nanofiber meshes that mimic morphological properties and bioactivity of basement membranes. Tissue Eng Part CMethods 2009;15:11–21.

[71] Um IC, Fang D, Hsiao BS, Okamoto A, Chu B. Electro-spinning and electro-blowing of hyaluronic acid. Biomacromolecules 2004;5:1428–36.

[72] Ji Y, Ghosh K, Shu XZ, Li B, Sokolov JC, Prestwich GD, Clark RA, Rafailovich MH. Electrospun three-dimensional hyaluronic acid nanofibrous scaffolds. Biomaterials 2006;27:3782–92.

[73] Ji Y, Ghosh K, Li B, Sokolov JC, Clark RA, RafailovichMH.Dual-syringe reactive electrospinning of cross-linked hyaluronic acid hydrogel nanofibers for tissue engineering applications. Macromol Biosci 2006;6:811–7.

[74] Ma Z, He W, Yong T, Ramakrishna S. Grafting of gelatin on electrospun poly(caprolactone) nanofibers to improve endothelial cell spreading and proliferation and to control cell Orientation. Tissue Eng 2005;11:1149–58.

[75] Duan Y, Wang Z, Yan W, Wang S, Zhang S, Jia J. Preparation of collagen-coated electrospun nanofibers by remote plasma treatment and their biological properties. J Biomater Sci Polym Ed 2007;18:1153–64.

[76] Koh HS, Yong T, Chan CK, Ramakrishna S. Enhancement of neurite outgrowth using nano-structured scaffolds coupled with laminin. Biomaterials 2008;29:3574–82.

[77] Chen J, Chu B, Hsiao BS. Mineralization of hydroxyapatite in electrospun nanofibrous poly(L-lactic acid) scaffolds. J Biomed Mater Res A 2006;79:307–17.

[78] Yu HS, Jang JH, Kim TI, Lee HH, Kim HW. Apatite-mineralized polycaprolactone nanofibrous web as a bone tissue regeneration substrate. J Biomed Mater Res A 2009;88:747–54.

[79] Zhu Y, Leong MF, Ong WF, Chan-Park MB, Chian KS. Esophageal epithelium regeneration on fibronectin grafted poly(L-lactideco- caprolactone) (PLLC) nanofiber scaffold. Biomaterials 2007;28:861–8.

[80] Nisbet DR, Yu LM, Zahir T, Forsythe JS, Shoichet MS. Characterization of neural stem cells on electrospun poly(epsilon-caprolactone) submicron scaffolds: evaluating their potential in neural tissue engineering. J Biomater Sci Polym Ed 2008;19:623–34.

[81] Park K, Ju YM, Son JS, Ahn KD, Han DK. Surface modification of biodegradable electrospun nanofiber scaffolds and their interaction with fibroblasts. J Biomater Sci Polym Ed 2007;18:369–82.

[82] Patel S, Kurpinski K, Quigley R, Gao H, Hsiao BS, Poo MM, et al. Bioactive nanofibers: synergistic effects of nanotopography and chemical signaling on cell guidance. Nano Lett 2007;7:2122–8.

[83] Chua KN, Chai C, Lee PC, Ramakrishna S, Leong KW,Mao HQ. Functional nanofiber scaffolds with different spacers modulate adhesion and expansion of cryopreserved umbilical cord blood hematopoietic stem/progenitor cells. Exp Hematol 2007;35:771–81.

[84] Bakowsky U, Schumacher G, Gege C, Schmidt RR, Rothe U, Bendas G. Cooperation between lateral ligand mobility and accessibility for receptor recognition in selectin-induced cell rolling. Biochemistry 2002;41:4704–12.

[85] Houseman BT, Mrksich M. The microenvironment of immobilized Arg-Gly-Asp peptides is an important determinant of cell adhesion. Biomaterials 2001;22:943–55.

[86] Choi JS, Leong KW, Yoo HS. In vivo wound healing of diabetic ulcers using electrospun nanofibers immobilized with human epidermal growth factor (EGF). Biomaterials 2008;29:587–96.

[87] Li W, Guo Y, Wang H, Shi D, Liang C, Ye Z, Qing F, Gong J. Electrospun nanofibers immobilized with collagen for neural stem cells culture. J Mater Sci Mater Med 2008;19:847–54.

[88] Kim TG, Park TG. Biomimicking extracellular matrix: cell adhesive RGD peptide modified electrospun poly(D,L-lactic-co-glycolic acid) nanofiber mesh. Tissue Eng 2006;12:221–33.

[89] Zhang D, Chang J, Zeng Y. Fabrication of fibrous poly(butylene succinate)/ wollastonite/apatite composite scaffolds by electrospinning and biomimetic process. J Mater Sci Mater Med 2008;19:443–9.

[90] HeW,MaZ, Yong T, TeoWE,Ramakrishna S. Fabrication of collagencoated biodegradable polymer nanofiber mesh and its potential for endothelial cells growth. Biomaterials 2005;26:7606–15.

[91] Ma K, Chan CK, Liao S, Hwang WY, Feng Q, Ramakrishna S. Electrospun nanofiber scaffolds for rapid and rich capture of bone marrow-derived hematopoietic stem cells. Biomaterials 2008;29:2096–103.

[92] Chew SY, Hufnagel TC, Lim CT, Leong KW. Mechanical properties of single electrospun drug-encapsulated nanofibres. Nanotechnology 2006;17:3880–91.

[93] Kim K, Luu YK, Chang C, Fang D, Hsiao BS, Chu B, et al. Incorporation and controlled release of a hydrophilic antibiotic using poly(lactide-co-glycolide)-based electrospun nanofibrous scaffolds. J Control Release 2004;98:47–56.

[94] Luu YK, Kim K, Hsiao BS, Chu B, Hadjiargyrou M. Development of a nanostructured DNA delivery scaffold via electrospinning of PLGA and PLA-PEG block copolymers. J Control Release 2003;89:341–53.

[95] Chew SY, Wen J, Yim EK, Leong KW. Sustained release of proteins from electrospun biodegradable fibers. Biomacromolecules 2005;6:2017–24.

[96] Maretschek S, Greiner A, Kissel T. Electrospun biodegradable nanofiber nonwovens for controlled release of proteins. J Control Release 2008;127:180–7.

[97] Sanders E, Kloefkorn R, Bowlin G, Simpson D, Wnek G. Two-phase electrospinning from a single electrified jet: microencapsulation of aqueous reservoirs in poly(ethylene-co-vinylacetate) fibers. Macromolecules 2003;36:3803–5.

[98] Luong-Van E, Grondahl L, Chua KN, Leong KW, Nurcombe V, Cool SM. Controlled release of heparin from poly(epsilon-caprolactone) electrospun fibers. Biomaterials 2006;27:2042–50.

[99] Qi H, Hu P, Xu J, Wang A. Encapsulation of drug reservoirs in fibers by emulsion electrospinning: morphology characterization and preliminary release assessment. Biomacromolecules 2006;7:2327–30.

[100] Li X, Su Y, He C, Wang H, Fong H, Mo X. Sorbitan monooleate and poly(L-lactide-co-epsilon-caprolactone) electrospun nanofibers for endothelial cell interactions. J Biomed Mater Res A 2009;91:878–85.

[101] Yang X, Shah JD, Wang H. Nanofiber enabled layer-by-layer approach toward three-dimensional Tissue formation. Tissue Eng Part A 2009;15:945–56.

[102] Taepaiboon P, Rungsardthong U, Supaphol P. Vitamin-loaded electrospun cellulose acetate nanofiber mats as transdermal and dermal therapeutic agents of vitamin A acid and vitamin E. Eur J Pharm Biopharm 2007;67:387–97.

[103] Erisken C, Kalyon DM, Wang H. A hybrid twin screw extrusion/ electrospinning method to process nanoparticle-incorporated electrospun nanofibers. Nanotechnology 2008;19:165302.

[104] Sun Z, Zussman E, Yarin A, Wendorff J, Greiner A. Compound core-shell polymer nanofibers by co-electrospinning. Adv Mater 2003;15:1929–32.

[105] Loscertales IG, Barrero A, Marquez M, Spretz R, Velarde-Ortiz R, Larsen G. Electrically forced coaxial nanojets for one-step hollow nanofiber design. J Am Chem Soc 2004;126:5376–7.

[106] Zhang YZ, Wang X, Feng Y, Li J, Lim CT, Ramakrishna S. Coaxial electrospinning of (fluorescein isothiocyanate-conjugated bovine serum albumin)-encapsulated poly(epsilon-caprolactone) nanofibers for sustained release. Biomacromolecules 2006;7: 1049–57.

[107] Yi F, LaVan DA. Poly(glycerol sebacate) nanofiber scaffolds by core/shell electrospinning. Macromol Biosci 2008;8:803–6.

[108] Horii A, Wang X, Gelain F, Zhang S. Biological designer self assembling Peptide nanofiber scaffolds significantly enhance osteoblast proliferation, differentiation and 3-D migration. PLoS ONE 2007;2:e190.

[109] Segers VF, Tokunou T, Higgins LJ, MacGillivray C, Gannon J, Lee RT. Local delivery of protease-resistant stromal cell derived factor-1 for stem cell recruitment after myocardial infarction. Circulation 2007;116:1683–92.

[110] Gelain F, Bottai D, Vescovi A, Zhang S. Designer self-assembling Peptide nanofiber scaffolds for adult mouse neural stem cell 3- dimensional cultures. PLoS ONE 2006;1:e119.

[111] Harrington DA, Cheng EY, Guler MO, Lee LK, Donovan JL, Claussen RC, et al. Branched peptide-amphiphiles as self-assembling coatings for tissue engineering scaffolds. J Biomed Mater Res A 2006;78:157–67.

[112] Matsuzaka K, Walboomers XF, de Ruijter JE, Jansen JA. The effect of poly-L-lactic acid with parallel surface micro groove on osteoblastlike cells in vitro. Biomaterials 1999;20:1293–301.

[113] Deligianni DD, Katsala N, Ladas S, Sotiropoulou D, Amedee J, Missirlis YF. Effect of surface roughness of the titanium alloy Ti-6Al-4V on human bone marrow cell response and on protein adsorption. Biomaterials 2001;22:1241–51.

[114] Curtis A, Wilkinson C. Nanotechniques and approaches in biotechnology. Trends Biotechnol 2001;19:97–101.

[115] Badami AS, Kreke MR, Thompson MS, Riffle JS, Goldstein AS. Effect of fiber diameter on spreading, proliferation, and differentiation of osteoblastic cells on electrospun poly(lactic acid) substrates. Biomaterials 2006;27:596–606.

[116] Li WJ, Danielson KG, Alexander PG, Tuan RS. Biological response of chondrocytes cultured in three-dimensional nanofibrous poly(epsilon-caprolactone) scaffolds. J Biomed Mater Res A 2003;67:1105–14.

[117] Li WJ, Jiang YJ, Tuan RS. Chondrocyte phenotype in engineered fibrous matrix is regulated by fiber size. Tissue Eng 2006;12:1775–85.

[118] Liu Y, Ji Y, Ghosh K, Clark RA, Huang L, Rafailovich MH. Effects of fiber orientation and diameter on the behavior of human dermal fibroblasts on electrospun PMMA scaffolds. J Biomed Mater Res A 2009;90:1092–106.

[119] Rubenstein D, Han D, Goldgraben S, El-Gendi H, Gouma PI, Frame MD. Bioassay chamber for angiogenesis with perfused explanted arteries and electrospun scaffolding. Microcirculation 2007;14:723–37.

[120] Li D, Xia Y. Electrospinning of nanofibers: reinventing the wheel? Adv Mater 2004;16:1151–70.

[121] Huang Z-M, Zhang Y-Z, Kotaki M, Ramakrishna S. A review on polymer nanofibers by electrospinning and their applications in nanocomposites. Composites Sci Technol 2003;63:2223–53.

[122] Rockwood DN, Akins Jr RE, Parrag IC, Woodhouse KA, Rabolt JF. Culture on electrospun polyurethane scaffolds decreases atrial natriuretic peptide expression by cardiomyocytes in vitro. Biomaterials 2008;29:4783–91.

[123] Xu CY, Inai R, Kotaki M, Ramakrishna S. Aligned biodegradable nanofibrous structure: a potential scaffold for blood vessel engineering. Biomaterials 2004;25:877–86.

[124] Yang F, Murugan R, Wang S, Ramakrishna S. Electrospinning of nano/micro scale poly(L-lactic acid) aligned fibers and their potential in neural tissue engineering. Biomaterials 2005;26:2603–10.

[125] Choi JS, Lee SJ, Christ GJ, Atala A, Yoo JJ. The influence of electrospun aligned poly(epsilon-caprolactone)/collagen nanofiber meshes on the formation of self-aligned skeletal muscle myotubes. Biomaterials 2008;29:2899–906.

[126] Corey JM, Lin DY, Mycek KB, Chen Q, Samuel S, Feldman EL, et al. Aligned electrospun nanofibers specify the direction of dorsal root ganglia neurite growth. J Biomed Mater Res A 2007;83:636–45.

[127] Chua KN, Lim WS, Zhang P, Lu H, Wen J, Ramakrishna S, et al. Stable immobilization of rat hepatocyte spheroids on galactosylated nanofiber scaffold. Biomaterials 2005;26:2537–47.

[128] Meng J, Kong H, Han Z, Wang C, Zhu G, Xie S, et al. Enhancement of nanofibrous scaffold of multiwalled carbon nanotubes/ polyurethane composite to the fibroblasts growth and biosynthesis. J Biomed Mater Res A 2009;88:105–16.

[129] Chua KN, Chai C, Lee PC, Tang YN, Ramakrishna S, Leong KW, et al. Surface-aminated electrospun nanofibers enhance adhesion and expansion of human umbilical cord blood hematopoietic stem/progenitor cells. Biomaterials 2006;27:6043–51.

[130] Finne-Wistrand A, Albertsson AC, Kwon OH, Kawazoe N, Chen G, Kang IK, et al. Resorbable scaffolds from three different techniques: electrospun fabrics, salt-leaching porous films, and smooth flat surfaces. Macromol Biosci 2008;8:951–9.

[131] Chen M, Patra PK, Warner SB, Bhowmick S. Role of fiber diameter in adhesion and proliferation of NIH 3T3 fibroblast on electrospun polycaprolactone scaffolds. Tissue Eng 2007;13:579–87.

[132] McKenzie JL, Waid MC, Shi R, Webster TJ. Decreased functions of astrocytes on carbon nanofiber materials. Biomaterials 2004;25:1309–17.

[133] Yuan Y, Cong C, Zhang J, Wei L, Li S, Chen Y, et al. Self-assembling peptide nanofiber as potential substrates in islet transplantation. Transplant Proc 2008;40:2571–4.

[134] Sangsanoh P, Waleetorncheepsawat S, Suwantong O, Wutticharoenmongkol P, Weeranantanapan O, Chuenjitbuntaworn B, et al. In vitro biocompatibility of schwann cells on surfaces of biocompatible polymeric electrospun fibrous and solution-cast film scaffolds. Biomacromolecules 2007;8:1587–94.

[135] Elias KL, Price RL, Webster TJ. Enhanced functions of osteoblasts on nanometer diameter carbon fibers. Biomaterials 2002;23:3279–87.

[136] Lee CH, Shin HJ, Cho IH, Kang YM, Kim IA, Park KD, et al. Nanofiber alignment and direction of mechanical strain affect the ECM production of human ACL fibroblast. Biomaterials 2005;26: 1261–70.

[137] Moffat KL, Kwei AS, Spalazzi JP, Doty SB, Levine WN, Lu HH. Novel nanofiber-based scaffold for rotator cuff repair and augmentation. Tissue Eng Part A 2009;15:115–26.

[138] Baker BM, Mauck RL. The effect of nanofiber alignment on the maturation of engineered meniscus constructs. Biomaterials 2007;28:1967–77.

[139] Garreta E, Genove E, Borros S, Semino CE. Osteogenic differentiation of mouse embryonic stem cells and mouse embryonic fibroblasts in a three-dimensional self-assembling peptide scaffold. Tissue Eng 2006;12:2215–27.

[140] Shih YR, Chen CN, Tsai SW,Wang YJ, Lee OK. Growth of mesenchymal stem cells on electrospun type I collagen nanofibers. Stem Cells 2006;24:2391–7.

[141] Nur EKA, Ahmed I, Kamal J, Schindler M, Meiners S. Three dimensional nanofibrillar surfaces promote self-renewal in mouse embryonic stem cells. Stem Cells 2006;24:426–33.

[142] Bashur CA, Shaffer RD, Dahlgren LA, Guelcher SA, Goldstein AS. Effect of fiber diameter and alignment of electrospun polyurethane meshes on mesenchymal progenitor cells. Tissue Eng Part A 2009;15:2435–45.

[143] Leong MF, Chian KS, Mhaisalkar PS, Ong WF, Ratner BD. Effect of electrospun poly(D,L-lactide) fibrous scaffold with nanoporous surface on attachment of porcine esophageal epithelial cells and protein adsorption. J Biomed Mater Res A 2009;89:1040–8.

[144] Baker BM, Gee AO, Metter RB, Nathan AS, Marklein RA, Burdick JA, Mauck RL. The potential to improve cell infiltration in composite fiber-aligned electrospun scaffolds by the selective removal of sacrificial fibers. Biomaterials 2008;29:2348–58.

[145] Li X, Gao H, Uo M, Sato Y, Akasaka T, Feng Q, et al. Effect of carbon nanotubes on cellular functions in vitro. J Biomed Mater Res A 2009;91:132–9.

[146] Maniotis AJ, Chen CS, Ingber DE. Demonstration of mechanical connections between integrins, cytoskeletal filaments, and nucleoplasm that stabilize nuclear structure. Proc Natl Acad Sci U S A 1997;94:849–54.

[147] McBeath R, Pirone DM, Nelson CM, Bhadriraju K, Chen CS. Cell shape, cytoskeletal tension, and RhoA regulate stem cell lineage commitment. Dev Cell 2004;6:483–95.

[148] Spiegelman BM, Ginty CA. Fibronectin modulation of cell shape and lipogenic gene expression in 3T3-adipocytes. Cell 1983;35:657–66.

[149] Thomas CH, Collier JH, Sfeir CS, Healy KE. Engineering gene expression and protein synthesis by modulation of nuclear shape. Proc Natl Acad Sci U S A 2002;99:1972–7.

[150] McBride SH, Knothe Tate ML. Modulation of stem cell shape and fate A: the role of density and seeding protocol on nucleus shape and gene expression. Tissue Eng Part A 2008;14:1561–72.

[151] Czaja W, Krystynowicz A, Bielecki S, Brown Jr RM. Microbial cellulose—the natural power to heal wounds. Biomaterials2006;27:145–51.

[152] Araujo JV, Martins A, Leonor IB, Pinho ED, Reis RL, Neves NM. Surface controlled biomimetic coating of polycaprolactone nanofiber meshes to be used as bone extracellular matrix analogues. J Biomater Sci Polym Ed 2008;19:1261–78.

[153] Ito Y, Hasuda H, Kamitakahara M, Ohtsuki C, Tanihara M, Kang IK, et al. A composite of hydroxyapatite with electrospun biodegradable nanofibers as a tissue engineering material. J Biosci Bioeng 2005;100:43–9.

[154] Deng XL, Sui G, Zhao ML, Chen GQ, Yang XP. Poly(L-lactic acid)/hydroxyapatite hybrid nanofibrous scaffolds prepared by electrospinning. J Biomater Sci Polym Ed 2007;18:117–30.

[155] Jeong SI, Ko EK, Yum J, Jung CH, Lee YM, Shin H. Nanofibrous poly(lactic acid)/hydroxyapatite composite scaffolds for guided tissue regeneration. Macromol Biosci 2008;8:328–38.

[156] Venugopal JR,LowS,ChoonAT,KumarAB, Ramakrishna S. Nanobioengineered electrospun composite nanofibers and osteoblasts for bone regeneration. Artif Organs 2008;32:388–97.

[157] Li C, Vepari C, Jin HJ,KimHJ, Kaplan DL. Electrospun silk-BMP-2 scaffolds for bone tissue engineering. Biomaterials 2006;27:3115–24.

[158] Catledge SA, Clem WC, Shrikishen N, Chowdhury S, Stanishevsky AV,KoopmanM, et al.Anelectrospun triphasic nanofibrous scaffold for bone tissue engineering. Biomed Mater 2007;2:142–50.

[159] Kim HW, Lee HH, Chun GS. Bioactivity and osteoblast responses of novel biomedical nanocomposites of bioactive glass nanofiber filled poly(lactic acid). J Biomed Mater Res A 2008;85:651–63.

[160] Kim HW, Song JH, Kim HE. Bioactive glass nanofiber-collagen nanocomposite as a novel bone regeneration matrix. J Biomed Mater Res A 2006;79:698–705.

[161] Sargeant TD, Oppenheimer SM, Dunand DC, Stupp SI. Titanium foam-bioactive nanofiber hybrids for bone regeneration. J Tissue Eng Regen Med 2008;2:455–62.

[162] Xin X, Hussain M, Mao JJ. Continuing differentiation of human mesenchymal stem cells and induced chondrogenic and osteogenic lineages in electrospun PLGA nanofiber scaffold. Biomaterials 2007;28:316–25.

[163] Yoshimoto H, Shin YM, Terai H, Vacanti JP. A biodegradable nanofiber scaffold by electrospinning and its potential for bone tissue engineering. Biomaterials 2003;24:2077–82.

[164] Nam J, Huang Y, Agarwal S, Lannutti J. Improved cellular infiltration in electrospun fiber via engineered porosity. Tissue Eng 2007;13:2249–57.

[165] Hosseinkhani H, Hosseinkhani M, Tian F, Kobayashi H, Tabata Y. Bone regeneration on a collagen sponge self-assembled peptideamphiphile nanofiber hybrid scaffold. Tissue Eng 2007;13:11–9.

[166] Wei G, Jin Q, Giannobile WV,Ma PX. The enhancement of osteogenesis by nano-fibrous scaffolds incorporating rhBMP-7 nanospheres. Biomaterials 2007;28:2087–96.

[167] Shin SY, Park HN, Kim KH, Lee MH, Choi YS, Park YJ, et al. Biological evaluation of chitosan nanofiber membrane for guided bone regeneration. J Periodontol 2005;76:1778–84.

[168] Kim KH, Jeong L, Park HN, Shin SY, Park WH, Lee SC, et al. Biological efficacy of silk fibroin nanofiber membranes for guided bone regeneration. J Biotechnol 2005;120:327–39.

[169] Ko EK, Jeong SI, Rim NG, Lee YM, Shin H, Lee BK. In vitro osteogenic differentiation of human mesenchymal stem cells and in vivo bone formation in composite nanofiber meshes. Tissue Eng Part A 2008;14:2105–19.

[170] Sargeant TD, Guler MO, Oppenheimer SM, Mata A, Satcher RL, Dunand DC, et al. Hybrid bone implants: self-assembly of peptide amphiphile nanofibers within porous titanium. Biomaterials 2008;29:161–71.

[171] da Silva MA, Crawford A, Mundy J, Martins A, Araujo JV, Hatton PV, et al. Evaluation of extracellular matrix formation in polycaprolactone and starch-compounded polycaprolactone nanofiber meshes when seeded with bovine articular chondrocytes. Tissue Eng Part A 2009;15:377–85.

[172] Li WJ, Jiang YJ, Tuan RS. Cell-nanofiber-based cartilage tissue engineering using improved cell seeding, growth factor, and bioreactor technologies. Tissue Eng Part A 2008;14:639–48.

[173] Li WJ, Tuli R, Okafor C, Derfoul A, Danielson KG, Hall DJ, et al. A three-dimensional nanofibrous scaffold for cartilage tissue engineering using human mesenchymal stem cells. Biomaterials 2005;26:599–609.

[174] Janjanin S, Li WJ, Morgan MT, Shanti RM, Tuan RS. Mold-shaped, nanofiber scaffold-based cartilage engineering using human mesenchymal stem cells and bioreactor. J Surg Res 2008;149:47–56.

[175] Shin HJ, Lee CH, Cho IH, Kim YJ, Lee YJ, Kim IA, et al. Electrospun PLGA nanofiber scaffolds for articular cartilage reconstruction: mechanical stability, degradation and cellular responses under mechanical stimulation in vitro. J Biomater Sci Polym Ed 2006;17:103–19.

[176] Lee SJ, Yoo JJ, Lim GJ, Atala A, Stitzel J. In vitro evaluation of electrospun nanofiber scaffolds for vascular graft application. J Biomed Mater Res A 2007;83:999–1008.

[177] He W, Yong T, Teo WE, Ma Z, Ramakrishna S. Fabrication and endothelialization of collagen-blended biodegradable polymer nanofibers: potential vascular graft for blood vessel tissue engineering. Tissue Eng 2005;11:1574–88.

[178] Xu C, Inai R, Kotaki M, Ramakrishna S. Electrospun nanofiber fabrication as synthetic extracellular matrix and its potential for vascular tissue engineering. Tissue Eng 2004;10:1160–8.

[179] Jeong SI, Kim SY, Cho SK, Chong MS, Kim KS, Kim H, et al. Tissue-engineered vascular grafts composed of marine collagen and PLGA fibers using pulsatile perfusion bioreactors. Biomaterials 2007;28:1115–22.

[180] Inoguchi H, Kwon IK, Inoue E, Takamizawa K, Maehara Y, Matsuda T. Mechanical responses of a compliant electrospun poly(Llactide- co-epsilon-caprolactone) small-diameter vascular graft. Biomaterials 2006;27:1470–8.

[181] Matsuda T, Ihara M, Inoguchi H, Kwon IK, Takamizawa K, Kidoaki S. Mechano-active scaffold design of small-diameter artificial graft made of electrospun segmented polyurethane fabrics. J Biomed Mater Res A 2005;73:125–31.

[182] He W, Ma Z, Teo WE, Dong YX, Robless PA, Lim TC, et al. Tubular nanofiber scaffolds for tissue engineered small-diameter vascular grafts. J Biomed Mater Res A 2009;90:205–16.

[183] Nottelet B, Pektok E, Mandracchia D, Tille JC, Walpoth B, Gurny R, et al. Factorial design optimization and in vivo feasibility of poly(epsilon-caprolactone)-micro- and nanofiber-based small diameter vascular grafts. J Biomed Mater Res A 2009;89:865–75.

[184] Inanc B, Arslan YE, Seker S, Elcin AE, Elcin YM. Periodontal ligament cellular structures engineered with electrospun poly(DL-lactideco- glycolide) nanofibrous membrane scaffolds. J Biomed Mater Res A 2009;90:186–95.

[185] Riboldi SA, Sampaolesi M, Neuenschwander P, Cossu G, Mantero S. Electrospun degradable polyesterurethane membranes: potential scaffolds for skeletal muscle tissue engineering. Biomaterials 2005;26:4606–15.

[186] Wu Y, Zheng Q, Du J, Song Y, Wu B, Guo X. Self-assembled IKVAV peptide nanofibers promote adherence of PC12 cells. J Huazhong Univ Sci Technol Med Sci 2006;26:594–6.

[187] Yang F, Murugan R, Ramakrishna S, Wang X, Ma YX, Wang S. Fabrication of nano-structured porous PLLA scaffold intended for nerve tissue engineering. Biomaterials 2004;25:1891–900.

[188] Corey JM, Gertz CC, Wang BS, Birrell LK, Johnson SL, Martin DC, et al. The design of electrospun PLLA nanofiber scaffolds compatible with serum-free growth of primary motor and sensory neurons. Acta Biomater 2008;4:863–75.

[189] Valmikinathan CM, Tian J, Wang J, Yu X. Novel nanofibrous spiral scaffolds for neural tissue engineering. J Neural Eng 2008;5:422–32.

[190] Guo J, Su H, Zeng Y, Liang YX, Wong WM, Ellis-Behnke RG, et al. Reknitting the injured spinal cord by self-assembling peptide nanofiber scaffold. Nanomedicine 2007;3:311–21.

[191] Panseri S, Cunha C, Lowery J, Del Carro U, Taraballi F, Amadio S, et al. Electrospun micro- and nanofiber tubes for functional nervous regeneration in sciatic nerve transections. BMC Biotechnol 2008;8:39.

[192] Wang W, Itoh S, Matsuda A, Ichinose S, Shinomiya K, Hata Y, et al. Influences of mechanical properties and permeability on chitosan nano/microfiber mesh tubes as a scaffold for nerve regeneration. J Biomed Mater Res A 2008;84:557–66.

[193] Katti DS, Robinson KW, Ko FK, Laurencin CT. Bioresorbable nanofiber-based systems for wound healing and drug delivery: optimization of fabrication parameters. J Biomed Mater Res B Appl Biomater 2004;70:286–96.

[194] Chong EJ, Phan TT, Lim IJ, Zhang YZ, Bay BH, Ramakrishna S, et al. Evaluation of electrospun PCL/gelatin nanofibrous scaffold for wound healing and layered dermal reconstitution. Acta Biomater 2007;3:321–30.

[195] Venugopal J, Ramakrishna S. Biocompatible nanofiber matrices for the engineering of a dermal substitute for skin regeneration. Tissue Eng 2005;11:847–54.

[196] Powell HM, Boyce ST. Fiber density of electrospun gelatin scaffolds regulates morphogenesis of dermal-epidermal skin substitutes. J Biomed Mater Res A 2008;84:1078–86.

[197] Sun T, Mai S, Norton D, Haycock JW, Ryan AJ, MacNeil S. Self-organization of skin cells in three-dimensional electrospun polystyrene scaffolds. Tissue Eng 2005;11:1023–33.

[198] Schneider A, Garlick JA, Egles C. Self-assembling peptide nanofiber scaffolds accelerate wound healing. PLoS ONE 2008;3:e1410.

[199] Pietramaggiori G, Yang HJ, Scherer SS, Kaipainen A, Chan RK, Alperovich M, et al. Effects of poly-N-acetyl glucosamine (pGlcNAc) patch on wound healing in db/db mouse. J Trauma 2008;64:803–8.

[200] Powell HM, Supp DM, Boyce ST. Influence of electrospun collagen on wound contraction of engineered skin substitutes. Biomaterials 2008;29:834–43.

[201] MengH, Chen L, Ye Z,WangS, Zhao X. The effect of a self-assembling peptide nanofiber scaffold (peptide) when used as a wound dressing for the treatment of deep second degree burns in rats. J Biomed Mater Res B Appl Biomater 2009;89B:379–91.

[202] Blackwood KA, McKean R, Canton I, Freeman CO, Franklin KL, Cole D, et al. Development of biodegradable electrospun scaffolds for dermal replacement. Biomaterials 2008;29:3091–104.

[203] Nerurkar NL, Elliott DM, Mauck RL. Mechanics of oriented electrospun nanofibrous scaffolds for annulus fibrosus tissue engineering. J Orthop Res 2007;25:1018–28.

[204] Nesti LJ, Li WJ, Shanti RM, Jiang YJ, Jackson W, Freedman BA, et al. Intervertebral disc tissue engineering using a novel hyaluronic acid-nanofibrous scaffold (HANFS) amalgam. Tissue Eng Part A 2008;14:1527–37.

[205] Wang S, Nagrath D, Chen PC, Berthiaume F, Yarmush ML. Three-dimensional primary hepatocyte culture in synthetic selfassembling peptide hydrogel. Tissue Eng Part A 2008;14:227–36.

[206] Navarro-Alvarez N, Soto-Gutierrez A, Rivas-Carrillo JD, Chen Y, Yamamoto T, Yuasa T, et al. Self-assembling peptide nanofiber as a novel culture system for isolated porcine hepatocytes. Cell Transplant 2006;15:921–7.

[207] Hashemi SM, Soleimani M, Zargarian SS, Haddadi-Asl V, Ahmadbeigi N, Soudi S, et al. In vitro differentiation of human cord blood-derived unrestricted somatic stem cells into hepatocyte-like cells on poly(epsilon-caprolactone) nanofiber scaffolds. Cells Tissues Organs 2009;190:135–49.

[208] Navarro-Alvarez N, Rivas-Carrillo JD, Soto-Gutierrez A, Yuasa T, Okitsu T, Noguchi H, et al. Reestablishment of microenvironment is necessary to maintain in vitro and in vivo human islet function. Cell Transplant 2008;17:111–9.

[209] Stankus JJ, Soletti L, Fujimoto K, Hong Y, Vorp D, Wagner WR. Fabrication of cell microintegrated blood vessel constructs through electrohydrodynamic atomization. Biomaterials 2007;28:2738–46.

[210] van Aalst JA, Reed CR, Han L, Andrady T, Hromadka M, Bernacki S, et al. Cellular incorporation into electrospun nanofibers: retained viability, proliferation, and function in fibroblasts. Ann Plast Surg 2008;60:577–83

[211] Pham QP, Sharma U, Mikos AG. Electrospun poly(epsiloncaprolactone) microfiber and multilayer nanofiber/microfiber scaffolds: characterization of scaffolds and measurement of cellular infiltration. Biomacromolecules 2006;7:2796–805.

[212] Eichhorn SJ, Sampson WW. Statistical geometry of pores and statistics of porous nanofibrous assemblies. J R Soc Interface 2005;2:309–18.

[213] Balguid A, Mol A, van Marion MH, Bank RA, Bouten CV, Baaijens FP. Tailoring fiber diameter in electrospun poly(epsilon-caprolactone) scaffolds for optimal cellular infiltration in cardiovascular tissue engineering. Tissue Eng Part A 2009;15:437–44.

[214] Tuzlakoglu K, Bolgen N, Salgado AJ, Gomes ME, Piskin E, Reis RL. Nano- and micro-fiber combined scaffolds: a new architecture for bone tissue engineering. JMater Sci Mater Med 2005;16:1099–104.

[215] Santos MI, Tuzlakoglu K, Fuchs S, Gomes ME, Peters K, Unger RE, et al. Endothelial cell colonization and angiogenic potential of combined nano- and micro-fibrous scaffolds for bone tissue engineering. Biomaterials 2008;29:4306–13.

[216] Park SH, Kim TG, Kim HC, Yang DY, Park TG. Development of dual scale scaffolds via direct polymer melt deposition and electrospinning for applications in tissue regeneration. Acta Biomater 2008;4:1198–207.

[217] Thorvaldsson A, Stenhamre H, Gatenholm P, Walkenstrom P. Electrospinning of highly porous scaffolds for cartilage regeneration. Biomacromolecules 2008;9:1044–9.

[218] Yixiang D, Yong T, Liao S, Chan CK, Ramakrishna S. Degradation of electrospun nanofiber scaffold by short wave length ultraviolet radiation treatment and its potential applications in tissue engineering. Tissue Eng Part A 2008;14:1321–9.

[219] Ki CS, Park SY,KimHJ, JungHM,Woo KM, Lee JW, et al. Development of 3-D nanofibrous fibroin scaffold with high porosity by electrospinning: implications for bone regeneration. Biotechnol Lett 2008;30:405–10.

[220] Leong MF, Rasheed MZ, Lim TC, Chian KS. In vitro cell infiltration and in vivo cell infiltration and vascularization in a fibrous, highly porous poly(D,L-lactide) scaffold fabricated by cryogenic electrospinning technique. J Biomed Mater Res A 2009;91:231–40.

[221] Ekaputra AK, Prestwich GD, Cool SM, Hutmacher DW. Combining electrospun scaffolds with electrosprayed hydrogels leads to three-dimensional cellularization of hybrid constructs. Biomacromolecules 2008;9:2097–103.

[222] Nair S, Kim J, Crawford B, Kim SH. Improving biocatalytic activity of enzyme-loaded nanofibers by dispersing entangled nanofiber structure. Biomacromolecules 2007;8:1266–70.

[223] Ki CS, Kim JW, Hyun JH, Lee KH, Hattori M, Rah DK, et al. Electrospun three-dimensional silk fibroin nanofibrous scaffold. J Appl Polym Sci 2007;106:3922–8.

[224] Teo WE, Liao S, Chan CK, Ramakrishna S. Remodeling of three dimensional hierarchically organized nanofibrous assemblies. Curr Nanosci 2008;4:361–9.

[225] Srouji S, Kizhner T, Suss-Tobi E, Livne E, Zussman E. 3-D Nanofibrous electrospun multilayered construct is an alternative ECM mimicking scaffold. J Mater Sci Mater Med 2008;19:1249–55.

[226] Ishii O, Shin M, Sueda T, Vacanti JP. In vitro tissue engineering of a cardiac graft using a degradable scaffold with an extracellular matrix-like topography. J Thorac Cardiovasc Surg 2005;130:1358–63.

CHAPTER 3

3. EFFECTS OF ELECTROSPINNING PARAMETERS ON THE NANOFIBER DIAMETER AND LENGTH

3.1 Introduction

The fabrication of polymer nanofibers by electrospinning has received much attention in recent years. Polymer nanofibers exhibit several properties that make them favorable for many applications. Nanofibers have a very large surface area to volume ratio, flexibility in surface functionalities, and mechanical properties superior to larger fibers [1–3]. Some potential applications for nanofibers include: tissue engineering scaffolds, filtration devices, sensors, materials development, and electronic applications [2–13].

In a typical electrospinning process, fibers are drawn from a solution or melt through a blunt needle by electrostatic forces. Electrospun nanofibers are most commonly collected as randomly oriented or parallel-aligned mats. Randomly oriented fiber mats result when a simple static collecting surface is used, and parallel-aligned mats have been collected by several methods [1]. Parallel aligned fiber mats are most commonly collected with a rotating mandrel used as the collecting device. Nanofibers can also be collected across an air gap between two parallel plates in a linear orientation [14]. The electric field produced between two parallel plates causes fibers to align perpendicular to the plates and stretch across them. Because individual nanofibers can be collected by this method, it expands the potential applications of electrospinning. Once collected these fibers may be further processed to form structures suitable for specific applications. When exploring the types of structures that could potentially be developed, it may be of importance to have some idea of the maximum length of polymer fibers that is achievable by the parallel plate technique. Li et al. collected poly (vinal pyrrolidone) nanofibers across two conductive silicone strips up to several centimeters

in length and Teo and Ramakrishna collected PCL nanofibers across two thin steel blades at lengths up to 10 cm [14,15].

We theorized that longer fibers could be collected with a larger collecting device and that the maximum fiber length collected with this device would be affected by the electrospinning parameters. The characteristics of electrospun fibers are determined by many different parameters such as solution composition, polymer solution feed rate, applied voltage, and drop height. The maximum length of fibers that can be collected by the parallel plate method should be affected by these parameters and by the geometry and material characteristics of the collecting device. Optimization of these parameters could lead to the production of longer continuous fibers of a desired length and diameter. In this study the effect of these parameters on length and diameter is measured in order to gain an understanding of the factors that influence fiber diameter, uniformity, and maximum fiber length.

3.2 Materials and methods

Fibers were electrospun from polymer solutions containing 8, 11, 14, 17, and 20% w/v PCL (Mn 80,000, Sigma) and 0.06% w/v NaCl. Solution shear viscosities were approximately 0.12, 0.22, 0.45, 0.56, and 0.82 Pa respectively as measured with a TA Instruments AR100 rheometer. A 7:3 mixture of dichloromethane (DCM, Alfa Aesar) and methanol (Fisher Scientific) respectively was used as the solvent. To prepare polymer solutions, 6 mg of NaCl was dissolved in 3 ml of methanol and the resulting solution was added to 7 ml of DCM. The desired amount of PCL was then added to obtain the appropriate concentrations. A second 14% PCL solution was mixed without the addition of NaCl. The PCL solutions were transferred to 5 ml syringes and connected to a 30, 23, or 21 gauge blunt tipped needle with

polyethylene tubing. The needle tip was connected to a high voltage power source (Gamma High Voltage ES40P-10W) operating at 10, 15 or 20 kV, and polymer solution was feed into the needle at a rate of 0.010, 0.017, or 0.025 ml/min by a syringe pump (Medex inc. Medfusion 2010i). Two identical grounded aluminum plates were used as the collecting device. Three different sizes of plates were used. Dimensions were 30.5×7.5×0.7, 15×4×0.35, and 7.5×2×0.15 cm for large, medium, and small plates respectively. The plates were placed flat with an orientation that made their heights 7.5, 4, or 2 cm and arranged to be parallel along the longest dimension with a gap between them. The electrospinning setup is shown in Figure 3.1.

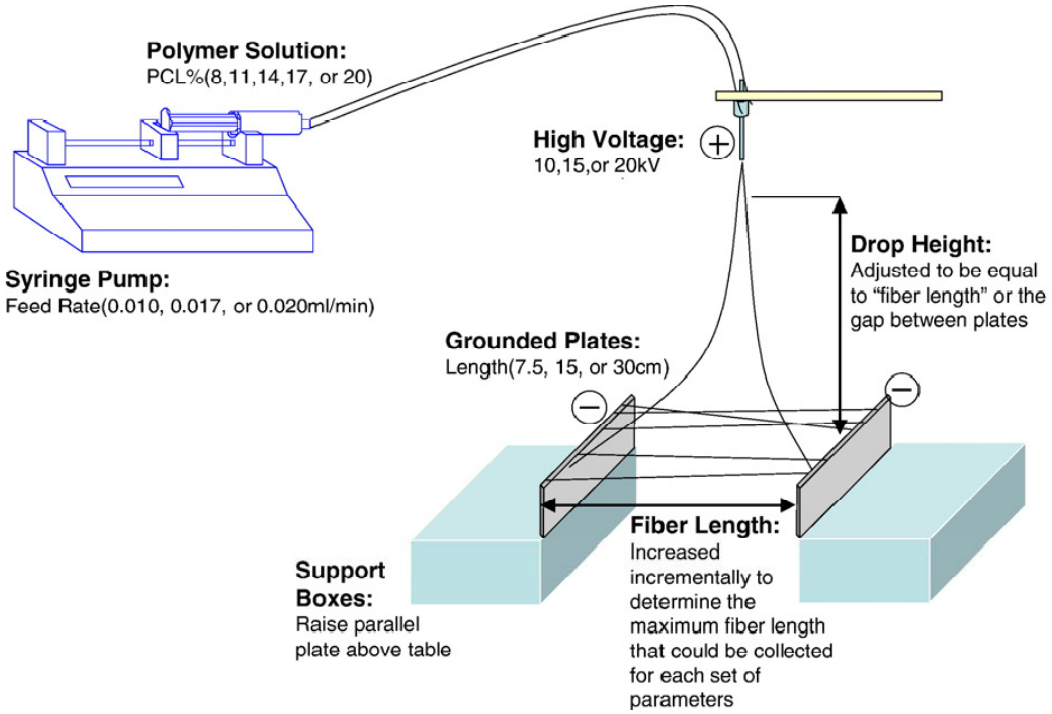

Figure 3.1: Experimental setup for electrospinning across two parallel plates.

The air gap between the two plates was set at a distance estimated to be close to the maximum fiber length and the needle tip was kept at a height equal to the distance between

the parallel plates. The gap between the plates and the drop height of the needle tip were adjusted in 2.5 cm increments to determine the maximum distance at which polymer fibers could be collected across the parallel plates. It has been previously shown that fiber collection rate decreases with increasing gap distance and constrains the maximum length at which fibers can be collected [15], therefore extending the length between the plates in increments allows an estimate of the maximum fiber length. Criteria used in making this determination were: (1) Polymer fibers stretched across the gap with each end attached to one of the parallel plates (2) Polymer fibers could be collected at an estimated amount of at least 50 fibers during a 2 min period (3) Polymer fiber collection at that distance was repeatable at least twice consecutively.

In group one, polymer concentration was varied with plate size set at 30.5×7.5×0.7 cm and NaCl concentration set at 0.06%. In group two, plate size was varied with polymer concentration set at 14% and NaCl concentration set at 0.06%. In group three, NaCl concentration was varied with polymer concentration set at 14% and plate size set at 30.5×7.5×0.7. Data was collected for all values in each group for all possible combinations of 10, 15, and 20 kV and 0.010, 0.017, and 0.025 ml/min.

Polymer fibers deposited across the parallel plates were adhered to an electron microscope stub moved through the air gap perpendicular to the fibers. Fibers contacting the stub stuck to its surface and were pulled off of the parallel plates. The samples were sputter coated with gold at a thickness of 50–70 nm using a Cressington 108 AUTO sputtercoater with a current of 30 mA for 2 min. Images of the samples were taken at 10,000 times magnification using a scanning election microscope (SEM, Hitachi TM-1000). The diameters of individual fibers were measured using Image-Pro Plus 4.0 and averaged for each group

using 17 to 40 measurements per group. Standard deviation % was calculated as the standard deviation of measured fiber diameters for one set of parameters divided by the average fiber diameter for that set of parameter. For this experiment, standard deviation % was used as a measure of the uniformity of the collected fibers. The presence of beaded fibers was quantified by measuring the ratio of the maximum to minimum diameter along the length of randomly selected fiber segments from 10,000 X SEM images. At least 65 fiber segments were averaged for 14% PCL solutions with and without NaCl added.

The effects of five different parameters were investigated: PCL %, plate size, NaCl concentration, voltage, and feed rate. The effects of polymer concentration, plate size, and NaCl concentration were analyzed within their groups and the effects of voltage and feed rate were analyzed using all of the data points. The Kruskal–Wallis test was used to determine whether the properties of maximum fiber length, resultant fiber diameter, or uniformity (standard deviation %) were affected by polymer concentration, plate size, NaCl concentration, voltage, or feed rate. The Holm's test was used to further investigate the relationships within the groups that had differences of Kruskal–Wallis significance.

Because of the instabilities in the jet, there was a random factor associated with fiber collection. The rate of fiber collection and the repeatability of fiber collection for a specific electrospinning setup were associated with the probability that fibers were being ejected in a direction that allowed them to collect in the desired location. The maximum fiber length was determined from the distance when the probability of fiber collection across the gap was too low to easily collect samples for analysis based of repeatability (two times consecutively) and rate of collection (estimated minimum of 50 fibers in a 2 min period). A P-value of <0.01 was selected to determine significance because of the variability involved

with random fluctuations in the electrospinning jet, and because of the error associated with human observation.

3.3 Results

Continuous fibers were successfully collected across the parallel aluminum plates for most groups. PCL nanofibers with an average diameter of less than 500 nm were collected at lengths up to 42.5 cm, and PCL nanofibers with an average diameter of less than 1 μm were collected at lengths up to 50 cm. Collected fibers tended to be oriented perpendicular or near perpendicular to the plates. Fibers were also observed to collect on nearby structures that were not part of the collecting device.

Fibers were successfully collected across the parallel plates for all parameter combinations except for at 8% PCL, 0.025 ml/min, and 20 kV; 20% PCL, 10 ml/min, and 15 kV; and all three flow rates in combination with 20% PCL and 20 kV. It appeared from observation that collection was impeded in the 8% PCL, 0.025 ml/min, and 20 kV group because of rapid deposition of unoriented fibers that collided with and broke the fibers collecting across the parallel plates. In the other four groups that failed to collect, fiber formation appeared to be impeded by solution properties.

Fiber collection is limited by a number of different factors. In some cases fibers extending across the plates were pulled down off the collecting plates. It was hypothesized that this was due to the electrostatic attraction to the surrounding objects because of the high acceleration observed. In several cases fiber collection proceeded from the bottom up, as electrostatic repulsion from other fibers were able to hold up new fibers on top. Fibers were also observed to fall off the plates because of collisions with other fibers. At some distances fibers were not observed stretching across the plates at all. Data points from the variable

polymer concentration and plate size groups are plotted in Figure 3.2. Voltage for each data point can be obtained from the legend, but differences in feed rate are not represented.

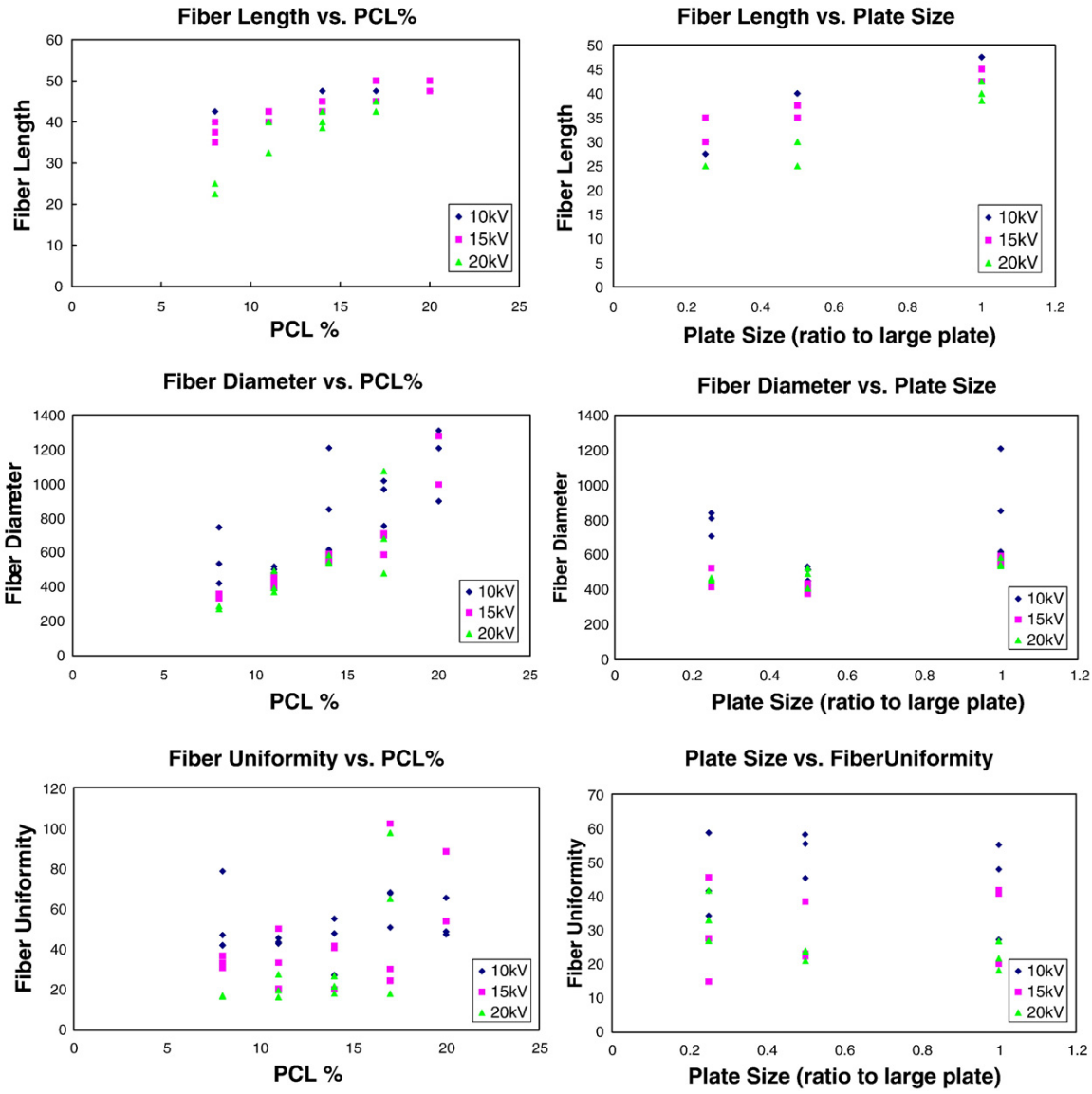

Figure 3.2: Fiber length, diameter, and uniformity versus polymer concentration and plate size.

3.3.1 Feed rate

Feed rate was not found to have a significant effect on maximum fiber length, diameter or uniformity over all parameter variations. Once the feed rate is sufficient for forming fibers,

higher feed rate only provides more polymer solution than needed, since it was observed that the amount of excess polymer solution formed at the needle tip increased with increasing feed rate (Table 3.1).

3.3.2 Polymer concentration

Maximum fiber length and fiber diameter increased with increasing polymer concentration at significant levels with plate size (30.5×7.5×0.7 cm) and NaCl concentration (0.06%) fixed and variable voltage and feed rate. Significant variation between 8% and 17%, 11% and 17%, and 11% and 20% PCL concentration groups for fiber length was identified by Holm's test. Holm's test also identified significant variation between 11% and 14%, 11% and 17%, and 11% and 20% PCL concentration groups for fiber diameter. Uniformity was observed to decrease with increasing polymer concentration, but not at the required level of significance. Fiber formation was sometimes impeded by the high viscosity of the solution at very high polymer concentration (20%) (Table 3.1).

3.3.3 Voltage

Fiber length and diameter decreased with increasing voltage over all data points, but only fiber diameter decreased at the desired level of significance. Uniformity of the fibers formed increased with increasing voltage at significant levels. Subsequent analysis of individual groups by Holm's test resulted in significant differences between the 10 kV and 15 kV and 10 kV and 20 kV groups for both fiber diameter and fiber uniformity (Table 3.1).

3.3.4 NaCl

Addition of salts to the polymer solution increases the conductivity of the solution and the surface charge density of the solution jet. Previously, addition of salts to polymer solutions reduced bead defects and decreased fiber diameter when a rotating drum was used as the collecting device [16]. Removal of NaCl from the polymer solution in this experiment did not result in any significant differences in maximum fiber length, diameter, or uniformity for the two NaCl concentration groups with polymer concentration (14%) and plate size fixed (30.5×7.5×0.7). There was however some observed decrease in fiber diameter with increasing NaCl concentration and fibers with beads were observed only when NaCl was not present in the polymer solution. The presence of beaded fibers due to lack of NaCl was quantified by the ratio of the maximum to minimum diameter of fiber segments in 10,000 times SEM images. The mean diameter ratio for fibers spun with and without NaCl added was 1.16 and 1.66 respectively ($p<0.01$). Beaded fibers electrospun from 14% PCL solution with no NaCl added are compared to fibers electrospun with 0.06% NaCl in solution in Figure 3.3 (Table 3.1).

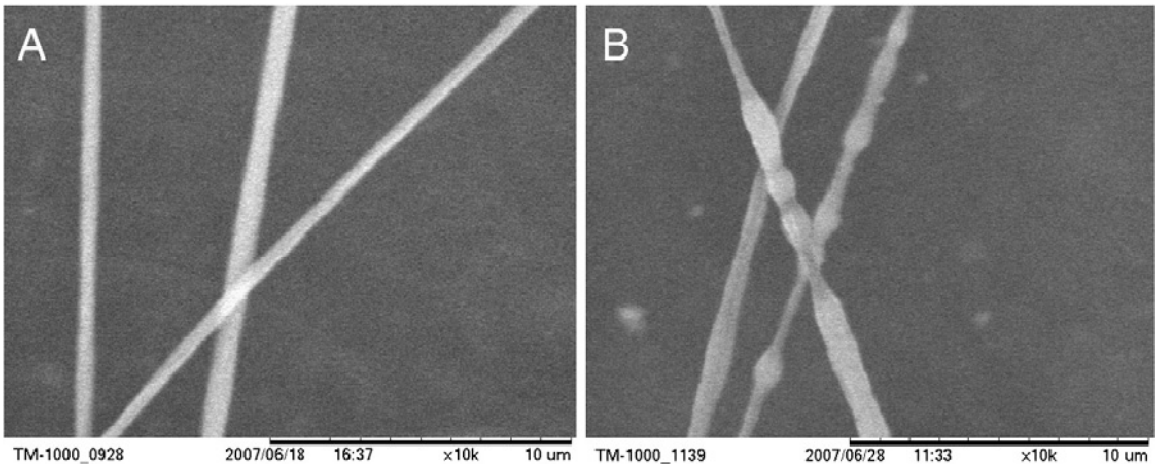

Figure 3.3: Fibers electrospun from 14% PCL solution feed at 10 ml/min and 10 kV applied voltage with (A) and without 0.06% w/v NaCl (B).

3.3.5 Plate size

A significant increase was observed for maximum fiber length and fiber diameter for variations in plate size with PCL concentration (14%) and NaCl content (0.06%) fixed. Analysis of individual groups by Holm's test resulted in significant differences in the small and large, and medium and large plates for fiber length and the medium and large plates for fiber diameter (Table 3.1).

Table 3.1: Effect of electrospinning parameters on length, diameter, and uniformity of the resultant fibers

Feed rate comparison	Kruskal P-Value
Length	0.9
Diameter	0.6
Standard Dev	0.7

PCL% Comparison	Kruskal P-Value
Length	0.00005
Diameter	0.00002
Standard Dev	0.03

NaCl concentration	Kruskal P-Value
Length	0.8
Diameter	0.1
Standard Dev	0.8

Voltage	Kruskal P-Value
Length	0.01
Diameter	0.003
Standard Dev	0.00008

Plate size	Kruskal P-Value
Length	0.00007
Diameter	0.003
Standard Dev	0.743

3.3.6 Diameter

Maximum fiber length was compared to fiber diameter (Figure 3.4) to determine if fiber diameter had a limiting relationship on maximum fiber length. There appeared to be some correlation between maximum fiber length and fiber diameter, but this correlation was determined weak by observation.

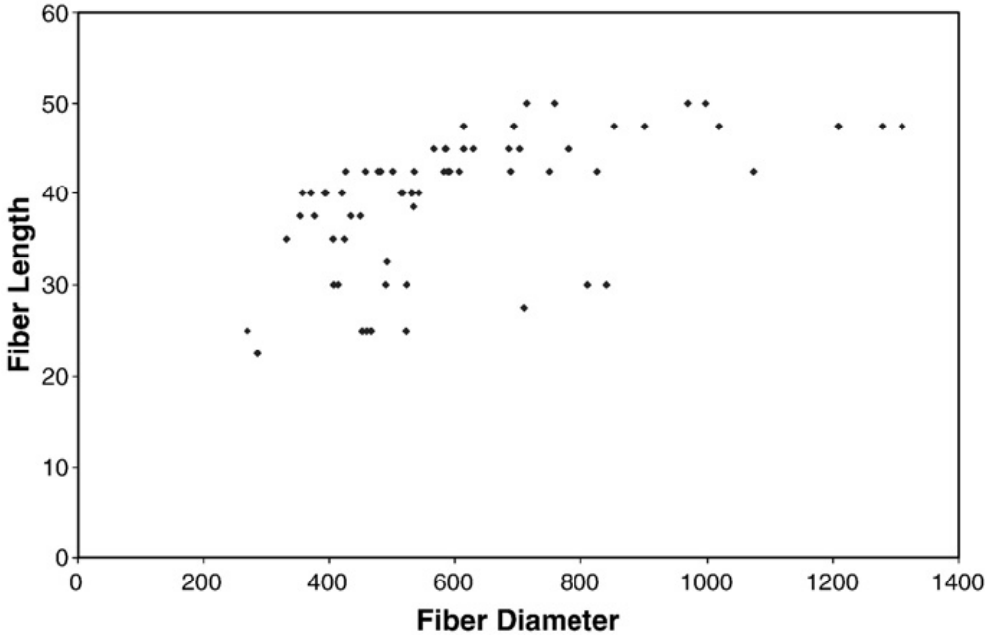

Figure 3.4: Fiber diameter versus maximum fiber length.

3.4 Discussion

The data would suggest that of the variables investigated, polymer concentration, applied voltage, and plate size had significant effects on the characteristics of fibers collected by the parallel plate method. The most interesting aspect of this experiment is the question of what the maximum length of PCL nanofibers is under optimum experimental conditions. In analyzing this question it is important to consider whether the limiting factor for maximum fiber length is the formation of continuous correctly oriented fibers or the adhesion of those fibers to the plates without fracture. It has previously been reported that under certain conditions fibers extended across two parallel plates, but broke under their own weight [14].

The data suggests that the electrical properties of the jet and the electric field have an effect on both fiber length and fiber diameter as indicated by the observed effect of polymer concentration and applied voltage on maximum fiber length. The forces acting on the fibers after contact with the plate are: adhesion to the plates, the weight of the fiber, electrostatic

attraction to the plates, electrostatic attraction to the ground, electrostatic repulsion from other collected fibers, and collisions with other fibers. A diagram of these forces is illustrated in Figure 3.5.

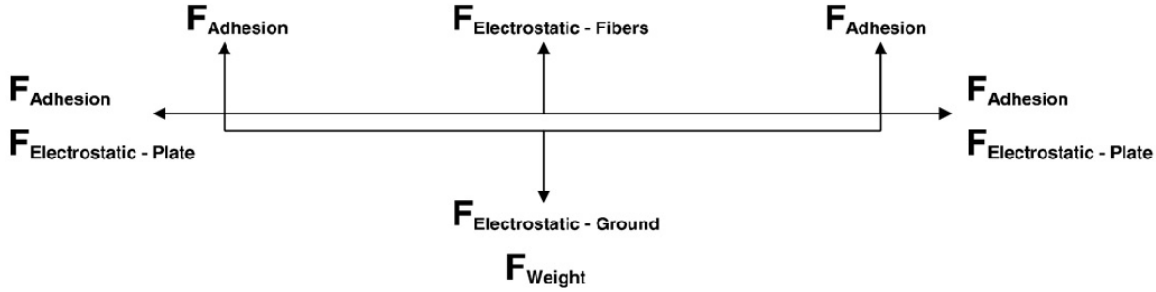

Figure 3.5: Forces acting on a single nanofiber electrospun across two parallel plates.

Fiber diameter is a variable that reflects all of the forces acting on the fiber after contacting the plate, therefore if plate adherence or fiber strength were major factors in limiting maximum fiber length then it could be expected that fiber diameter would be strongly related to fiber length.

The data shows some trend of increasing maximum fiber length with increasing fiber diameter, but the wide range of diameters for each fiber length suggests a weak correlation of maximum fiber length and fiber diameter. This would tend to discount the theory that plate adhesion or fiber strength has a strong limiting effect on the maximum fiber length for PCL, a relatively elastic material, across two parallel plates at the distances investigated.

The data suggests that it would be possible to extend the maximum length by increasing the polymer solution concentration or increasing the size of the plates. Polymer solution concentration can only be increased to a certain extent before the viscosity impedes jet formation, but the plate size can be increased without limit to any reasonable size. It is hypothesized that increasing the plate size can increase maximum fiber length to an undetermined value when using the parallel plate method, and it may be of future interest to

determine how long electrospun nanofibers can be made by this method under optimum conditions. Nanofibers are a very promising material, but the fabrication of the long continuous individual nanofibers that are required for many applications remains a challenge. Fabrication of increasingly longer nanofibers collected by the parallel plate method using increasingly larger plates will expand the potential uses of electrospinning fabrication to applications that require longer continuous nanofibers.

3.5 Conclusions

This experiment showed that continuous individual PCL nanofibers with diameters in the range of approximately 350 nm to 1 μm could be collected at lengths of 35 to 50 cm, and that polymer concentration, voltage, and plate size had significant effects on maximum fiber length, fiber diameter, and fiber uniformity. Fibers of this length could potentially be used as single fibers or further assembled into structures for many applications. For practical applications it will be desirable to obtain high quality fibers of a desired length and diameter, with a high degree of uniformity in diameter. It has been shown that all of these parameters can be controlled by changing the electrospinning conditions. It may be of interest to produce relatively long nanofibers for certain applications and it was shown that fiber length could be increased by increasing the PCL concentration in solution and the plate size. Because plate size can be increased without disrupting the electrospinning process, it is hypothesized that plates larger than those used in this experiment could be used to collect significantly longer PCL fibers up to an unknown maximum length. Parallel plate electrospinning could be used to create devices suitable for many different applications and by understanding how to create longer continuous fibers with controlled properties we can expand the versatility of this technique.

3.6 References

[1] Huang ZM, Zhang YZ, Kotaki M ,Ramakrishna S. A review on polymer nanofibers by electrospinning and their applications in nanocomposites. Composites Science and Technology 2003;63:2223-53.

[2] Zhang Y, Lim CT, Ramakrishna S, Huang ZM. Recent development of polymer nanofibers for biomedical and biotechnological applications. J Mater Sci Mater Med 2005; 16(10):933-46.

[3] Kwon IK, Kidoaki S, Matsuda T, Electrospun nano- to microfiber fabrics made of biodegradable copolyesters: structural characteristics, mechanical properties and cell adhesion potential. Biomaterials 2005;26(18):3929-39.

[4] Luong-Van E, Grondahl L, Chua KN, Leong KW, Nurcombe V, Cool SM. Controlled release of heparin from poly(epsilon-caprolactone) electrospun fibers. Biomaterials 2006; 27(9):2042-50.

[5] Chew SY, Wen J, Yim EK, Leong KW. Sustained release of proteins from electrospun biodegradable fibers. Biomacromolecules 2005;6(4):2017-24.

[6] Yang F, Murugan R, Wang S, Ramakrishna S. Electrospinning of nano/micro scale poly(L-lactic acid) aligned fibers and their potential in neural tissue engineering. Biomaterials 2005;26(15):2603-10.

[7] Chua KN, Chai C, Lee PC, Tang YN, Ramakrishna S, Leong KW, Mao HQ. Surface-aminated electrospun nanofibers enhance adhesion and expansion of human umbilical cord blood hematopoietic stem/progenitor cells. Biomaterials 2006;27(36):6043-51.

[8] Stitzel J, Liu J, Lee SJ, Komura M, Berry J, Soker S, Lim G, Van Dyke M, Czerw R, Yoo JJ, Atala A. Controlled fabrication of a biological vascular substitute. Biomaterials 2006;27(7):1088-94.

[9] Ahn P, Park S, Kim G, Hwang Y, Lee C, Shin H, Lee J. Development of high efficiency nanofilters made of nanofibers. Current Applied Physics 2006;6:1030-1035.

[10] Barhate RS, Ramakrishna S. Nanofibrous filtering media: Filtration problems and solutions from tiny materials. Journal of Membrane Science 2007;296:1-8.

[11] Dong F, Zhenyu L, Huang H, Yang F, Zheng W, Wang C. Fabrication of semiconductor nanostructures on the outer surfaces of polyacrylonitrile nanofibers by in-situ electrospinning. Materials Letters 2007;61:2556-2559.

[12] Li G, Peng L, Yunhua Y, Jia X, Zhang S, Yang X, Ryu S. Novel carbon fiber/epoxy composite toughed by electrospun polysulfone nanofibers. Materials Letters 2008;62:511-14.

[13] Aussawasathien D, Dong JH, Dai L. Electrospun polymer nanofiber sensors. Synthetic Metals 2005;154:37-40.

[14] Li D, Wang Y, Younan X, Electrospinning of Polymeric and Ceramic Nanofibers as Uniaxially Aligned Arrays. Nano Letters 2003;3(8):1167-71.

[15] Teo WE, Ramakrishna S. Electrospun fibre bundle made of aligned nanofibers over two fixed points. Nanotechnology 2005;16:1878-84.

[16] Zong X, Kim K, Fang D, Ran S, Hsiao B, Chu B. Structure and process relationship of electrospun bioabsorbable nanofiber membranes. Polymer 2002;43:4403-4412.

CHAPTER 4

4. FABRICATION OF LOOSE NANOFIBER ARRAYS FROM AN ELECTROSPINNING JET

4.1 Introduction

The fabrication of nanofibers using the electrospinning technique has generated a great amount of attention and research in recent years. Nanofibers have favorable geometric properties and superior mechanical properties when compared to larger fibers [1-2]. The surface area to volume ratio of a 500 nm diameter fiber is 8 million m^2/m^3 and 1000 times higher than that of a 500 um diameter fiber. The percentage of functional groups exposed on the surface of a polymer nanofiber is approximately three orders of magnitude greater than the percentage of functional groups on the surface of a microfiber [3]. A high percentage of surface area may result in improved cell-substrate interactions such as attachment, proliferation, and differentiation [4-7], increased sensor sensitivity [8], and improved filter efficiency. The potential of nanofibers in strong lightweight composites and fabrics is highlighted by experimental mechanical testing that shows that the Young's modulus of polymer fibers can be increased up to three times by reducing the diameter of the fibers [2].

Polymer nanofibers can be easily fabricated by electrospinning. Typically a polymer solution or melt is feed through a blunt needle tip that is connected to a high voltage power source. A thin liquid jet is ejected from the needle tip toward a grounded target as electrostatic forces overcome the surface tension forces in the needle. The jet thins and dries or cools as it travels toward the grounded target resulting in small diameter solid fibers. Electrospinning is a simple low cost method of producing polymer nanofibers. It is also a favorable technique for constructing biological scaffolds because drugs and biomolecules can

be incorporated into electrospun fibers for sustained release, while maintaining their functionality [9-11].

However, current technologies for fabricating structures from electrospun nanofibers are limited. Electrospun nanofibers have been fabricated using several methods of collection, such as flat surfaces, rotating mandrels, and parallel plates [2, 12-13]. Randomly oriented meshes collected on flat surfaces have been used to fabricate tissue engineering scaffolds and filtration devices, but their application is limited because only a random orientation is possible with this technique and because pore size is dependent on the fiber diameter [14]. Linearly aligned nanofiber scaffolds can be collected on a rotating mandrel, but only tubular structures, or segments cut from them, with a dense aligned or randomly oriented mesh are collected by this method. One major challenge with nanofiber fabrication is that nanofibers generated using electrospinning are not completely dry once they reach the collecting substrate. Due to the fact that nanofibers are formed from polymer solutions or polymer melts and that nanofibers are formed at relatively high speeds, there is not enough time to dry the fibers before they contact with each other. Therefore, all of the nanofibers are prone to stick to one another and form dense mats. This dense mat structure can cause a lot of problems in real life applications. For example, in tissue engineering applications, cells may only grow on the surface of the dense mat and be unable to penetrate inside the nanofiber scaffolds, which greatly limits the tissue formation process. Another challenge in nanofiber fabrication is the difficulties in the fabrication of ordered structures and a lack of continuous steady state fiber fabrication techniques for industrial scale up. In current electrospun nanofiber fabrication, the collection rates are not uniform and continuous due to charge buildup and shielding effects of deposited fibers, which repulse the deposition of subsequent

fibers.

In order to address the limitations of current electrospun nanofiber fabrication, a novel parallel mobile track based collecting technology was developed to allow continuous uniform aligned loose nanofiber collection. The electric field generated by two parallel conductive tracks causes charged nanofibers to deposit perpendicular to the tracks with one end fixed to the upper edge of each track, based on the similar principle demonstrated previously by Li et al [12]. Due to the incorporation of automation in these parallel conducting tracks, newly formed nanofibers are continuously pulled away from the collecting edge. There are three distinct advantages to this method: (1) Individual fibers are allowed enough time to dry on the mobile tracks before contacting other fibers in the final structure, thus reducing the chance of adhesion between adjacent fibers and even opening the door to electrospinning structures from slow evaporating solutions and high temperature melts. (2) Charge does not build up across the track as it does with the static parallel plate technique so fibers can be collected continuously, uniformly, and indefinitely. (3) Static loose nanofiber arrays on the tracks can be assembled into a structure during and after electrospinning. Complex structures that cannot be directly collected from the rapidly whipping electrospinning jet may be fabricated from the continuous supply of stabilized individual fibers.

In this work, two designs were developed to continuously collect fibers using mobile tracks. The first design uses tracks moving in the same direction as the jet to pull fibers down away from the collecting area and the second design used tracks moving in the direction normal to the jet to pull fibers sideways away from the collecting area. Figures 4.1A and D schematically show the motion of the tracks relative to the electrospinning nozzle

for each design.

The application of this technology was demonstrated in the fabrication of: (1) large area aligned nanofiber mats with controllable fiber density and unlimited thickness; (2) ultra-thin membranes with a highly controllable pore size that is dependent on fabrication parameters and not fiber diameter (3) Complex 3-dimensional structures with controlled fiber packing density.

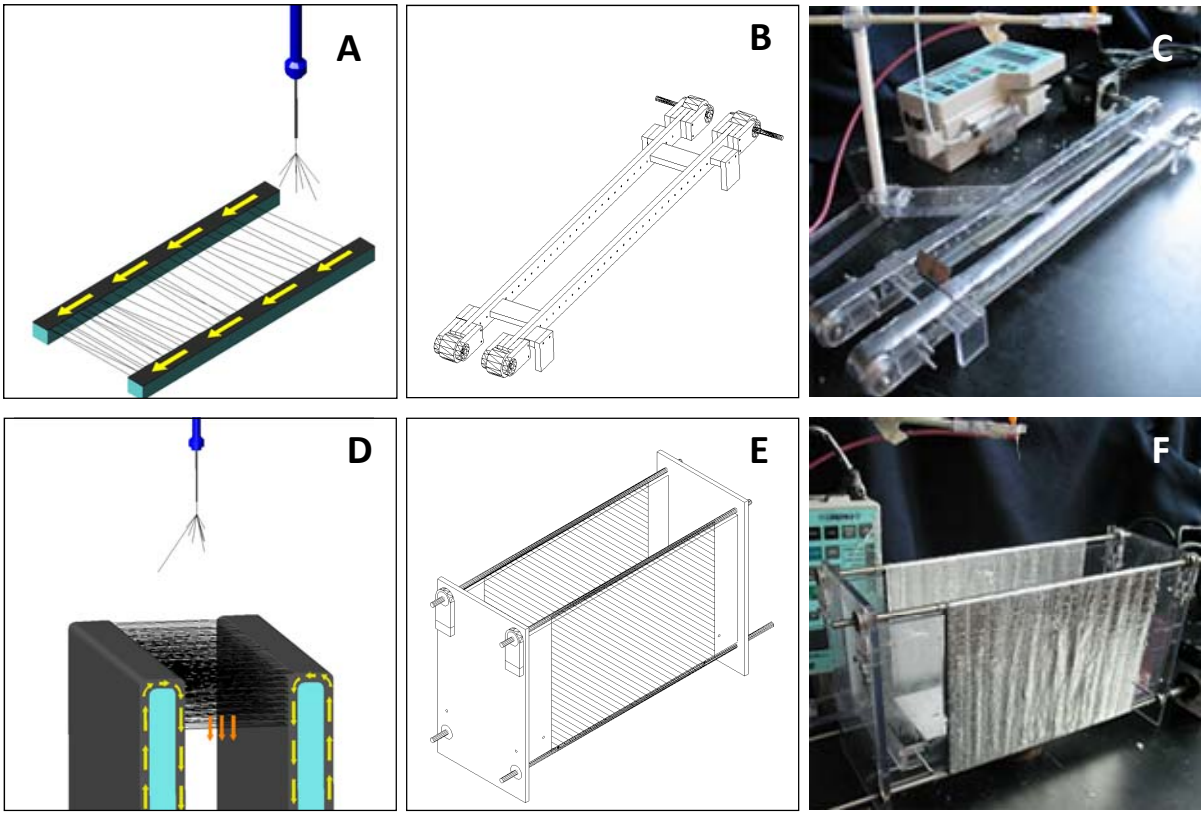

Figure 4.1: Schematics of track motion relative to an electrospinning jet (A&D), CAD drawings (B&E) and photographs (C&F) of two different types of mobile track based nanofiber collecting devices.

4.2. Materials and methods

4.2.1 Design of the Collecting Device

Two different devices were constructed to demonstrate the potential of utilizing automated mobile tracks to collect nanofibers from an electrospinning jet and assemble them into structures. Figure 4.1 contains a schematic (B and E) and a photograph (C and F) of both of the fabricated devices. All raw materials for constructing the devices were obtained from Smallparts (Miramar, FL) and McMaster-Carr (Atlanta, GA) unless otherwise specified. The frames of the devices were constructed from medical grade polycarbonate. Stainless steel rods were inserted into bearings and connected to Animatics SmartMotors (4-40C; Animatics Corporation. Santa Clara, CA) that controlled the movement of the mobile tracks. Two separate motors were used to turn each of the tracks synchronically at a controlled speed. The motion of the motors was controlled using Animatics SmartMotor Data Logger software. The tracks on the devices consisted of an inner layer made from a latex sheet, a center layer of double sided tape and an outer layer of aluminum foil. The tension applied to the tracks could be adjusted by increasing their length.

4.2.2 Electrospinning

Polycaprolactone (PCL Mn=80,000, Sigma, St Louis, MO), polyurethane (PU, Tecoflex SG-80A, Noveon, Cleveland, OH), Poly(L-lactide) (L-PLA Boehringer Ingelheim, L2095), P(DL-lactide) (DL-PLA LACTEL, B6014-1), P(DL-lactide-co-glycolide) (DL-PLG 85:15 LACTEL 85DG065), and a degradable PU (PU-D, synthesized in our lab) based on lysine diisocyanate (LDI, Kyowa Hakko Koygo Co., Ltd, Tokyo, Japan) and polycaprolactone diol (PCL-diol, Sigma) were electrospun from polymer solvent solutions. Tecoflex SG-80A was

dissolved in hexafluoro-2-propanol (HFIP, Oakwood, West Columbia, SC) at 5-8 wt/v% and degradable PU was dissolved in dichloromethane:dimethylformamide (3:1) (DCM:DMF, Sigma) at concentrations of 13-17 wt/v%. PCL was dissolved in DCM:Methonal (7:3; Sigma) at concentrations of 5-15% and in DCM:DMF (3:1) at concentrations of 13-18%. L-PLA was dissolved in HFIP at 7 wt/v% and DL-PLA was dissolved in HFIP at 35 wt/v%. DL-PLG was dissolved in 3:1 DCM:DMF at 30 wt/v%. Polymer solution was feed by a syringe pump (Medfusion 2010i; Medex Inc.) at adjustable feed rates of 0.008- 0.025 ml/min through 1/16" polyethylene tubing into a 30, 23, or 21g blunt tipped needle. A voltage of 8-20kV was applied to the needle tip with a high voltage power supply (Gamma High Voltage ES40P-10W). The needle tip was held at 5-20 cm above the level of the collecting device. The tracks of the collecting devices were run at speeds of 0 to 0.05 m/s.

4.2.3 Fiber Collection Rate Measurement

Two parallel strips of Scanning Electron Microscope (SEM) tape were placed on SEM stubs and aligned fiber arrays were collected for 1, 2.5, 5, or 7.5 minutes in an orientation perpendicular to the tape. Samples were analyzed using SEM. Fibers per unit length in the direction perpendicular to fiber alignment was counted using ImagePro Plus 4.0. Six measurements were averaged for each of three trials per collection time.

4.2.4 Pore size of crisscrossed mats

Squares of SEM tape were placed on SEM stubs. The inner dimensions of the squares were 8x8 mm. Fiber arrays were collected for 10s, 20s, 30s, 1 min, 2.5 min, or 5 min. Four layers of fiber arrays were collected for each collection time and transferred to the SEM stubs. The stub was rotated 90° between each layer to make a crisscross pattern. Samples were analyzed

using SEM and the space between crisscrossed fibers was measured using ImagePro Plus 4.0. Approximately 40 spaces were measured for each of three trials per collection time.

4.2.5 Scanning Electron Microscopy

Samples were sputter coated with gold at a thickness of 50-70 nm using a Cressington 108 AUTO sputter-coater with a current of 30 mA for 2 minutes. Images of the samples were taken at 500 to 10,000 times magnification using a scanning election microscope (SEM, Hitachi TM-1000).

4.2.6 Light microscopy

Light microscope images were taken using a Nikon Eclipse TE2000-S microscope with a Q-Imaging Micropublisher 3.3 RTV camera with Q-Capture software, or with a Zeiss Imager M2 microscope and AxioCam MRm with AxioVs40 software.

4.2.6 Laser Confocal Microscopy

In order to visualize the nanofibers in laser confocal fluorescent microscope, DiO (Invitrogen) was added to polymer solution at a concentration of 0.03mg/ml. A Leica confocal microscope (TCS SP5 AOBS) was used to visualize the nanofiber scaffolds.

4.2.7 Image Processing

ImagePro Plus 4.0 (Media Cybernetics, L.P.) was used to analyze images of nanofibers taken using SEM. Fiber diameter, number of fibers per unit length, and the space between crisscrossed fibers were all analyzed with ImagePro Plus.

4.2.8 In Vitro Cell Culture

To demonstrate the 3-dimensional cell growth and penetration of cells into the 3D nanofiber arrays, human osteoblast cells, human neural stem cells, and mouse myoblasts were cultured on aligned loose 3D nanofiber arrays (fabricated using design shown in Figure 4.1D-F) for 5 days with appropriate cell culture medium for each cell types. For all cell types, media was filled just above the level of the nanofiber arrays and cells were seeded by dripping cell suspension above the area of the scaffolds.

4.2.9 Immunocytochemistry and Histology

All cells were fixed in 4% paraformaldehyde. Some samples were directly stained using standard immunocytochemistry procedures. Some specimens were embedded in O.C.T. compound and sectioned at 20um thickness along the nanofiber direction. Some sections were stained with hemotoxilin and eosin and coversliped. Some sections were processed for immunocytochemistry staining. Osteoblasts were stained with AlexaFluor 488 Phalloidin (Invitrogen) for the actin filament inside the cells. C2C12 cells were immunostained against skeletal muscle heavy chain myosin and neurospheres were immunostained against BIII-tubulin. Aligned polymer nanofibers were visualized by confocal microscopy using reflection, and 4'-6-Diamidino-2-phenylindole (DAPI, Invitrogen) stained for the cell nuclei.

4.3. Results

4.3.1 Fiber collection

PCL, PU, PU-D, PLA, P(DL)GA, and P(DL)A nanofibers were successfully collected using the described mobile track devices. Nanofibers were collected using a number of different electrospinning parameters and the diameter and length of these fibers could be predictably adjusted. Individual fiber length was equal to the distance between the tracks of the collecting devices. The distance between tracks was adjusted to collect fibers of all polymer types to different length. Solution properties and electrospinning parameters were adjusted to predictably fabricate 8 cm long PCL fiber arrays with diameters of 250, 500, and 1000 nm. Fiber collection rate was affected by the specific electrospinning parameters selected. When fibers were collected across the parallel tracks in the static state, electrostatic repulsive forces on the deposited fibers resisted further collection. Limitation of accumulation at the collection area was readily overcome with track motion and this allowed continuous collection of aligned loose nanofiber arrays. At very low track speeds, the collected fibers stayed in the collecting area longer, which resulted in an observed repulsive force. This repulsive force caused large amounts of electrospun fibers to move away from the collecting area and accumulate elsewhere on the surface of the device or in the area surrounding the device. Fibers were continuously collected with track velocities of up to 0.05 m/s. It was not attempted to increase the track velocities further.

Fibers arrays were collected for 1, 2.5, 5 and 7.5 minutes (with electrospinning parameters and track speed fixed) to confirm continuous and uniform nanofiber collection. The results (Figure 4.2) of this experiment suggest a continuous linear collection rate. Fiber arrays were continuously collected for attempted time periods of up to eight hours.

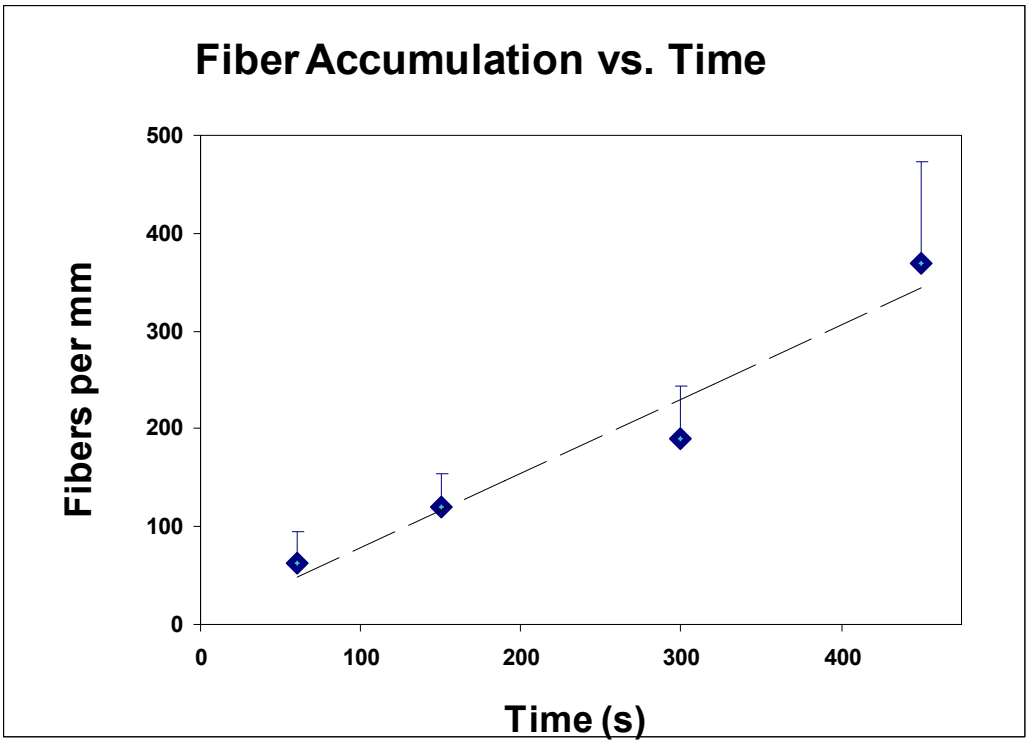

Figure 4.2: Nanofiber delivery rate of a mobile track device (shown in Figure 1D-F) with motion parallel to the direction of an electrospinning jet.

4.3.2 Collection of aligned nanofiber structures

Unidirectional aligned nanofiber arrays were easily assembled by placing a polycarbonate rectangular rack in between the two tracks of the device. The rack was held in place by holders placed on the collecting device. A very small space (~0.25cm) was left between the edge of the rack and the wall of the collecting device to allow the mobile track to pass in between. Shear forces generated on the fibers as the track moved past the rack easily cut the fibers off, leaving the fibers deposited perpendicularly across the rack. A PCL nanofiber array collected across such a rack is displayed in Figure 4.3.

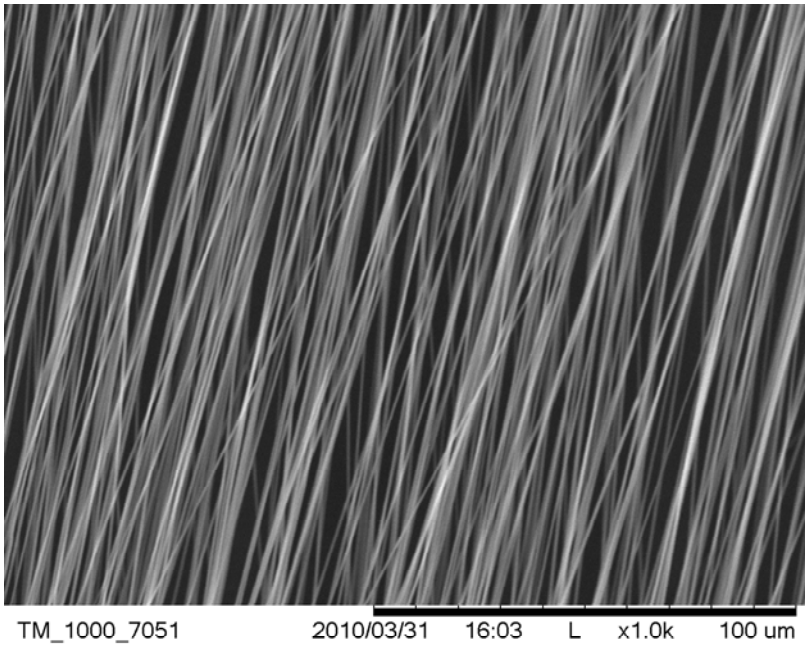

Figure 4.3: SEM image of an aligned nanofiber array collected using a mobile track device (shown in Figure 1D-F) with motion in the direction of an electrospinning jet.

4.3.3 Thin membranes with controlled porosity

Ultra thin perpendicularly crisscrossed nanofiber sheets (Figure 4.4A) were assembled by rotating a collecting rack in 90° increments at the bottom of the device. The pore size of these mats was dependent on fiber density and not fiber diameter. Collection time determined fiber density and thus the average area between crisscrossed fibers. Four layers of perpendicular fiber arrays were collected for 10 seconds to 5 minutes per layer and the average pore size was measured (Figure 4.4B&C). The average area between crisscrossed fibers decreased with increasing collection time as displayed in Figure 4.4A. It appeared that pore size was related to collection time by a power law as would be expected.

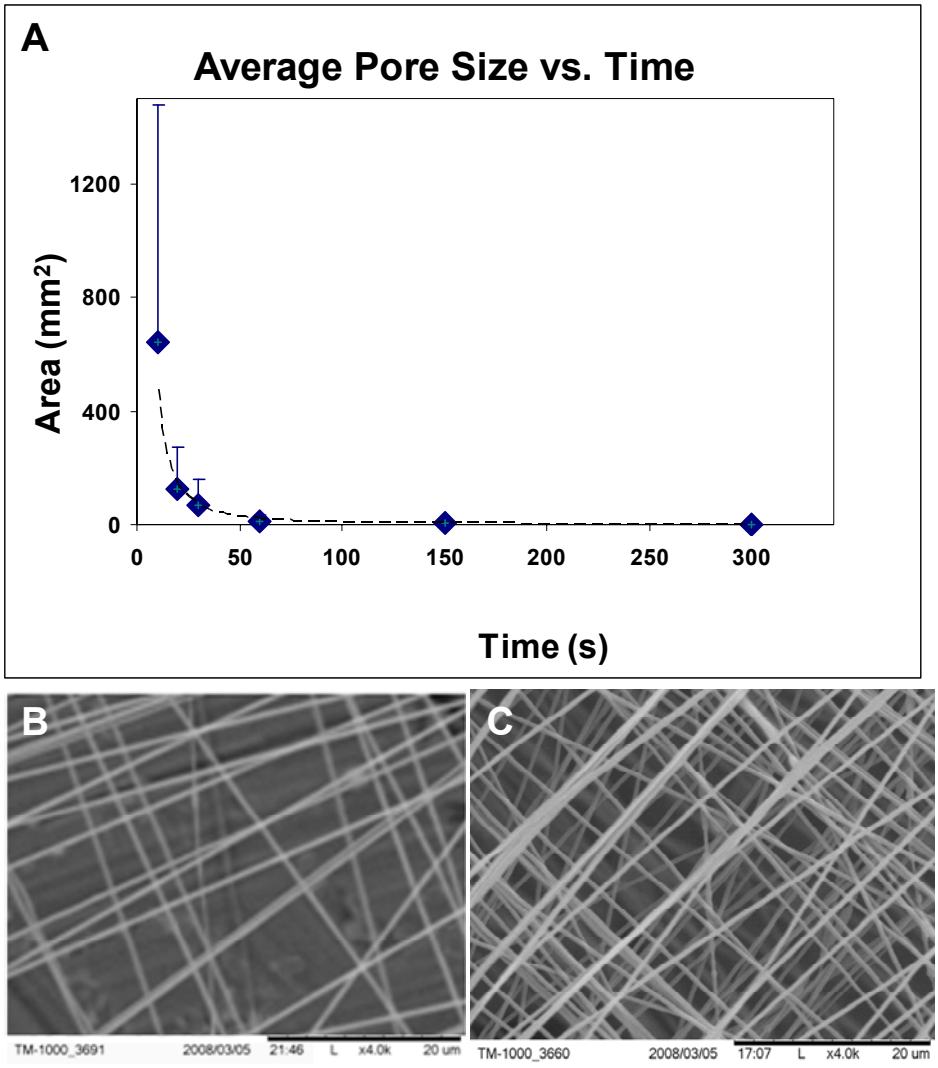

Figure 4.4: Crisscross patterned nanofiber membranes: (A) Plot of average pore size versus fiber layer collection time. SEM images of thin sheet/membranes with four layers collected for (B) one and (C) five minute each.

4.3.4 Fabrication of 3-dimensional aligned structures with controlled fiber packing density

A 3-dimensional volume of aligned nanofibers (Figure 4.5A, light reflection allows visualization of the small diameter (~600 nm) nanofibers with the naked eye) is naturally created as fibers travel down the tracks of the device described in Figures 4.1A-C. The fiber density of this volume is related to the track speed. In addition, a layer-by-layer approach was utilized to fabricate three-dimensional structures with controlled fiber density across a

rack at the bottom of the device when spacers were placed intermittently between layers of collected fibers. Nanofibers could be collected for uniform time intervals and spacers of different thickness could be placed in between nanofiber layers. For example, an aligned loose nanofiber structure of 10 mm thickness and 5cm in width can be readily fabricated when approximately two hundred 50μm spacers are used to separate 200 nanofiber arrays collected for 20 seconds per layer. Figure 4.5B is such a structure labeled with DiO and visualized by confocal microscopy. Another such structure was immersed in aqueous solution and analyzed by confocal microscopy. The fibers in the stacked array structure remained separated from neighboring fibers and intact after contact with water demonstrating the potential of these 3-dimensional arrays as components for composite assembly.

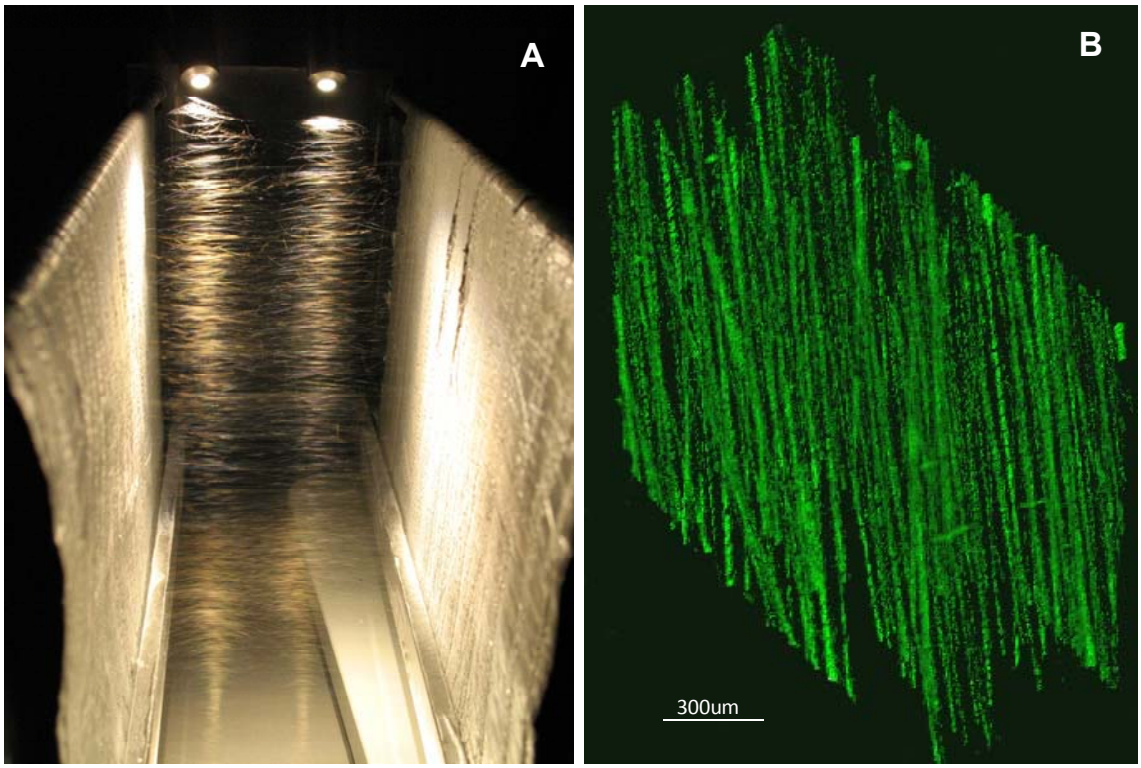

Figure 4.5: (A) Image of parallel nanofibers suspended throughout the interior space of a mobile track device (shown in Figure 1D-F) with track motion parallel to the direction of an electrospinning jet during collection. (B) Confocal images of a three-dimensional loose nanofiber array fabricated using mobile track collecting device and layer spacers.

4.3.5 Tissue engineering constructs

The potential of this technology in 3-dimensional tissue growth was demonstrated by seeding different types of cells on the surface of the fabricated loose aligned nanofiber arrays (Figure 4.6). When human neural stem cells were seeded on the nanofiber array under neural differentiation condition, 3-dimensional aligned neurites sprouted from human neural stem cells aligned with the nanofibers and grew inside the nanofiber arrays to form 3D nerve fibers (Figure 4.6A&E). When human osteoblasts were seeded on the nanofiber arrays, cytoskeletal actin filaments inside the cells are highly aligned along the loose nanofibers and formed 3-dimensional tissue structure. When mouse myoblasts were seeded on the nanofiber arrays under myo-differentiation condition, myotubes were formed on both sides of loose nanofiber array even though myoblasts were seeded only on one side, which also proved the ability of cells to migrate through the loose nanofiber array (Figure 4.6C&F). Myoblasts cultured on thick loose non-adherent aligned nanofiber array were able to penetrate deep into the fiber mats after just one week in culture, and after 3 weeks of culture myoblasts populated the entire thickness of nanofiber array and formed skeletal muscle like tissue (Horizontal sections along the nanofiber direction, Figures 4.6D&H). It is hypothesized that loose nanofiber arrays (i.e., without fiber-fiber adhesions) allowed for good cell penetration throughout the nanofiber bundles.

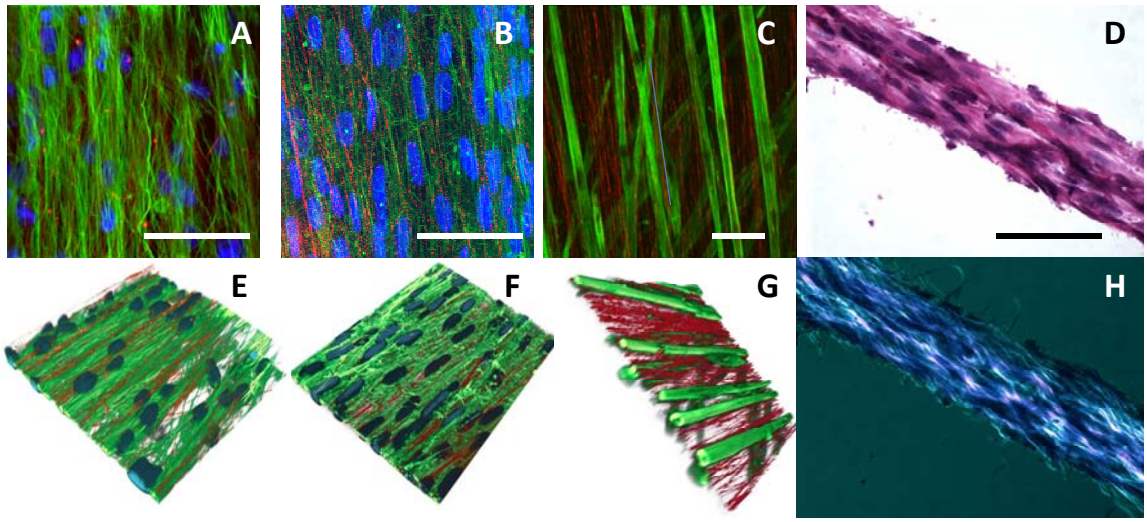

Figure 4.6: Three-dimensional cell-nanofiber structure formed after seeding cells on the surface of the nanofiber arrays and grown for 5 days: Human neural stem cells(A and E), human osteoblasts(B and F), and 21 days: mouse myoblasts(C and G). A horizontal section of an aligned loose nanofiber array seeded with myoblast shows good penetration of cells and form skeletal muscle like tissue structure after 3 weeks in culture stained with H&E and taken in bright field (D) and DIC mode (H). Scale bar= 50um

4.4 Discussion

Nanofiber structures are commonly obtained from an electrospinning jet using a flat plate, rotating collection device, or parallel plate collector. While each of these techniques is different, they are all limited in the kinds of nanofiber structures that can be fabricated because all utilize nanofiber assembly directly from an unstable highly charged electrospinning jet. A novel technology was developed that allows for an intermediate step in between the stabilization of nanofibers from the electrospinning jet and the assembly of nanofibers into a structure.

The two described collecting devices demonstrated the potential of this technology to maintain continuous and uniform collection of aligned nanofibers for an indefinite time period. Unlike most methods of fiber collection, this technology allows for a consistent electrical field. Charge build up and electrical shielding by deposited fibers cause variations in the electric field when previous available collection methods are employed. Variations in

the electrical field can affect the rate of collection as well as limit it. The described devices demonstrated fiber collection rates that were uniform and indefinitely continuous (verified continuous collection tested up to 8 hours).

The continuously collected fiber arrays are maintained as individual fibers until further post-processing assembly, thus providing additional time for evaporation of residual solvent or cooling of melts before the individual fibers contact one another. This results in the elimination of any unwanted fiber-fiber adhesions in the final assemblies and may even open the door for electrospun nanofiber structure assembly using slow-evaporating solutions and high temperature melts. Control over evaporation/cooling time will also allow greater versatility in a variety of applications. One example is that this novel technology may also allow for direct live cell loading within the nanofiber arrays during the fabrication/assembly process since this technology allows extra time for solvent evaporation or cooling, where toxic solvents and high temperatures can damage cells.

Several structures were assembled from nanofiber arrays collected by automated tracks in order to demonstrate the potential of this method. Easily fabricated ultra-thin nanofiber mats with controllable pore size could have potential use as filtration devices or guidance tissue regeneration (GTR) membranes. Importantly the pore size of these ultra thin structures was not dependent on the fiber diameter as is seen in conventional randomly oriented nanofiber meshes. Independent control over pore size and fiber diameter allows for the assembly of structures with both optimized fiber diameter and optimized pore size. Ultra thin crisscrossed mats have been previously fabricated from static parallel electrodes [12, 15], but fabrication with incorporation of automated tracks offers advantages in maximum overall mat area, minimum pore size, uniformity, and practicality in the manufacturing process.

Fabricated aligned loose nanofiber arrays allow many different types of cells to attach, grow, and penetrate inside the 3-dimensional arrays. As shown in Figure 4.6A and 4.6E, nerve fibers sprout from neural stem cells and form aligned nerve fiber bundles along the loose nanofiber arrays. The same is true for osteoblasts and myoblasts, where thick aligned loose nanofiber arrays allow good cell penetration deep into the scaffolds. It is hypothesized that cell penetration was facilitated because this fabrication procedure addresses some of the problems that may be encountered when conventional rotating mandrel or parallel plate collectors are used in nanofiber collection. The rotating mandrel method requires high rotation speeds that generate tangential velocities of several meters per seconds [13]. This results in a tightly wound structure that contributes to poor cell penetration properties. The static parallel plate method utilizes a gentler nanofiber collection process, but a thick aligned nanofiber scaffold cannot be fabricated by this method alone because of charge resistance and shielding caused by previously deposited fibers [16]. In addition, the rotating mandrel, the static parallel plate method, and all other collecting methods developed before this method have inherent problems of fiber to fiber adhesions due to incomplete drying or cooling of fibers that are in contact with one another soon after formation. Fiber to fiber adhesions can limit cell penetration into nanofibrous structures.

This automatic dynamic collecting device allows fabrication of 3-dimensional aligned nanofiber structures that could not be possible using previous methods. The applicability of electrospun nanofiber structures is limited by the difficulty in fabricating ordered 3-dimensional structures. It was demonstrated that this technology is capable of fabricating large volume 3-dimensional aligned fiber arrays with controllable uniform packing density. Fiber alignment with large volume and uniform spacing among individual nanofibers make

those structures unique to this system of fabrication. The ability of these 3-dimensional fiber arrays to maintain their structure in liquid highlights a potential for composite fabrication and tissue regeneration.

The most substantial impact of this technology may come not from the types of structures that can be assembled, but the practicality for industrial scale up. Most nanofiber structures are assembled directly from the electrospinning jet and are thus restricted by the unstable jet, which experiences violent whipping motions and high electrical charges. Difficulties involved in predictably controlling this jet seriously limit the possibility of assembling complex nanofiber structures with electrospun nanofibers. Other potential problems facing conventional electrospinning for industrial scale up include non-uniform/limited fiber collection rates and clogging, spitting, and increased unpredictability during the beginning of each electrospinning collection cycle. The presented technologies demonstrated continuously delivered individual nanofibers in stable aligned arrays, where after they can be post-processed into more complex structures by mechanical methods. Delivery of continuous stable nanofiber arrays on automated tracks in a highly controllable fashion opens the door for countless innovative ways to assemble complex nanofiber structures that may not be feasible by available techniques.

The exceptional versatility of this technology was demonstrated by the successful fabrication and operation of two fiber collecting devices. Continuous aligned nanofiber arrays were collected for a variety of materials with controlled fiber diameter and length. The simplicity of this system makes it conducive for combination with other electrospinning techniques such as; addition of auxiliary electrodes, magnetic fields, and alternating currents; and mechanical assembly techniques such as rapid prototyping technologies [17-19].

4.5 Conclusions

A novel technology for collecting nanofibers using parallel automated tracks was developed. Parallel tracks were moved in two different planes to collect nanofibers and deliver them for assembly into various structures. A uniform electric field is maintained because movement of fibers away from the collecting area alleviates repulsive charge accumulation. Steady state indefinitely continuous delivery of immobilized nanofiber arrays by motorized tracks was verified. The described method also allows an indefinite amount of extra time for individual fibers to dry or cool before contacting other fibers in the final structure. Thus, potential fiber-fiber adhesions due to incomplete drying or cooling can be eliminated. It is hypothesized that nanofiber arrays collected and distributed with motorized collecting tracks could be assembled into complex ordered structures that cannot be practically fabricated using other current methods. This novel method of fiber collection adds an intermediate step that outputs stable aligned fiber arrays collected from the violent highly charged electrospinning jet. Fixation and organization of the fibers permits feasible post processing of electrospun nanofibers into complex structures by mechanical means. Several structures were fabricated to demonstrate the potential of this technology. 1) Thick aligned loose nanofiber array with good cell penetration properties due to the assembly techniques. 2) Three dimensional aligned fiber arrays with uniform fiber packing densities and theoretically unlimited width and depth. And 3) Ultrathin crisscrossed meshes fabricated with independent control of both nanofiber diameter and pore size. All these structures are difficult to fabricate using other current collecting techniques due to the unpredictable electrospinning jet. With a mobile parallel track based nanofiber fabrication technology, it is very practical for scale up with a variety of automated mechanical assembly methods for the fabrication of nanofiber

containing structures that are not feasible with current methods.

4.6 References

[1] Huang MH, Zhang YZ, Kotaki M, Ramakrishna S. A review on polymer nanofibers by electrospinning and their applications in nanocomposites. Composite Science and Technology 2003;63:2223-2253.

[2] Kwon IK, Kidoaki S, Matsuda T, Electrospun nano- to microfiber fabrics made of biodegradable copolyesters: structural characteristics, mechanical properties and cell adhesion potential. Biomaterials 2005;26(18):3929-39.

[3] Zhang Y, Lim CT, Ramakrishna S, Huang ZM. Recent development of polymer nanofibers for biomedical and biotechnological applications. J Mater Sci Mater Med 2005; 16(10):933-46.

[4] Nur-E-Kamal A, Ahmed I, Kamal J, Schindler M, Meiners S. Three-dimensional nanofibrillar surfaces promote self-renewal in mouse embryonic stem cells. Stem Cells 2006;24(2):426-33.

[5] Chua KN, Chai C, Lee PC, Tang YN, Ramakrishna S, Leong KW, Mao HQ. Surface-aminated electrospun nanofibers enhance adhesion and expansion of human umbilical cord blood hematopoietic stem/progenitor cells. Biomaterials 2006;27(36):6043-51.

[6] Yang F, Murugan R, Wang S, Ramakrishna S. Electrospinning of nano/micro scale poly(L-lactic acid) aligned fibers and their potential in neural tissue engineering. Biomaterials 2005;26(15):2603-10.

[7] Beachley V, Wen X. Polymer nanofibrous structures: Fabrication, biofunctionalization, and cell interactions. Prog Polym Sci 2010;35(7):868-892.

[8] Aussawasathien D, Dong JH, Dai L. Electrospun polymer nanofiber sensors. Synthetic Metals 2005;154:37-40.

[9] Luong-Van E, Grondahl L, Chua KN, Leong KW, Nurcombe V, Cool SM. Controlled release of heparin from poly(epsilon-caprolactone) electrospun fibers. Biomaterials 2006; 27(9):2042-50.

[10] Qi H, Hu P, Xu J, Wang A. Encapsulation of drug reservoirs in fibers by emulsion electrospinning: morphology characterization and preliminary release assessment. Biomacromolecules 2006;7(8):2327-30.

[11] Xie J, Wang CH. Electrospun micro- and nanofibers for sustained delivery of paclitaxel to treat C6 glioma in vitro. Pharm Res 2006;23(8):1817-26.

[12] Li D, Wang Y, Younan X, Electrospinning of Polymeric and Ceramic Nanofibers as Uniaxially Aligned Arrays. Nano Letters 2003;3(8):1167-71.

[13] Courteny T, Sacks MS, Stankus J, Guan J, Wagner WR. Design and analysis of tissue engineering scaffolds that mimic soft tissue mechanical anisotropy. Biomaterials 2006; 27(19):3631-8.

[14] Pham QP, Sharma U, Mikos AG. Electrospun poly(epsilon-caprolactone) microfiber and multilayer nanofiber/microfiber scaffolds: characterization of scaffolds and measurement of cellular infiltration. Biomacromolecules 2006;7(10):2796-805.

[15] Li D, Wang Y, Xia Y. Electrospinning Nanofibers as Uniaxially Aligned Arrays and Layer-by-Layer Stacked Films. Advanced Materials 2004;16(4):361-366.

[16] Teo WE, Ramakrishna S. A review on electrospinning design and nanofibre assemblies. Nanotechnology 2006;7:R89-106.

[17] Deitzel JM, Kleinmeyer JD, Hirvonen JK, Beck Tan NC. Controlled deposition of electrospun poly(ethylene oxide) fibers. Polymer 2001;42:8163-70.

[18] Liu Y, Xinping Z, Xia Y, Yang H. Magnetic-Field-Assisted Electrospinning of Aligned Straight and Wavy Polymeric Nanofibers. Advanced Materials 2010;22(22): p2454-57.

[19] Kim, GH, Electrospinning process using field-controllable electrodes. Journal of Polymer Science Part B-Polymer Physics 2006;44(10):1426-33.

CHAPTER 5

5. FABRICATION OF NANOFIBER REINFORCED PROTEIN STRUCTURES FOR TISSUE ENGINEERING

5.1. Introduction

Many tissue engineering strategies involve the use of scaffolds that support cell attachment, survival and proliferation, and formation of tissue-like structures. Natural extracellular matrices (ECMs), such as collagen, gelatin, laminin and fibronectin, promote cell attachment, survival, and growth. However, without extra-cross-linking, these materials are structurally very weak after in vitro processing, which greatly limits their potential use for guiding tissue regeneration [1]. In addition, ECMs without appropriate alignment may not offer directional guidance to attached cells. On the other hand, degradable electrospun nanofibers support cell attachment, and provide excellent directional guidance to the attached cell [2–5]. Like ECMs, individual degradable nanofibers are also very fragile and difficult to handle unless a relatively dense mat or dense bundle of nanofibers is formed. However, densely packed nanofibers provide a barrier for cell penetration inside the nanofiber bundles, especially in the case of aligned nanofibers, and thus preventing the use of 3D structures of aligned nanofibers as effective tissue engineering scaffolds. Interestingly, a combination of ECMs and loose degradable nanofiber arrays may help to address the weakness of each component as a scaffold. Nanofibers can offer directional cues to the ECMs, and also provide extra structural integrity with nanofiber reinforcement. ECMs can act as a substrate to immobilize individual nanofibers and serve as spacers among nanofibers, thus creating nanofiber arrays with loose nanofiber packing that also provides adequate structural integrity. Since ECMs may degrade very fast in the body, the resulting spaces will allow cells to populate into the space among

the nanofibers. To this end, degradable loose nanofibers were embedded in protein matrix in an attempt to fabricate a composite scaffold with improved properties; such as improved strength, guidance, spacing among nanofibers, etc. The goal of this study was to design a method of fabricating hybrid protein structures by combining degradable nanofibers and protein matrices. The model system tested was the electospun PCL nanofibers embedded into gelatin thin films and the properties of these hybrid structures were evaluated with mechanical testing and in vitro cell culture.

5.2. Materials and methods

5.2.1. Electrospinning

Polycaprolactone (PCL, Mn =80,000, Sigma, St. Louis, MO) was dissolved in dichloromethane and dimethylformamide (3:1) (DCM: DMF, Sigma) at a concentration of 18%wt/v. A hydrophobic cyanine dye, 1,1′-dioctadecyl-3,3,3′3′-tetramethylindocarbocyanine perchlorate (DiI, Invitrogen, Carlsbad, CA, USA), was added to the polymer solution at concentrations of 0.025 mg/ml to label the fabricated nanofibers. Polymer solution was feed by syringe pump (Medfusion 2010i; Smiths Medial Inc., Carlsbad, CA, USA) at a rate of 0.015 ml/min through a 23 G blunt tipped needle. A voltage of 8 KV was applied to the needle tip with a high voltage power supply (ES40P-10 W, Gamma High Voltage Research, Ormond Beach, FL, USA). The needle tip was held at 10 cm above a custom built collecting device designed in our lab to collect large loose arrays of parallel nanofibers across a rectangular rack [6]. This device utilized parallel mobile tracks that pulled electrostatically aligned electrospun fiber arrays into a secondary collection area at a vertical speed of 16.9 mm/s.

5.2.2. Composite film fabrication

Parallel electrospun nanofibers were collected continuously across a rectangular rack (Figure 5.1A) for 3 or 6 min. This fiber array was then transferred to a two-piece polycarbonate frame that was held together with screws (Figure 5.1B and C). Composite films were fabricated with two different fiber orientations: unidirectional straight fibers (Figure 5.2 A, C, and E) and bi-directional/criss-crossed fibers (Figure 5.2B, D, and F). During the fabrication of unidirectional composites, nanofibers were collected for 6 min first and transferred to a

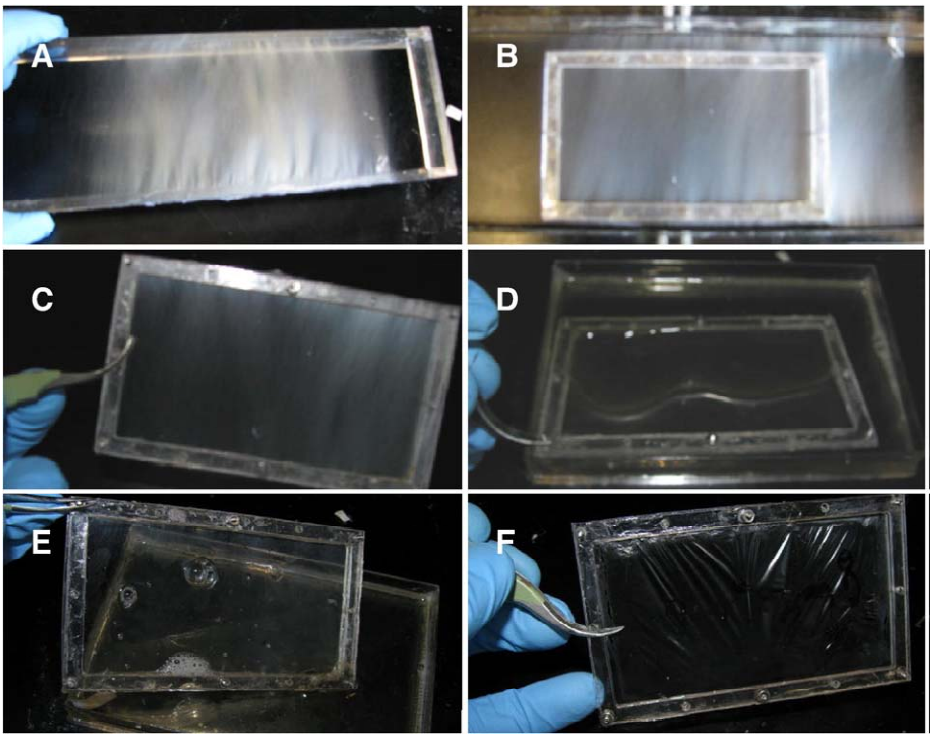

Figure: 5.1 Hybrid film fabrication: (A) PCL nanofibers on collecting rack (B) nanofiber array is transferred to smaller frame (C) nanofiber array inside of frame (D) nanofiber array is wetted in gelatin solution (E) nanofiber array is removed from gelatin solution and (F) dried hybrid film.

polycarbonate frame. For fabrication of bi-directional composites, nanofibers were collected twice for 3 min at two different directions and then transferred to the polycarbonate frame. The frames holding the nanofiber arrays were then coated in a 1 wt.% gelatin aqueous

solution (Bovine skin type B, Sigma, St. Louis, MO, USA) and allowed drying. Some of the composite films were cross-linked with 1-Ethyl-3-(3-dimethylaminopropyl) carbodimide (EDC, TCI America). All the films were sterilized with 75% ethanol.

5.2.3. Visualization

All SEM images were taken at 1000 to 5000 times magnification using a scanning electron microscope (SEM, Hitachi TM-1000). Samples were not sputter coated. In order to visualize the embedded fibers, the composite film edges were selected for taking pictures. All

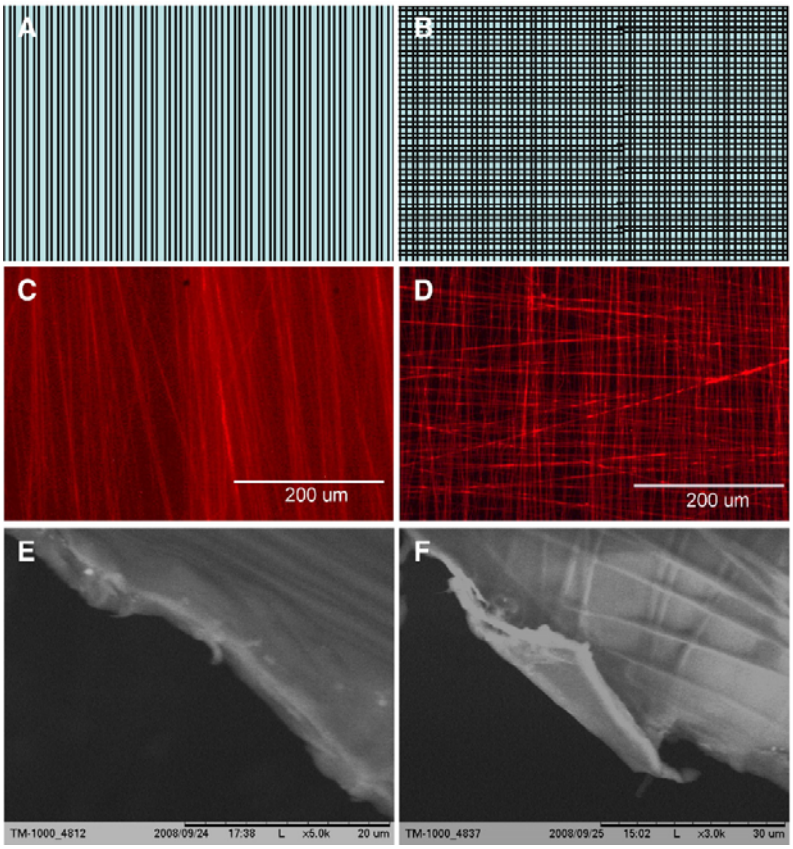

***Figure 5.2:** Hybrid gelatin/PCL nanofiber membranes: (A) Schematic of unidirectional aligned nanofiber reinforced protein membrane. (B) Schematic of criss-cross nanofiber reinforced protein membrane. (C) Fluorescent image of gelatin/PCL membrane. PCL fibers dyed with DiI in a unidirectional pattern. (D) Fluorescent image of gelatin/PCL membrane. PCL fibers dyed with DiI in a bi-directional pattern. (E) SEM image of gelatin/PCL membrane. PCL fibers are in a unidirectional pattern and (F) PCL fibers are in a bi-directional pattern.*

fluorescent and light microscope images were taken using a Nikon Eclipse TE2000-S microscope with an EXFO X-cite 120 fluorescence illumination system, and a Q-Imaging Micropublisher 3.3 RTV camera with Q-Capture software. ImagePro Plus 4.0 (Media Cybernetics Inc., Bethesda, MD, USA) was used to measure the average thickness of composite film samples using SEM images of the cross sections.

5.2.4. Mechanical testing

Mechanical properties of the hybrid PCL nanofiber reinforced gelatin films were characterized using both biaxial tensile testing and uniaxial tensile testing. Biaxial tensile testing was performed using a BioTester5000 Biaxial Test System (CellScale division of Waterloo Instruments Inc., Waterloo, Ontario, Canada) to examine the mechanical properties of the membrane samples in two directions. In brief, gelatin/PCL nanofiber based thin film (5 mm×5 mm) was attached with 20 tungsten finger grips (300 μm diameter, five on each side) and stretched in the nanofiber direction or perpendicular to the nanofiber direction in dry condition (Figure 5.3A). Each set of five finger grips was attached to an actuator, and load cells measured the force along the two pulling axes. The load cell used was 2500mN. The samples were sequentially tested with 3% strain, 5% stain and 7% strain and each stain rate was done in 20s. Uniaxial tensile testing was performed in a Shimadzu EZ Graph tensile tester (Nakagyo-ku, Kyoto, Japan) with Trapezium 2.32 software for data acquisition to examine the strength and stiffness of the thin films. SEM tape was adhered to both ends of 20mm×5mm rectangular strips of composite film and these were attached to the tensile tester's grips leaving an initial length of 10 mm of sample between the grips prior to elongation. The purpose of the tape was to limit stress concentrations on the thin films and to prevent slippage from the grips. A total of 20 samples were fabricated for mechanical testing,

with 5 samples for each of 4 groups: (1) Unidirectional (2) Bidirectional (3) Unidirectional+EDC and (4) Bi-directional+EDC. Strips were cut from the samples in the direction of the aligned fibers (90°) and perpendicular to the direction of the aligned fibers (180°). Strips cut from each sample were tensile tested in both directions under both wet and dry conditions. Under wet conditions the samples were secured in the grips of the tensile

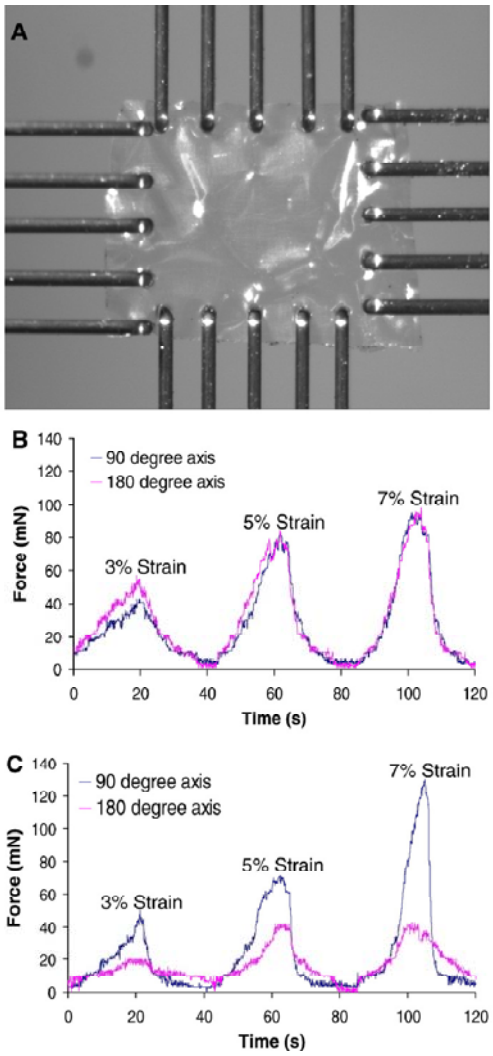

Figure 5.3: ***Biaxial tensile testing on hybrid gelatin membrane embedded with PCL degradable nanofiber arrays. (A) Example of a gelatin/PCL membrane mounted in the biaxial tester. (B) Gelatin membrane embedded with criss-crossed PCL fibers were tested at 3% strain, 5% strain and 7% strain condition. (C) Gelatin membrane embedded with unidirectional aligned PCL fibers were tested at 3% strain, 5% strain and 7% strain condition.***

tester and then hydrated. The elastic modulus, maximum stress, and elongation were measured from the stress strain curves. Statistical analysis was done using SPSS 15.0 software (SPSS Inc. Chicago, Illinois, USA). All p-values (p) were calculated using the Mann–Whitney test.

5.2.5. In vitro cell culture study

Circular pieces of unidirectional and bi-directional EDC cross-linked hybrid film with a diameter of 19mm were cut and placed at the bottom of 12 well cell culture plates. Half-inch sections of polycarbonate rod (Outer Diameter: 19mm, Inner Diameter: 13mm) were place on top of the films to hold them down. Sample wells were sterilized with 75% ethanol and 80,000 3T3 fibroblast cells were seeded on each sample and allowed to incubate for 3 days. Cells were fixed in 4% paraformaldehyde and stained with AlexaFluor 488 Phalloidin (Invitrogen) for the actin filament inside the cells and 4′-6-Diamidino-2-phenylindole (DAPI, Invitrogen) for the cell nuclei.

5.3. Results

5.3.1. Hybrid film fabrication

Thin gelatin/PCL degradable nanofiber hybrid films were fabricated using the techniques described above. The surface tension of the gelatin solution caused the formation of a thin film over both unidirectional and bi-directional nanofiber arrays. A thin hybrid film remained intact after drying. Fluorescent and SEM microscopy confirmed that the nanofibers remained embedded in the gelatin films in their original configurations (Figure 5.2C–F). The average thickness of the films was 2.73um with a standard deviation of 0.28. It was estimated from previously collected data that PCL fibers were approximately 585nm in diameter and

collected at a rate of approximately 0.05 fibers/um/min (data not shown), therefore the estimated volume fraction of PCL nanofibers embedded in the composite films was around 3% v/v. The volume fraction and the size of the nanofibers can be readily adjusted by controlling the nanofiber fabrication conditions and collecting time. Fabricated films demonstrated the strength and structural integrity for manipulation into complex shapes.

5.3.2. Mechanical testing

Results for biaxial testing in dry conditions can be observed in Figure 5.3A. Hybrid membranes reinforced with PCL nanofibers in crisscross pattern possessed similar mechanical properties in both 90^{o} and 180^{o} directions (Figure 5.3B). In contrast, membranes with PCL nanofibers in a unidirectional pattern had significant differences in strength in different directions (Figure 5.3C).

Uniaxial tensile testing was done in the 90° and 180° planes under both wet and dry conditions for samples that were uncrosslinked and cross-linked with EDC. The elastic modulus and failure strength for each set of conditions is displayed in Figure 5.4. Fiber orientation had significant effects on the strength of composite films for unidirectional samples with and without EDC in the dry and hydrated state. The elastic modulus of unidirectional hybrid films were 392% ($p = 0.05$), 231% ($p = 0.02$), and 164% ($p = 0.03$) higher in the direction of the aligned fibers for hydrated, hydrated+EDC, and dry films respectively. The failure strength of unidirectional hybrid films were 1265% ($p=0.05$), 437% ($p=0.03$), and 212% ($p=0.02$) higher in the direction of the aligned fibers for hydrated, hydrated+EDC, and dry films respectively. Composite films cross-linked with EDC were stronger than films without EDC cross-linking over all fiber orientations ($p< 0.05$). The elastic modulus of cross-linked films were 36% ($p=0.02$) higher in the dehydrated state, and 306% ($p< 0.01$) higher

when hydrated. The failure strength of cross-linked films were 86% ($p < 0.01$) higher in the dehydrated state, and 139% ($p = 0.01$) higher when hydrated.

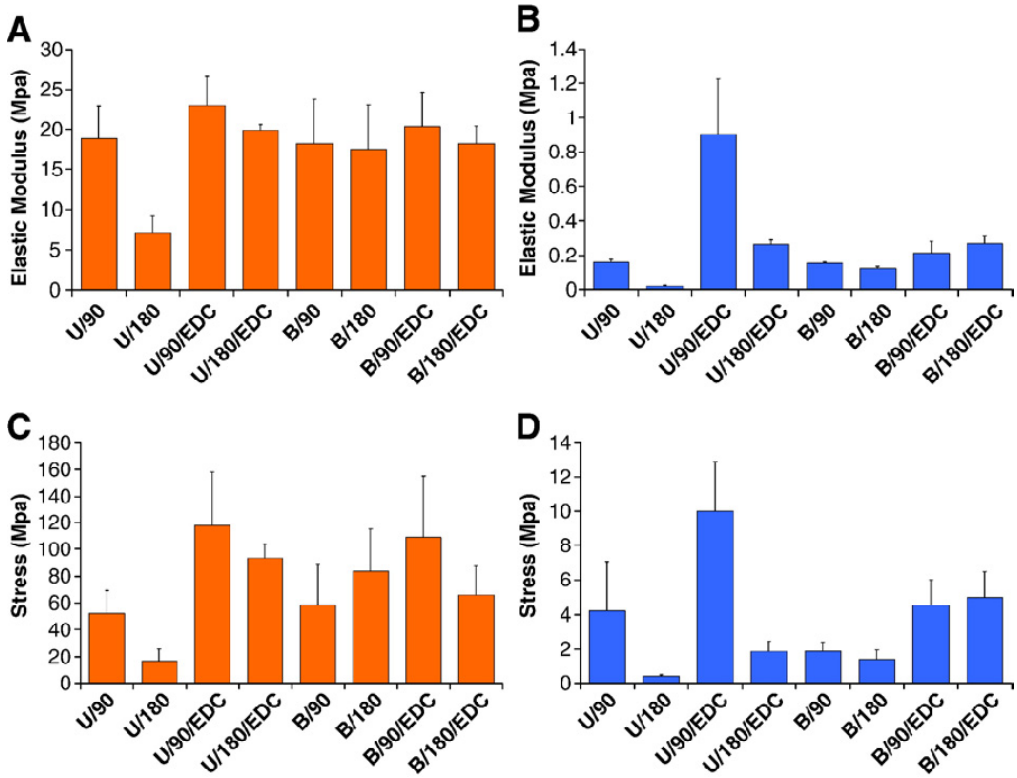

Figure 5.4: Elastic modulus of samples tested under (A) dry and (B) wet conditions and failure stress of samples tested under (C) dry and (D) wet conditions: U=unidirectional sample, B=bi-directional sample, 90=force applied in the direction of aligned fibers, 180=force applied perpendicular to aligned fibers, EDC=cross-linked sample.

5.3.3. In vitro cell culture study

PCL nanofiber/gelatin hybrid thin films maintained their integrity under cell culture conditions and promoted the attachment of 3T3 fibroblast cells. Since the membrane is very thin, cells were able to sense the embedded PCL nanofibers. Fibroblast cells on composite films containing bi-directional nanofibers adopted a somewhat random orientation, although it appeared that some cells may have oriented in the criss-crossed pattern of the fibers (Figure 5.5A). Fibroblast cells on composite films containing unidirectional nanofibers however, clearly elongated in the direction of the aligned nanofibers (Figure 5.5B).

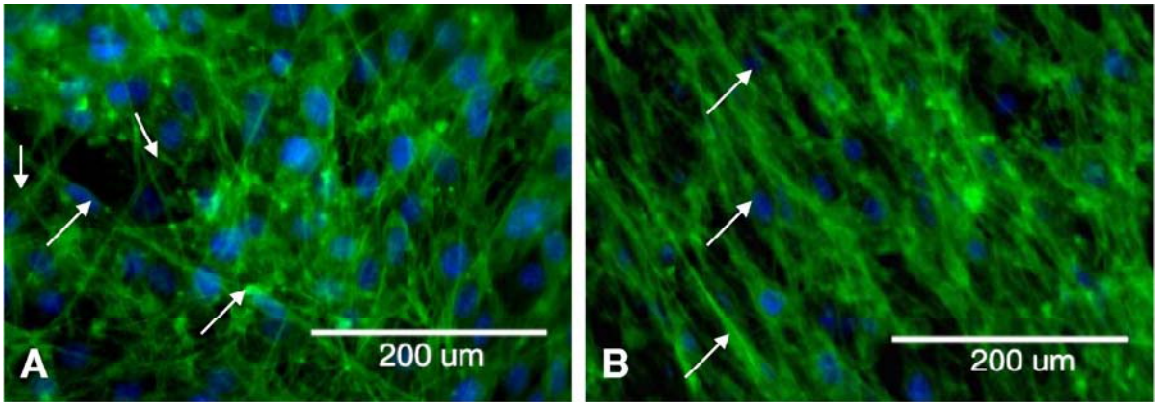

Figure 5.5: 3T3 fibroblasts grown on gelatin/PCL nanofiber composites with (A) bi-directional and (B) unidirectional fiber orientations.

5.4. Discussion

Extracellular matrix proteins, such as collagen, gelatin, laminin, fibronectin, etc. have favorable properties as tissue engineering scaffolds. Because most of these materials are naturally found in the body, they promote cell attachment, survival and growth and are fully biodegradable. The concern about the immunogenicity can be overcome by using human recombinant ECM molecules. Unfortunately natural ECMs are mechanically weak after in vitro manipulation, which limits their practicality as tissue engineering scaffolds. Structural weakness not only limits these proteins as coating materials or applications in non-load bearing environment, but it also makes them very difficult to handle and manipulate in the fabrication, processing, and implantation steps.

Degradable polymer nanofibers exhibit many properties that make it an excellent substrate to add to protein matrices to construct hybrid structures with improved structural properties. Nanofibers mimic the size and structure of the natural guidance cues and therefore provide physical guidance for tissue regeneration, which is critical for regenerating aligned tissues such as nerve, tendon/ligament, or muscle tissue. Nanofibers can provide mechanical strength due to their high surface area to volume ratio and act as a barrier to crack

propagation because of their long continuous length.

The combination of polymer nanofibers with gelatin in a hybrid membrane expands the versatility of both of these promising materials or structures. The addition of as low as 3% v/v PCL nanofibers improved the strength of gelatin film in the direction of unidirectional aligned fibers when compared to the strength in the direction perpendicular to the fibers, especially for hydrated samples. It could be hypothesized that addition of a greater percentage of nanofibers could strengthen protein matrices much further. And furthermore, chemical modification of the nanofiber surface to promote the covalent bonding between nanofibers and protein matrix will further improve the mechanical properties of the composite structures. These hybrid structures also address one of the greatest limitations of nanofibers as a scaffolding material. Nanofibers are very difficult to handle, process and implant into the body, and in addition, the tendency of forming dense nanofiber mats greatly limits cell population inside the nanofiber structure. The protein matrix in hybrid structures allows the fabrication of scaffolds containing loose nanofiber arrays with sufficient space for cell growth inside the nanofiber bundles, which can provide directional guidance without obstructing cell penetration.

The fabrication techniques used to manufacture these composite films is readily adaptable for scale up and use in a Good Manufacturing Practices (GMP) fabrication facility for human tissue regeneration applications. Because the films were fabricated in atmospheric conditions there is no need to remove them from any substrate and they can be easily handled and manipulated. Complex two and three-dimensional structures assembled from dry composite films become gelatinous scaffolds once again upon rehydration, and thus this material may be a versatile tool in the fabrication of tissue engineering scaffolds.

5.5. Conclusions

A method for fabricating nanofiber and protein hybrid thin membranes was developed. Hybrid membranes could be fabricated with a relatively consistent thickness between 2 and 4um. The hybrid films were structurally robust enough for handling and manipulation into complex structures. Hybrid membranes could be fabricated with unidirectional and bi-directional embedded fibers, and cross-linking with EDC strengthened the films significantly. Increased strength of films in the direction of unidirectional nanofibers suggests that an embedded volume fraction of PCL nanofibers as low as 3% can improve the mechanical properties of gelatin significantly. In vitro culture of fibroblasts confirmed that these composite films supported cell attachment, survival, and growth, and that embedded nanofibers could provide directional guidance to cells growing on the hybrid membranes. It was shown that nanofibers and protein matrices can be easily combined into a composite structure that has improved properties as a tissue engineering scaffold when compared to either component alone. This versatile technique can be used to develop tissue scaffolds that are biodegradable and biocompatible; promote cell attachment, survival, and growth; provide directional guidance; and possess the structural stability required for practical handling. Studies in progress are evaluating direct cell loading into the hybrid membrane and the use of nanofiber reinforced protein structures for engineering blood vessel, skeletal muscle, tendon/ligament and nervous tissue.

5.6 References

[1] Wang X, Li X, Yost MJ. Microtensile testing of collagen fibril for cardiovascular tissue engineering J. Biomed. Mater. Res. A 2005;74(2):263-8.

[2] Chua KN, Chai C, Lee PC, Tang YN, Ramakrishna S, Leong KW, Mao HQ. Surface-aminated electrospun nanofibers enhance adhesion and expansion of human umbilical cord blood hematopoietic stem/progenitor cells. Biomaterials 2006;27(36):6043-51.

[3] Nur-E-Kamal A, Ahmed I, Kamal J, Schindler M, Meiners S. Three-dimensional nanofibrillar surfaces promote self-renewal in mouse embryonic stem cells. Stem Cells 2006;24(2):426-33.

[4] Schnell E, Klinkhammer K, Balzer S, Brook G, Klee D, Dalton P, Mey J. Guidance of glial cell migration and axonal growth on electrospun nanofibers of poly-e-caprolaction and a collagen/poly-e-caprolactone blend. Biomaterials 2007;28(19):3012-25.

[5] Yang F, Murugan R, Wang S, Ramakrishna S. Electrospinning of nano/micro scale poly(L-lactic acid) aligned fibers and their potential in neural tissue engineering. Biomaterials 2005;26(15):2603-10.

[6] Beachley, V. and X. Wen, Fabrication of three dimensional aligned nanofiber array, US-7828539, 2010. Clemson University (Clemson, SC, US).

CHAPTER 6

6. A NOVEL FABRICATION TECHNOLOGY FOR CREATING NANOFIBER COMPOSITES THAT MIMIC THE MICROSTRUCTURE AND MECHANICAL PROPERITES OF NATURAL BLOOD VESSELS

6.1 Introduction

Cardiovascular disease causes more fatalities in the United States than any other disease [1]. Highly diseased coronary artery and peripheral vessels must be repaired or replaced to restore healthy blood flow patterns. Current treatments for occluded vessels are limited by low patency rates in small diameter (<6 mm) vessels and in addition, the use of autologous grafts is limited by the lack of adequate donor tissue in many patients [2,3]. There exists a great need for a small diameter synthetic vascular graft with improved long-term patency. Failure of synthetic grafts is brought about by one of three primary mechanisms: thrombosis due to the lack of an adequate endothelium; restenosis brought about by inflammatory responses and compliance mismatch; and infection [4]. An engineered vascular graft must be made from biocompatible materials with a lumen that promotes strong endothelial cell attachment and with mechanical properties that closely match those of natural tissue.

The technology to fabricate blood compatible vascular grafts through the use of biocompatible materials and surface modification of the graft is well established. The other critical factor for achieving graft patency is that the mechanical properties match with natural vessels. The property of 'compliance' is commonly used when comparing the mechanical properties of vessel grafts to natural vascular tissue. Compliance describes how the mechanical properties of a vessel or graft change depending on the internal hemodynamic pressure (and thus distention). It is reported that compliance mismatch between vessel grafts and surrounding the vasculature causes intimal hyperplasia or aneurysm and that poor vessel

graft patency may be the result of turbulent flow brought about by compliance mismatch [5,6]. Hemodynamic flow variations arise due to the compliance mismatch of vascular grafts [7] and cause areas of both increased shear stress, which damages the endothelium, and decreased shear stress [8], which leads areas of stagnation, pooling of chemokine factors [9], and increased platelet interactions and oscillatory forces [10]. It is therefore paramount that the structure of such a graft be designed to replicate the mechanical properties of the native artery as closely as possible to maximize patency [11]. Mechanical property mismatches can also cause increased stress concentrations at the anastomosis of a graft and the surrounding vasculature. Stress concentrations can bring about remodeling that leads to intimal thickening and eventual graft failure.

Natural blood vessels are composite structures with complex mechanical properties, and mimicking these properties may be the most challenging aspect of designing a synthetic vascular graft. Blood vessels do not exhibit a linear stress-strain curve in the circumferential direction. Instead they exhibit a non-linear 'J-shaped' stress-strain curve, which has a relatively elastic region at low values of vessel distension (less than 140-160% of initial radius) that transitions into a relatively stiff region as distension increases [11-14] (Figure 6.1). This type of dual stress-strain behavior is a necessity in the vascular system because of physiological requirements. Blood vessels must be elastic in order to provide pulse smoothing and capacitance, but they must also have the stiffness required to provide a stable geometry over a wide variety of pressures.

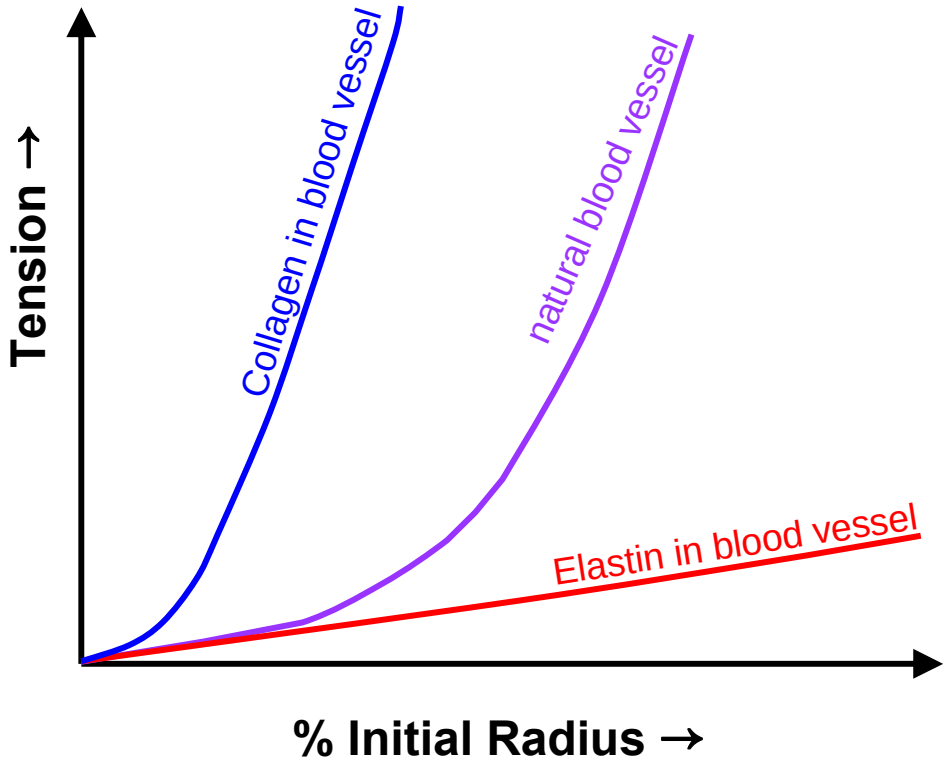

Figure 6.1: Schematics of stress-strain profile of natural blood vessels (purple curve), collagen fibers remaining (blue curve; Trypsin was used to digest elastin from natural blood vessel), and elastin fibers remaining (red curve; Formic-acid was used to digest collagen from natural blood vessel) (Modified from [13])

Several studies have shown that the collagen and elastin fiber components of blood vessels are associated with the two regions of the J-shaped stress-strain curve (Figure 6.1) [13, 15]. In the natural blood vessel, collagen fibers have a wavy or helical orientation at mean physiological pressure [16] (Figure 6.2a,b,c). Because these bundles of collagen fibers do not appear to be taut at lower values of vessel distention, they may offer little resistance to expansion until the vessel wall is distended enough to fully straighten them [17]. This mechanism would allow the mechanical properties of the blood vessel to exhibit elastin dominated elastic behavior at low levels of vessel distention and collagen dominated stiff behavior at high levels of vessel distention as seen in the J-shaped stress-strain curve. At low

levels of pressure and thus distension, the highly elastic elastin fibers dominate the vessels mechanical properties. As pressure and thus distension increase, progressive recruitment of relatively inelastic collagen fibers bring about collagen dominated vessel mechanical properties. The geometry of the fibrous microstructure in blood vessels could be the mechanism that allows collagen to provide stiffness at high levels of distention without compromising elasticity at low levels of distention. Therefore, we hypothesize that a fibrous graft with components designed to mimic the mechanical properties and microstructure of elastin and collagen fibers in natural vessels will exhibit bulk mechanical properties similar to natural blood vessels.

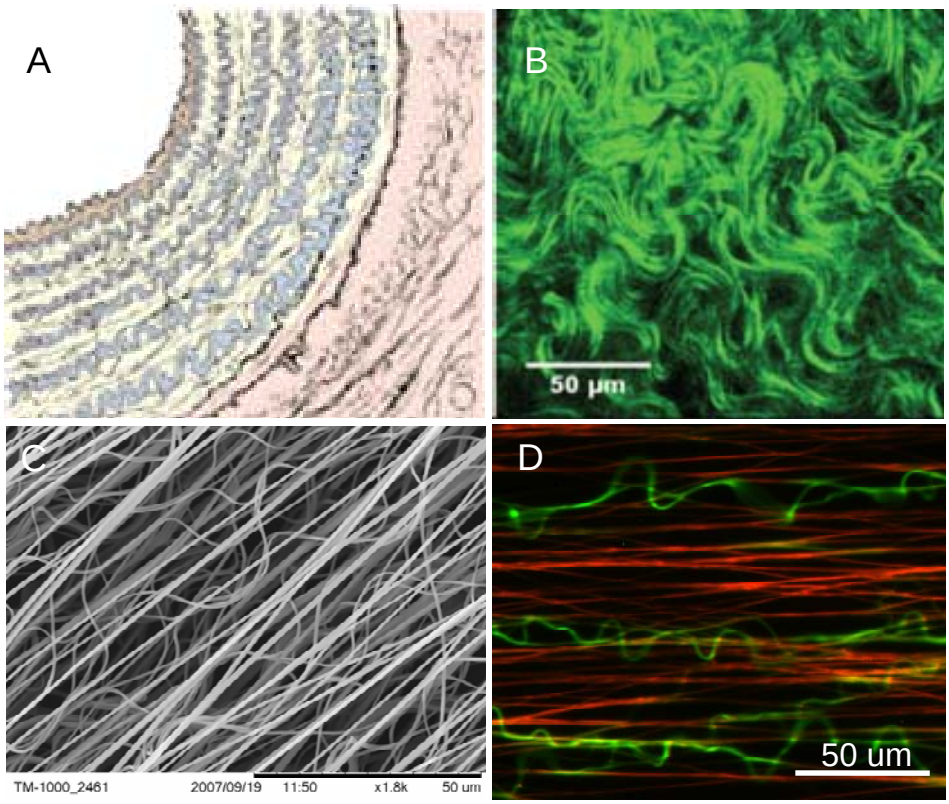

Figure 6.2: Schematic (A) and fluorescent (B) images of collagen fiber microstructure in natural vessels. SEM (C) and fluorescent (D) images of straight/PU – wavy/PCL nanofiber composites. PU fibers are dyed red with DiI and PCL fibers are dyed green with DiO.

The suitability of polymer nanofibers as a vascular implant material has been previously investigated. A wide range of polymer materials are available and the properties of polymers can be specifically tailored for applications to a certain extent. Because of this, a material based on polymer fibers offers great flexibility for optimization throughout the design process. Some types of polymers such as polyurethane (PU), polycaprolactone (PCL), and poly(DL-lactide-co-glycolide) (PLGA) have shown excellent biocompatibility when used as implants [18-20]. Polymer nanofibers have several properties that make them excellent scaffolding structures when compared to larger polymer fibers. Because of their small size, nanofibers are recognized by cells, which align in the direction of aligned nanofibers [19, 21]. Polymer nanofibers have also been shown to support cell attachment [22, 23]. In addition, drugs and proteins that can be directly incorporated into electrospun nanofibers and retain bioactivity and exhibit extended release kinetics [24-26]. Several groups have fabricated tubular vascular grafts from electrospun nanofibers, but these materials did not closely match the mechanical properties of natural blood vessel tissue [18, 27].

The goal of this study was to develop a technology to fabricate a polymer composite graft, with similar compliance to natural vessels, by mimicking the mechanical properties and microstructure of the elastin and collagen fibers found in native tissue.

6.2 Materials and Methods

6.2.1 Electrospinning

Polycaprolactone (PCL Mn=80,000, Sigma, St Luois, MO), polyurethane (PU, Tecoflex SG-80A, Noveon, Cleveland, OH), Poly(L-lactide) (PLLA, L2095, Boehringer Ingelheim, Ingelheim Germany),and P(DL-lactide-co-glycolide) (PLGA 85:15, LACTEL, Cupertino, CA) were electrospun from polymer solvent solutions. PU was dissolved in hexafluoro-2-propanol (HFIP, Oakwood, West Columbia, SC) at 8% wt/v and PLLA was dissolved in HFIP at 7% wt/v. PCL was dissolved in dichloromethane:dimethylformamide (3:1) (DCM:DMF, Sigma) at a concentrations of 18% wt/v and PLGA was dissolved in 3:1 DCM:DMF at 30% wt/v. Polymer solution was feed by a syringe pump (Medfusion 2010i; Smiths Medial Inc., Carlsbad, CA, USA) at feed rates of 0.015 ml/min for PU and PLLA, and 0.10ml/min for PLGA and PCL, through 1/16" polyethylene tubing into a 23g blunt tipped needle (Smallparts, Miramar, FL). A voltage of 8kV was applied to the needle tip with a high voltage power supply (ES40P-10W, Gamma High Voltage Research, Ormond Beach, FL). The needle tip was held at 10 cm above a custom build collecting device. In cases where nanofibers were stained, DiI or DiO (, Invitrogen, Carlsbad, CA) was added to the polymer solution at a concentration of 0.025 mg/ml.

6.2.2 Composite fiber mat assembly

Two fabrication processes with the same principle were used to fabricate the vascular grafts. In one method, custom build device designed in our laboratory [28] was used to collect 9 cm long parallel-aligned nanofibers and deposit them across an adjustable rectangular rack. This device utilized two parallel mobile tracks to collect aligned fiber arrays and pull them down

to a secondary collecting area at a vertical speed of 10mm/second. Composite fiber mats were constructed using a stepwise procedure (Figure 6.3). First a layer of elastic PU fibers was collected across the adjustable rack at a length and then elastic PU fibers were stretched. Stiffer polymer fibers (PCL, PLA, or DL-PLG) were then deposited on top of the PU fibers and the rack was relaxed back to its original width. This process could be repeated for multilayer mats.

In the second method, a rotating mandrel was used to collect aligned elastic PU fibers. Mandrel diameter was increased to stretch the PU fibers and stiffer aligned polymer fibers (PCL, PLA, or DL-PLG) were then deposited on top of the PU fibers. The diameter was then relaxed back to its original width. This second method could also be repeated for multilayer mats

In order to investigate the effect of the 'compression' distance (ΔD in Figure 6.3) of the stiff fibers, PCL fibers were collected, by the method described above on top of a layer of 4 cm PU fibers that were stretched to a distance of 6.25, 5.25, or 4cm before relaxation back to 4cm (ΔD = 2.25, 1.25, 0 respectively from Figure 6.3). A theoretical schematic of the effect of 'compression' distance on composite mat microstructure is shown in Figure 6.3 (a-c).

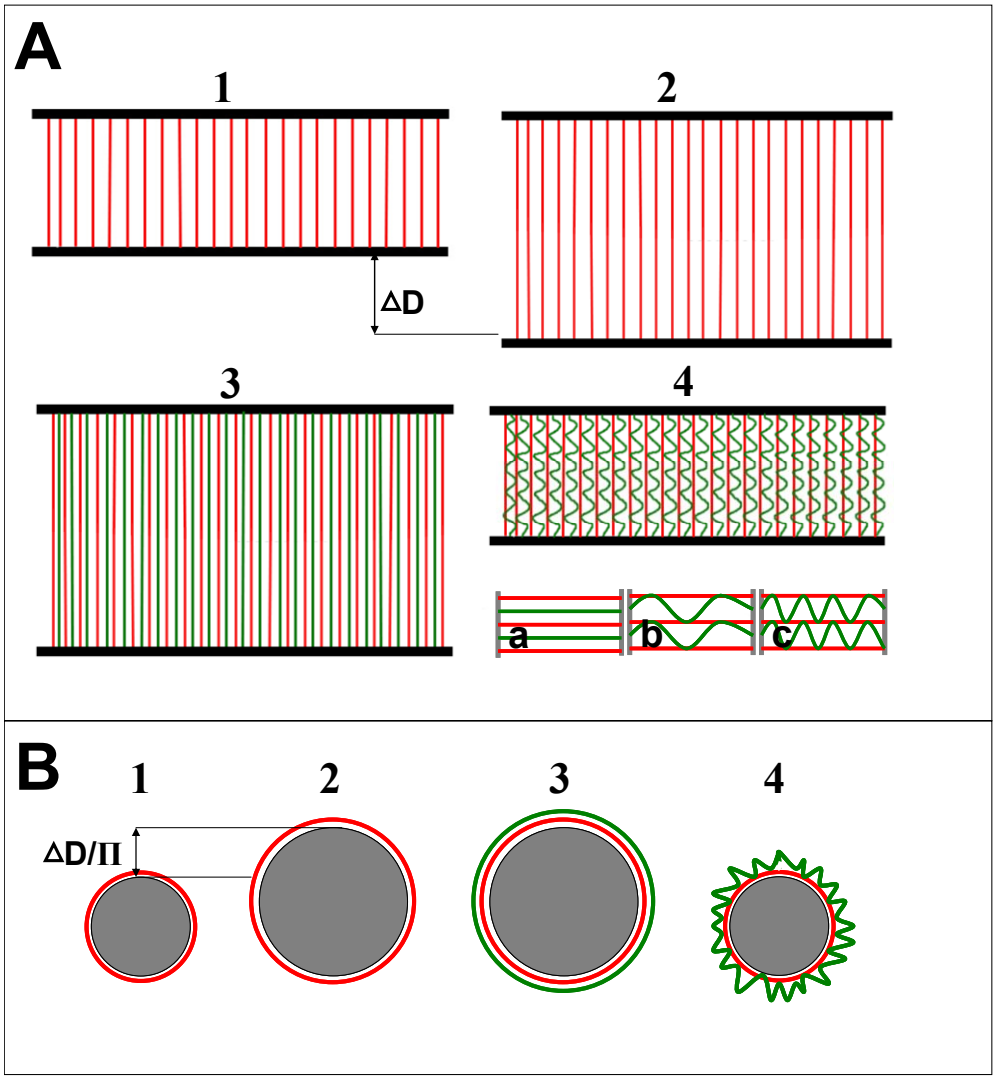

Figure 6.3: Fabrication of straight-elastic/wavy-stiff nanofiber composites. Elastic fibers (PU in red) were collected either (A) across a rack or (B) around a mandrel (1) and stretched distance ΔD (2). Stiff fibers (PCL in green) were collected on top of elastic PU fibers (3) and pulled into a wavy orientation by elastic PU fibers upon relaxation back to their original length (4). A schematic of PCL fiber orientation for composites with increasing ΔD is shown in figures a-c.

In order to investigate the effect of the ratio of elastic to stiff fibers, PU-PCL composite fiber mats with varied PU and PCL collection times were fabricated. Three groups of composite mats were fabricated with PU:PCL collection times of 15:5, 10:10, and 5:15 minutes, where an estimated 3000 PCL fibers (diameter = 600nm) or 600 PU fibers (diameter = 1200nm) were collected in a 5 minute time period.

6.2.3 Mechanical Testing

To prepare the samples for mechanical testing, the first fabrication method was used. Samples of composite mat were mounted in 1x1cm sections on rectangular paper frames. Samples were clamped into a Bose 3220 tensile testing machine with a 22N load cell with the aligned PU fibers in the direction of the applied force. Prior to testing, the two sides of the paper frame were carefully cut, so that they did not offer any resistance, and the load was zeroed. Samples were pulled at 0.05mm/second and data was collected at a rate of 13 points per second. Stress-strain curves were calculated from the force displacement data recorded by Bose WinTest software. For stress calculations, the cross sectional area of each sample was determined by multiplying the estimated number of fibers in the sample by the estimated cross-sectional area of each fiber. In order to estimate the number of fibers per sample, PU and PCL fibers were collected for 5 minutes under the exact conditions used in composite mat fabrication. The resulting aligned fiber array was transferred onto an electron microscope stub and the average fiber diameter and the rate of fiber collection (fibers/um/min) was determined using Image Pro Plus 4.0.

After the stress-strain data was calculated, a one hundred point moving average was applied to smooth the curve. Elastic moduli were calculated using points from linear regions of the stress-strain curve. A one hundred point moving average of the first and second derivative were also calculated and plotted. The local maximum of the second derivative in the region of the 'elastic to stiff' transition point was used as a quantitative representation of the location of the transition region. The stress-strain curve of straight fiber composites immediately exhibited stiff behavior and was therefore given a quantitative value of zero for the 'elastic to stiff' transition point.

6.2.4 Microscopy

All samples imaged using scanning electron microscopy (SEM) were sputter coated with gold at a thickness of 50-70 nm using a Cressington 108 AUTO sputter-coater with a current of 30 mA for 2 minutes. Images of the samples were taken at 500 to 10,000 times magnification using an SEM (Hitachi TM-1000). Fluorescent and light microscope images were taken using a Nikon Eclipse TE2000-S microscope with an EXFO X-cite 120 fluorescence illumination system, and a Q-Imaging Micropublisher 3.3 RTV camera with Q-Capture software.

6.2.5 Cell culture

Rat Smooth Muscle Cells (ATCC# CRL-1444) and adult rat aortic endothelial cells (RAEC, passage 6–8; Cell Applications, San Diego, CA) were cultured on bare culture plate or on coated or uncoated glass slides using 12 well culture dishes. Glass slides were coated with PU film, PCL film, or PU/PCL nanofiber composite. Alamar blue (Serotec) assay was used to determine cell viability and proliferation at days 1, 2, 4, and 7 using an absorbance plate reader (Spectra max 384 Plus, Molecular Devices). At day 7, cells were fixed in 4% paraformaldehyde and stained with AlexaFluor 488 or 543 Phalloidin (Invitrogen) for the actin filament inside the cells and 4'-6-Diamidino-2-phenylindole (DAPI, Invitrogen) for the cell nuclei.

6.2.6 Statistical Analysis

Statistical analysis was performed using SPSS 15.0 version software. The Kruskal Wallis test was used to compare mechanical properties obtained from the stress-strain curves using 5 samples per group. Students-t-test was used for analysis of Alamar blue metabolic assay.

6.3 Results

6.3.1 Composite mat microstructure

With our novel fabrication technology, elastic polyurethane (PU) fibers were used as model structure to mimic elastin fibers which remained straight and aligned, while polycaprolactone (PCL) fibers were used to mimic collagen fibers adopted a wavy aligned orientation. Figure 6.2 (C and D) shows the straight-wavy aligned microstructure of a PU-PCL composite mat. It was confirmed by fluorescent microscopy that the elastic PU fibers in red remained straight while PCL fibers in green adopted a wavy orientation.

6.3.2 Mechanical behavior

6.3.2.1 Stress-strain curve

Composite grafts with a straight-wavy microstructure adopted a J-shaped stress-strain behavior, while composite grafts without wavy microstructure did not (Figures 6.4, 6.6a).

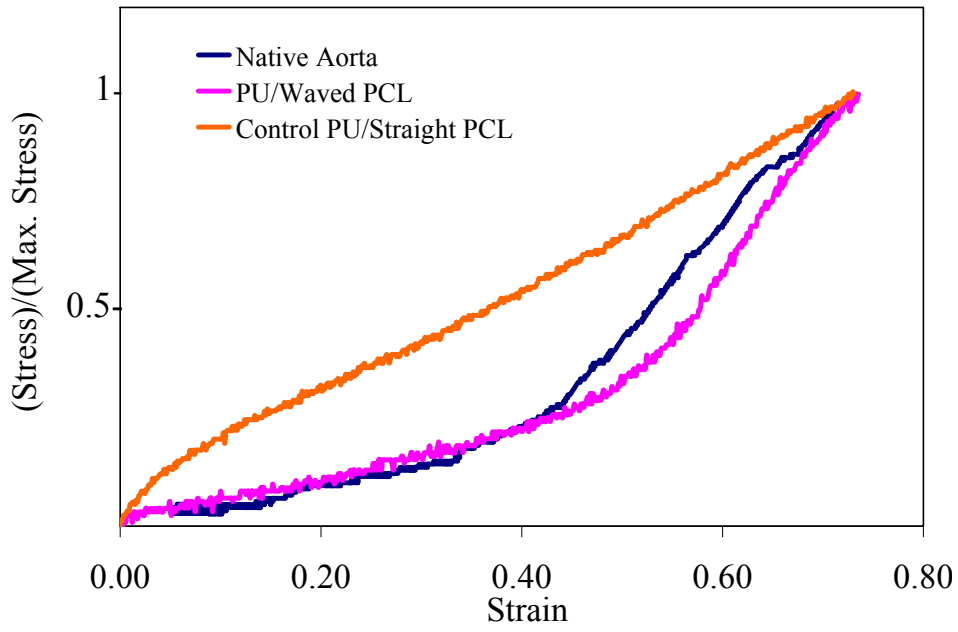

Figure 6.4: Normalized stress-strain curves of PU/PCL composites and native aorta tissue

Straight-wavy composite graft displayed an initial region with a low elastic modulus that transitioned into a secondary region of high elastic modulus, while control straight fiber composites graft displayed an initial high slope region that transitioned into a low slope region. Stress-strain curves of straight-wavy and control straight fiber composites plotted against native aorta tissue (Figure 6.4) confirm that straight-wavy fiber composites display mechanical behavior similar to natural blood vessel tissue. Stress values for the three curves in Figure 6.4 were normalized by dividing all values of stress by the maximum stress. Normalization allows comparison of the shapes of the stress-strain curves, independent of the stress differences. It was confirmed that the location of the elastic-to-stiff region on the stress-strain curve for straight/wavy composites corresponded with the straightening of the stiff PCL fibers (Figure 6.5).

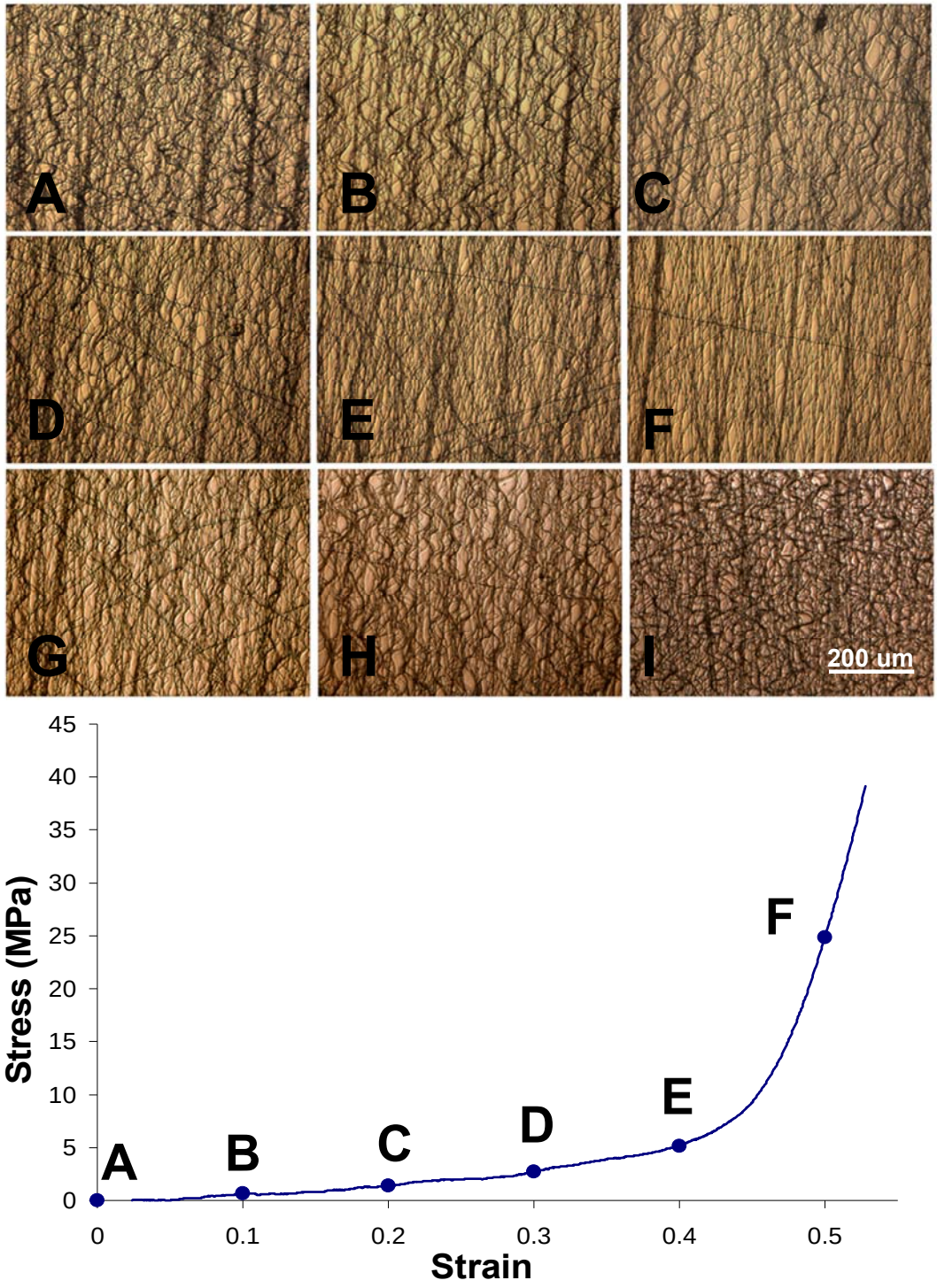

Figure 6.5: A PU-PCL composite fiber mat stretched to a strain of: 0, 0.1, 0.2, 0.3, 0.4, 0.5, and then relaxed to 0.3, 0.1, and 0 (A-I respectively)

6.3.2.2 Transition point location shift

PU-PCL composite fiber grafts that were fabricated with different degrees of rack extension (ΔD from Figure 6.3) resulted in composite fiber mats with different degrees of PCL 'compression'. PCL fibers were collected on top of PU fibers with extension of ΔD=56%, 31%, and 0%, and they were pulled into a wavy orientation by the elastic PU fibers upon relaxation back to ΔD=0. The average 'elastic to stiff' transition point on the stress-strain curve was 0.38, 0.17, and 0 (σ = 0.05, 0.06, 0 respectively) for the extension of ΔD=56%, 31%, and 0% respectively. It was found that the transition point was significantly shifted to the right of the stress-strain curve according to the degree of PCL compression ($p<.01$) (Figure 6.6a).

6.3.2.3 Curve shape

PU-PCL composite fiber mats were fabricated with different material composition ratios. The stress-strain curves of three groups with PU:PCL collection times of 15:5, 10:10, and 5:15 were compared. The shape of the curve was quantitatively calculated as the ratio of the slope of the initial and secondary linear regions of the stress-strain curve. The ratio of these two elastic modulus were 3.2, 6.5, and 8.8 MPa (σ = 0.9, 1.7, 2.4 MPa respectively) for PU:PCL collection times of 15:5, 10:10, and 5:15 min respectively. The difference in elastic modulus ratio according to PU:PCL collection times was significant ($p<.01$) and its relation to curve shape is displayed in (Figure 6.6b).

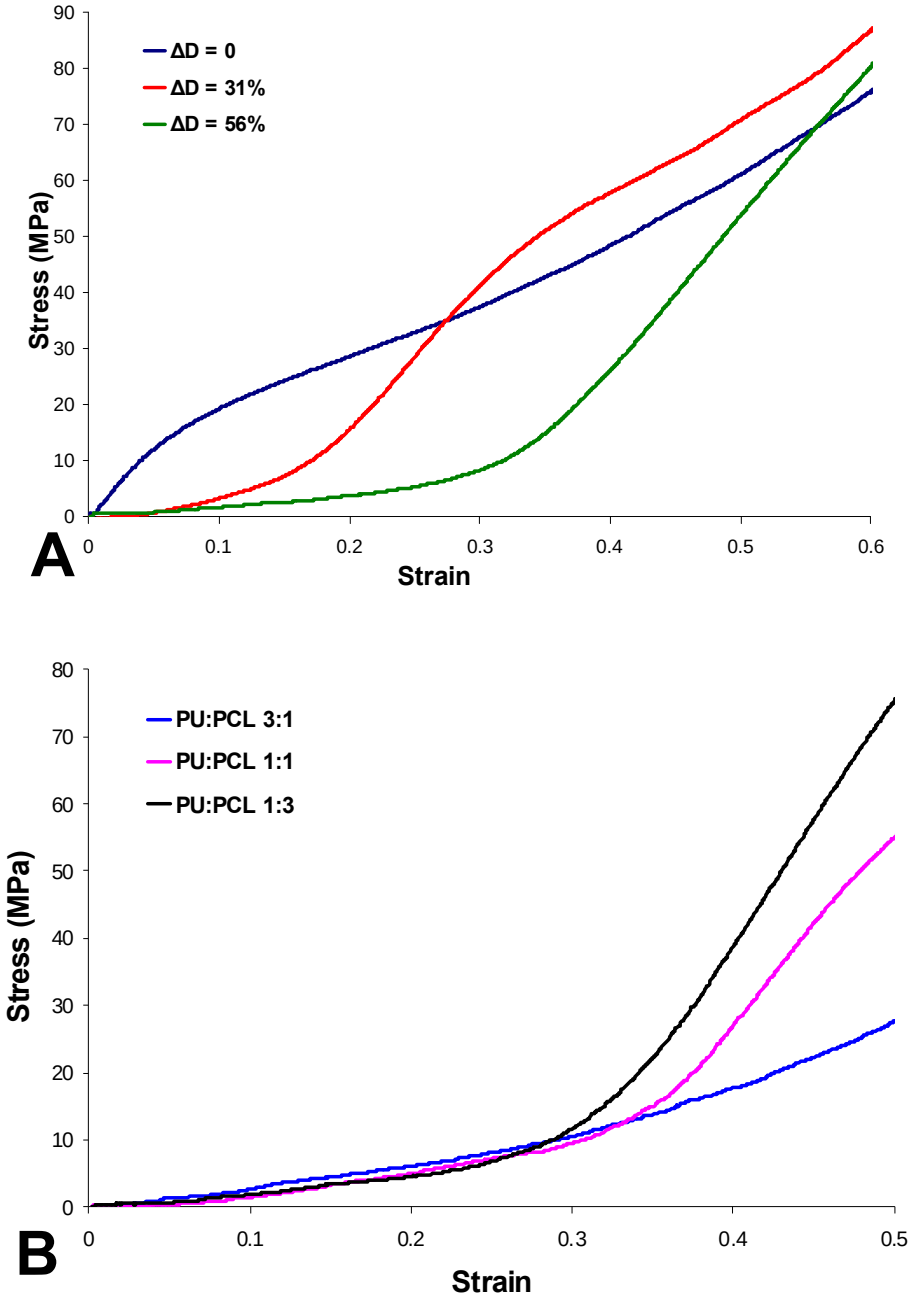

Figure 6.6: Stress-strain curves for PU-PCL composites with (A) varied PU expansion rate (ΔD in Figure 2) and (B) varied PU to PCL fiber ratios

6.3.2.4 Cyclic Loading

It is essential that any material used as a vascular graft is able to maintain its integrity under cyclic loading. It was determined that the stress-strain curve of electrospun PU fibers fabricated by our protocol are weakened after the first cycle and then maintain a consistent stress-strain behavior for subsequent cycles. A stress-strain curve of a straight PU-PCL composite was tested under cyclic loading and it was found that the stress-strain curve had some weakening in the elastic region after the first cycle, and consistent mechanical behavior for subsequent cycles (Figure 6.7). Visual inspection confirmed that the unique microstructure of these composite grafts returned to its initial state after loading and subsequent relaxation (Figure 6.5).

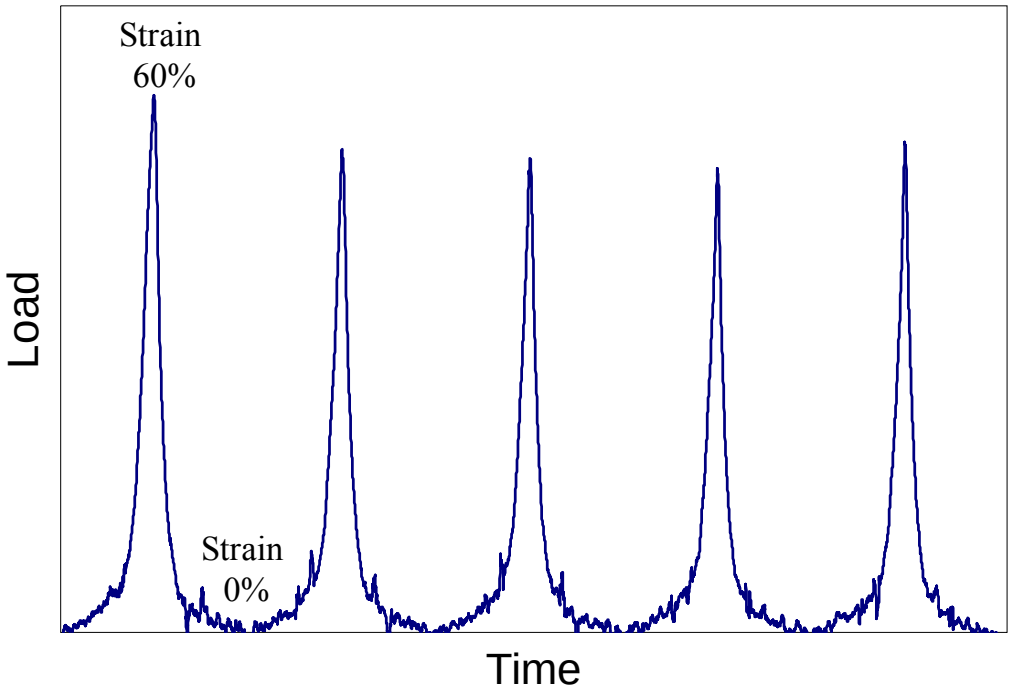

Figure 6.7: Straight-PU/Wavy/PCL composite fiber mat loaded from 0 to 60% strain at 0.05mm/s.

6.3.3 In vitro

Cell viability and proliferation were analyzed using the Alamar Blue metabolic assay. The metabolic activity of smooth muscle cells and endothelial cells grown on PU-PCL fiber composite graft was compared to that of cells grown on PU film, PCL film, and glass on days 1, 2, 4, and 7 of culture. Endothelial cells (ECs) and smooth muscle cells (SMCs) grown on fiber mats had higher metabolic scores than cells grown on PU-PCL films for all time points, but the increase reached significance only in endothelial cell culture on day 7 ($p<0.05$). Both smooth muscle cells and endothelial cells adopted an aligned morphology in the direction of the aligned PU fibers when grown on composite fiber mats, but not on the films. (Figure 6.8 a,b,c & d).

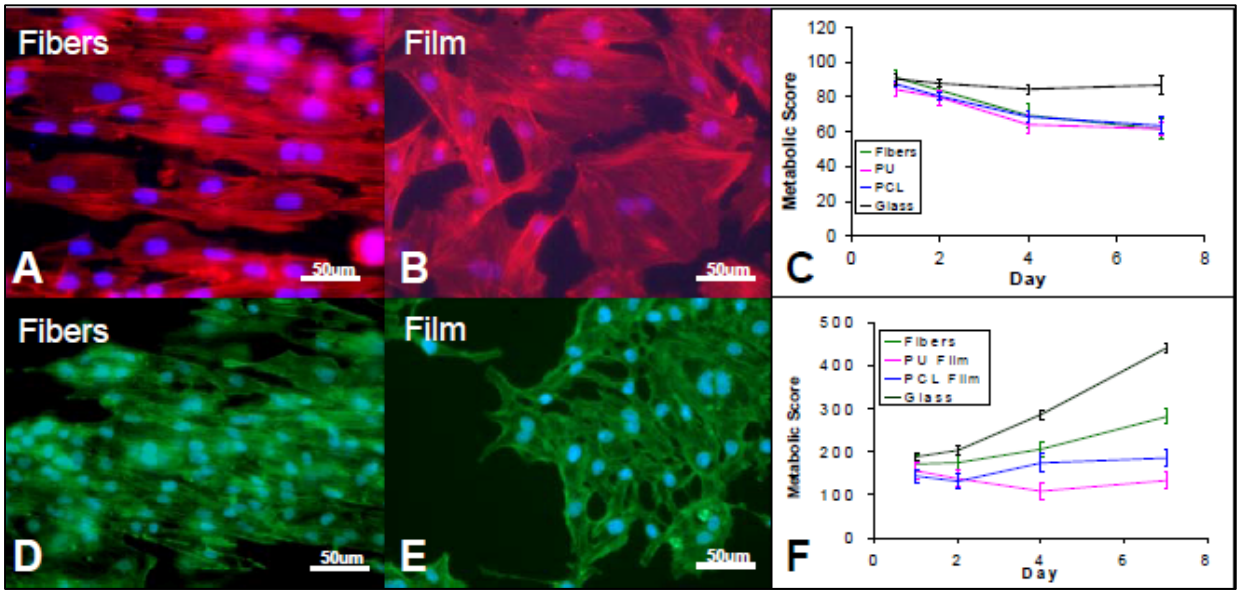

Figure 6.8: SMCs (A,B) and endothelial cells (C,D) cultured on PU-PCL fiber composites (A,D) and PCL films (B,E). The alamar blue metabolic score of SMCs versus cells cultured on well plate control are displayed in C, and the alamar blue metabolic scores of endothelial cells versus no cell control wells are displayed in D.

6.4 Discussion

According to 2008 estimates of the American Heart Association, the US health care system will incur over $448.5 billion in costs for treatment and management of cardiovascular disease [29]. Treatment for the most severe cases requires mechanical repair or replacement of diseased vessels. Stenting, the most common repair strategy, is an adequate short term solution in some cases, but faces may limitations such as restenosis, platelet activation, and vessel wall damage [30, 31]. While stenting comprises 70-90% of revascularization procedures, restensosis rates of 20-30% are still seen up to 6 months after surgery in small diameter (<5mm) vessels [32, 33]. The gold standard replacement strategy, autologous vein transplant, also faces severe limitations. Venous tissue is structurally different from arterial tissue and this is reflected in mechanical properties mismatches that lead to restenosis. In addition, healthy vein tissue in diseased subjects is often unavailable, especially in repeated procedures, and there is morbidity and cost associated with the harvesting procedure. While synthetic grafts are currently available, these grafts do not match the compliance of natural vessels and they are less effective that vein transplants. The patency of rates of polytetrafluorethyle (ePTFE) or Dacron grafts when used for infrapopliteal arterial reconstruction are 20-30% at 4-5 years [34].

An ideal synthetic graft must be biocompatible, promote the formation of a strongly attached endothelial layer, and match the mechanical properties of the connecting vessel tissue. In this attempt to develop an ideal graft for blood vessel replacement, we primarily focused on matching the mechanical properties of the natural vessel in this work because it is the most challenging requirement. Our strategy was to mimic the mechanical properties and microstructure of the elastin and collagen structural components of natural blood vessels with

a polymer nanofiber composite. Using this strategy we were able to create materials that exhibited the J-shaped stress-strain curve characteristic of the natural blood vessel. In the future study, we will further improve the chemistry of the graft for improved in vitro and in vivo outcome of the vascular grafts.

While the main focus of this study was to develop a novel technology to fabricate a graft that is more mechanically compliant with vascular tissue, this method of fabrication has biological advantages as well. Because of their geometrical similarities to the natural fibers of the ECM, electrospun polymer nanofibers provide excellent substrates for strong endothelial cell attachment in the lumen of vascular grafts and SMCs grown on the nanofiber scaffolds adopted an aligned morphology similar to that seen in natural blood vessels. The electrospinning method of fabrication also allows direct incorporation of drugs, proteins, and growth factors for slow release.

While mechanical testing results for this graft are very promising, the stresses experienced by an actual vessel implant are much more rigorous. Further testing will be required in the future to confirm whether or not this material is suitable as a vascular graft for long term implantation, but preliminary tests were promising. Most of the mechanical data collected was for dry samples, but straight-wavy composites that were hydrated did retain the same J-shaped stress-strain behavior. In addition it was determined that the straight/wavy microstructure and the mechanical behaviors associated with that microstructure remained consistent over multiple loading cycles. While this material still must be tested under in vivo physiological conditions, experimental evidence leads us to believe that it could withstand such conditions.

The greatest advantage of this method of fabrication is its versatility. The mechanical

properties of straight/wavy fiber composite materials can be modified by several methods to allow fine-tuning of mechanical properties. Fine-tuning may be accomplished by changing the material components of the composites or by changing their structure.

While most of these experiments were conducted using PU:PCL composite structures, this fabrication technology is by no means limited to any specific material. Preliminary data has shown that PU:PLGA and PU:PLLA composite nanofiber mats fabricated using the same procedure also adopted a straight-wavy microstructure and a J-shaped stress-strain profile. It is hypothesized that any material that can be electrospun could be incorporated into a straight-wavy composite material using this fabrication method. For instance, this fabrication method could be used to make both a degradable and a non-degradable vascular graft by changing the polymer materials used as the straight/elastic and wavy/stiff fibers. The mechanical properties of individual fibers can even be modified without changing material types. Electrospinning parameters can be modified to change the diameter and microstructure of individual fibers and thus their mechanical properties.

The mechanical properties of these straight-wavy fiber composite materials can also be modified without changing the material of its components. It was demonstrated that the location of the elastic-to-stiff region of the stress-strain curve is shifted when the degree of "waviness" of stiff fibers is modified. It was also demonstrated that the shape of the stress-strain curve of composites changes when the ratio of straight/elastic to stiff/wavy fibers is modified.

In summary, the mechanical properties of these fibrous composite materials can be fine tuned by: 1) the modification of individual fiber components, such as material selection and fiber microstructure (i.e. diameter, porosity…), and 2) the modification of composite

microstructure, such as the degree of stiff fiber "wavyness" and the ratio of fiber components. All of these versatilities allow great flexibility for designing straight-wavy electrospun nanofiber composites with fine tuned mechanical properties. In addition, while a two-component system was used in the examples presented, there is certainly no limit to the number of different components that may be used in the design of these composite grafts. Such versatility allows great potential for fabrication of nanofiber composite materials that closely match the mechanical properties of any vessel in the body.

Because this material can be assembled as very thin (a few microns) mechanically stable sheets, it is well suited for use as a component in tissue engineering strategies for vascular grafts. Several tissue engineered vascular grafts have been developed with promising results [1,4, 35]. Many of these strategies incorporate long term bioreactor culture to impart mechanical integrity. Thin nanofibrous composite sheets with optimized mechanical properties could offer additional mechanical strength and very quick cell alignment from this onset of graft fabrication.

6.5 Conclusions

Treatment of cardiovascular disease is currently limited by a lack of adequate vessel repair and replacement strategies. One of the likely mechanisms for failure of current vascular implants is the mismatch of mechanical properties when compared to natural tissue. Nanofibrous composite materials were fabricated that mimicked the microstructure and mechanical properties of the elastin and collagen fiber components of natural vessels. Mechanical testing confirmed that these composite materials demonstrated a J-shaped stress-strain behavior similar to natural blood vessels. The versatility for fine-tuning the mechanical properties of such a composite was demonstrated by altering the arrangement and ratio of the

elastic and stiff fiber components in composite scaffolds. The feasibility of these grafts for use as vascular implants was demonstrated by confirmation of endothelial and SMC attachment, survival, and alignment on composite materials. In addition it was confirmed that the mechanical properties and microstructure of composite materials maintained their integrity after cyclic loading and in both dry and hydrated state. An ideal synthetic graft must be biocompatible, allow for the formation of a strongly attached endothelial layer, and match the mechanical properties of the natural surrounding vasculature. These composite grafts address all three key requirements. The straight/elastic-stiff/wavy nanofibrous microstructure of these composite materials matched the mechanical properties of natural blood vessels and allowed for the strong attachment and alignment of endothelial and smooth muscle cells. The versatilities of these composite scaffolds allow for fine-tuning of mechanical properties that cannot be achieved with a single material structure. Vascular grafts with improved patency could be fabricated by incorporation of a straight/elastic-wavy/stiff nanofibrous microstructure that allows close matching of mechanical properties to that of surrounding vessel segments.

6.6 References

[1] Mitchell SL, Niklason LE. Requirements for growing tissue-engineered vascular grafts. Cardiovasc Pathol 2003;12:59-64.

[2] Cooper GJ, Underwood MJ, Deverall PB. Arterial and venous conduits for coronary artery bypass. A current review. Eur J Cardiothorac Surg 1996;10:129-40.

[3] Motwani JG, Topol, EJ. Aortocoronary saphenous vein graft disease: pathogenesis, predisposition, and prevention. Circulation 1998;97:916-31.

[4] L'Heureux N, Dusserre N, Marini A, Garrido S, de la Fuente L, McAllister T. Technology insight: the evolution of tissue-engineered vascular grafts--from research to clinical practice. Nat Clin Pract Cardiovasc Med 2007;4:389-95.

[5] Walden R, L'Italien GJ, Megerman J, Abbott WM. Matched elastic properties and successful arterial grafting. Arch Surg 1980;115:1166-9.

[6] Perktold K, Leuprecht A, Prosi M, Berk T, Czerny M, Trubel W, Schima H. Fluid dynamics, wall mechanics, and oxygen transfer in peripheral bypass anastomoses. Ann Biomed Eng 2002;30:447-60.

[7] Miyawaki F, How TV, Annis D. Effect of compliance mismatch on flow disturbances in a model of an arterial graft replacement. Med Biol Eng Comput 1990;28:457-64.

[8] Rittgers SE, Karayannacos PE, Guy JF, Nerem RM, Shaw GM, Hostetler JR, Vasko JS. Velocity distribution and intimal proliferation in autologous vein grafts in dogs. Circ Res 1978;42:792-801.

[9] Stewart SF, Lyman DJ. Effects of a vascular graft/natural artery compliance mismatch on pulsatile flow. J Biomech 1992;25:297-310.

[10] Sarkar S, Salacinski HJ, Hamilton G, Seifalian AM. The mechanical properties of infrainguinal vascular bypass grafts: their role in influencing patency. Eur J Vasc Endovasc Surg 2006;31:627-36.

[11] Karapinar K, Ulus AT, Tutun U, Aksoyek A, Apaydin N, Pamuk K, Can Z, Saritas Z, Kucukay F, Arda K, Katircioglu SF. Implantation of novel small-diameter polyurethane vascular prostheses interposed in canine femoral and carotid arteries. Eur Surg Res 2004;36:241-8.

[12] Pandit A, Lu X, Wang C, Kassab GS. Biaxial elastic material properties of porcine coronary media and adventitia. Am J Physiol Heart Circ Physiol 2005;288:H2581-7.

[13] Roach MR, Burton AC. The reason for the shape of the distensibility curves of arteries. Can J Biochem Physiol 1957;35:681-90.

[14] Shum-Tim D, Stock U, Hrkach J, Shinoka T, Lein J, Moses MA, Stamp A, Taylor G, Moran AM, Landis W, Langer R, Vacanti JP, Mayer JE. Tissue engineering of autologous aorta using a new biodegradable polymer. Ann Thorac Surg 1999;68:2298-304.

[15] Apter, JT. Correlation of visco-elastic properties with microscopic structure of large arteries. IV. Thermal responses of collagen, elastin, smooth muscle, and intact arteries. Circ Res 1967;21:901-18.

[16] O'Connell MK, Murthy S, Phan S, Xu C, Buchanan J, Spilker R, Dalman R, Zarins C, Denk W, Taylor C. The three-dimensional micro- and nanostructure of the aortic medial lamellar unit measured using 3D confocal and electron microscopy imaging. Matrix Biol 2008;27:171-81.

[17] Gupta BS, Kasyanov VA. Biomechanics of human common carotid artery and design of novel hybrid textile compliant vascular grafts. J Biomed Mater Res 1997;34:341-9.

[18] Stitzel J, Liu J, Lee SJ, Komura M, Berry J, Soker S, Lim G, Van Dyke M, Czerw R, Yoo JJ, Atala A. Controlled fabrication of a biological vascular substitute. Biomaterials 2006;27(7):1088-94.

[19] Schnell E, Klinkhammer K, Balzer S, Brook G, Klee D, Dalton P, Mey J. Guidance of glial cell migration and axonal growth on electrospun nanofibers of poly-e-caprolaction and a collagen/poly-e-caprolactone blend. Biomaterials 2007;28(19):3012-25.20.

[20] Grenier, S., Sandig, M., Holdsworth, D. W. & Mequanint, K. Interactions of coronary artery smooth muscle cells with 3D porous polyurethane scaffolds. J Biomed Mater Res A (2008).

[21] Yang F, Murugan R, Wang S, Ramakrishna S. Electrospinning of nano/micro scale poly(L-lactic acid) aligned fibers and their potential in neural tissue engineering. Biomaterials 2005;26(15):2603-10.

[22] Nur-E-Kamal A, Ahmed I, Kamal J, Schindler M, Meiners S. Three-dimensional nanofibrillar surfaces promote self-renewal in mouse embryonic stem cells. Stem Cells 2006;24(2):426-33.

[23] Chua KN, Chai C, Lee PC, Tang YN, Ramakrishna S, Leong KW, Mao HQ. Surface-aminated electrospun nanofibers enhance adhesion and expansion of human umbilical cord blood hematopoietic stem/progenitor cells. Biomaterials 2006;27(36):6043-51.

[24] Qi H, Hu P, Xu J, Wang A. Encapsulation of drug reservoirs in fibers by emulsion electrospinning: morphology characterization and preliminary release assessment. Biomacromolecules 2006;7(8):2327-30.

[25] Luong-Van E, Grondahl L, Chua KN, Leong KW, Nurcombe V, Cool SM. Controlled release of heparin from poly(epsilon-caprolactone) electrospun fibers. Biomaterials 2006; 27(9):2042-50.

[26] Xie J, Wang CH. Electrospun micro- and nanofibers for sustained delivery of paclitaxel to treat C6 glioma in vitro. Pharm Res 2006;23(8):1817-26.

[27] Inoguchi H, Kwon IK, Inoue E, Takamizawa K, Maehara Y, Matsuda T. Mechanical responses of a compliant electrospun poly(L-lactide-co-epsilon-caprolactone) small-diameter vascular graft. Biomaterials 2006;27:1470-8.

[28] Beachley, V. and X. Wen, Fabrication of three dimensional aligned nanofiber array, US-7828539, 2010. Clemson University (Clemson, SC, US).

[29] (American Heart Association, 2006).

[30] Farb A, Weber DK, Kolodgie FD, Burke AP, Virmani R. Morphological predictors of restenosis after coronary stenting in humans. Circulation 2002;105:2974-80.

[31] Farb A, Burke AP, Kolodgie FD, Virmani R. Pathological mechanisms of fatal late coronary stent thrombosis in humans. Circulation 2003;108:1701-6.

[32] Sallam M, Spanos V, Briguori C, DiMario C, Tzifios V, Dharmadhikari A, Albiero R, Colombo A. Predictors of re-occlusion after successful recanalization of chronic total occlusion. J Invasive Cardiol 2001;13:511-5.

[33] Dobesh PP, Stacy ZA, Ansara AJ, Enders JM. Drug-eluting stents: a mechanical and pharmacologic approach to coronary artery disease. Pharmacotherapy 2004;24:1554-77.

[34] Tai NR, Salacinski HJ, Edwards A, Hamilton G, Seifalian AM. Compliance properties of conduits used in vascular reconstruction. Br J Surg 2000;87:1516-24.

[35] Campbell JH, Efendy JL, Campbell GR. Novel vascular graft grown within recipient's own peritoneal cavity. Circ Res 1999;85:1173-8.

[36] Junquiera LC. Junquiera’s Basic Histology Text & Atlas (McGraw Hill, New York, 2005).

[37] Boulesteix T, Pena AM, Pages N, Godeau G, Sauviat MP, Beaurepaire E, Schanne-Klein MC. Micrometer scale ex vivo multiphoton imaging of unstained arterial wall structure. Cytometry A 2006;69:20-6.

CHAPTER 7

7. VASCULAR GRAFTS ASSEMBLED FROM BIOMIMETIC NANOFIBROUS COMPOSITES THAT MATCH THE MICROSTRUCTURE AND COMPLIANCE OF NATURAL BLOOD VESSELS

7.1 Introduction

Cardiovascular disease is the cause of more deaths than any other disease in Western societies, and costs our health care systems hundreds of billions of dollars each year [1]. Diseased blood vessels in the coronary and peripheral vascular system must be repaired or replaced with the goal of reestablishing normal blood flow patterns. While blood vessel replacement with synthetic grafts may be an ideal treatment in some cases, current synthetic grafts are not effective as small diameter (<6 mm) vessels replacements due to very low patency rates. For example, the patency of rates of polytetrafluorethyle (ePTFE) or Dacron grafts when used for infrapopliteal arterial reconstruction are 20-30% at 4-5 years [2].
A better synthetic vascular graft for small diameter vessel replacement is clearly a need.

It is hypothesized that a vascular graft may fail due to three primary mechanisms: (1)Thrombosis due to activation of the coagulation cascade by the graft. (2) Restenosis brought about by compliance mismatch or inflammatory response, and (3) infection [3]. Our goal is to develop a method to fabricate vascular grafts with optimized, highly tunable mechanical properties to address the issue of failure by compliance mismatch. The term 'compliance' is commonly used when the mechanical properties of a vascular graft are compared to that of its neighboring natural vascular. Compliance ($C=\Delta Volume/\Delta Pressure$) describes the relationship of vessel distention to the internal pressure and is related to the circumferential elasticity of the vessel wall. Compliance mismatch may result in hemodynamic blood flow disturbances and stress concentrations at the anatomosis of a

vascular graft as shown in Figure 7.1 [4]. Hemodynamic flow variations can result in areas of increased shear stress, which may damage the endothelium, and decreased shear stress [5], which may lead to areas of stagnation, chemokine pooling [6], and increased platelet interactions and oscillatory forces [7]. Stress concentrations can bring about tissue remodeling that results in intimal thickening, which eventually leads to graft failure. It has been reported that turbulent flow caused by compliance mismatch may bring about intimal hyperplasia or aneurysm and result in poor graft patency [8-9].

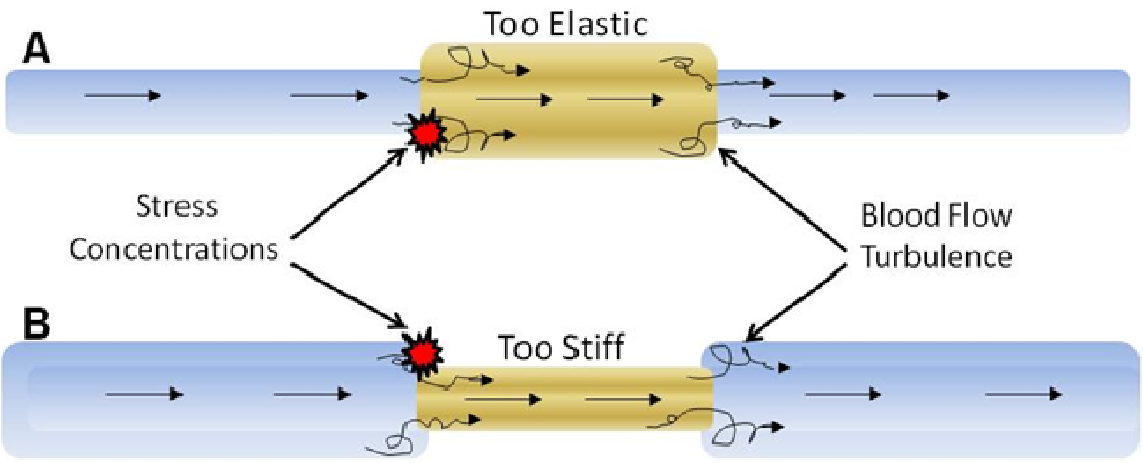

Figure 7.1: Schematic of non-compliant vascular grafts. (A) Grafts with compliance greater than neighboring vessels undergo a greater degree of expansion due to internal blood pressure, and (B) grafts with compliance lower than neighboring vessels undergo less expansion. In both case, geometric inconsistencies result in blood flow turbulence and stress concentrations at the anatomosis.

Designing a vascular graft with compliance that matches that of the natural vascular is difficult because the compliance of natural blood vessels is not uniform, and varies with the degree of wall distension. The vascular system must be elastic to provide capacitance and pulse smoothing to blood flow, but must also offer stability over a wide range of pressures. In order to address both of these needs, blood vessels are relatively elastic at low levels of vessel distention (less than around 140-160% of initial diameter), but and their stiffness increases rapidly at vessel distention above that value. The mechanical profile of the vascular

wall adopts a J-shaped curve that reflects this behavior as shown in Figure 6.1. It has been hypothesized that this J-shaped mechanical behavior is due to the contributions of the relatively elastic elastin fibers and much stiffer collagen fiber components of vascular wall. Roach and Burton [10] provided evidence to support this theory when they compared the mechanical properties of a vessel wall that had its elastic fiber component digested by trypsin to a vessel wall that had its collagen fiber component digested by formic acid. It was found that the sample containing elastic fibers had a mechanical profile similar to a control vessel as low levels of vessel distention, and that the sample containing collagen fiber had a mechanical profile similar to a control vessel at higher levels of distention (Figure 6.1). The mechanism that allows collagen to contribute to the strength of the vessel in such a way may be explained by the microstructural arrangement of collagen in the vessel wall. Collagen fibers in the natural blood vessel exhibit a wavy or helical orientation at mean physiological pressure [11]. Because these collagen fiber bundles do not appear to be taut at low levels of vessel distention, they may not contribute much to resisting expansion until the vessel wall is distended enough to where they are fully straightened [12]. It can be hypothesized that elastin fibers dominate the mechanical behavior of the vessel at low pressures and thus distention, and that as pressure and distention increases progressive recruitment of collagen fibers dominate the mechanical behavior and result in increasing stiffness.

We previously showed that the J-shaped mechanical behavior of blood vessels could be mimicked with a two component nanofiber structure where one component was relatively elastic and the other relatively stiff compared to one another and where the stiffer component exhibited a waved orientation [13]. It was our goal to use this novel concept to fabricate an implantable vascular graft that retained this optimized mechanical behavior, similar to natural

blood vessels, both in vitro and in vivo, and both before implantation and after implanted or retrieval.

7.2 Materials and Methods

7.2.1 Electrospinning

Wavy nondegradable nylon 6 (Arcos, New Jersey, USA) nanofibers and straight nondegradable medical grade aliphatic polyether polyurethane (PU, Tecoflex SG-80A, Noveon, Cleveland, OH) nanofibers were electrospun from their polymer solvent solutions. Nylon was dissolved in hexafluoro-2-propanol (HFIP, Oakwood, West Columbia, SC) at 30% wt/v and PU was dissolved in HFIP at 12% wt/v. Polymer solutions were doped with poly(ethylene glycol) (PEG, M.W. 400, Arcos, New Jersey, USA), amine terminated polypropylene glycol-block-PEG (PEG-NH2, Sigma 14527), or gelatin (Fisher S80023-1, Rochester, NY). Doping concentrations used were 1 & 10%(w/w) vs. PU and 2% vs. nylon, 3 & 30% vs. PU and 7% vs. nylon, and 5 & 20% vs. PU and 10% vs. nylon respectively. Aligned PU fibers were electrospun using low concentration doping agent solutions and randomly aligned PU fibers were electrospun using high doping agent solutions. Polymer solutions were feed by a syringe pump (Medfusion 2010i; Smiths Medial Inc., Carlsbad, CA,USA) at a feed rate of 0.025 ml/min through 1/16" polyethylene tubing into a 21g blunt tipped needle (Smallparts, Miramar, FL). A voltage of 8-12kV was applied to the needle tip with a high voltage power supply (ES40P-10W, Gamma High Voltage Research, Ormond Beach, FL). The needle tip was held at 10 cm above a custom build collecting device [14].

7.2.2 Biomimetic vascular graft fabrication

Biomimetic vascular grafts with wavy and straight nanofiber structures were made using a

custom build device designed in our laboratory [14] and detailed methods were described in Chapter 6.

7.2.3 Heparin immobilization

A 0.05M MES buffer was prepared with a pH of 5.6 and warmed to 37ºC. Heparin (Sigma, H4784), N-Hydroxysuccinimide (NHS, Sigma 130672), and 1-Ethyl-3-(3-dimethylaminopropyl) carbodimide (EDC, TCI America), were added to the buffer solution at 0.2%, 0.12%, and 0.2% respectively and incubated for 10 minutes to activate heparin. Samples were added to the solution and incubated for 4 hours then removed and washed in water 5 times over 24 hrs.

7.2.4 Mechanical testing

Mechanical tests were performed using a BioTester5000 Biaxial Test System (CellScale division of Waterloo Instruments Inc., Waterloo, Ontario, Canada) with a 10N load cell (ring samples ~1mm in length for data shown in Figure 7.6) and a Shimadzu EZ Graph tensile tester (Nakagyo-ku, Kyoto, Japan) with a 50N load cell (ring samples ~2.5 mm in length all other data). All mechanical testing was performed in PBS warmed to 37 ºC. Circumferential strength was evaluated by inserting two rods through the lumen of small ring samples of grafts or explant tissue followed by tensile displacement to failure. Force data was halved to reflect the wall strength of a single piece of vessel. Fatigue testing was performed by straining rings to around 200% diameter at 250um intervals for 100 cycles.

7.2.5 Surgical Implantation

Female New Zealand white rabbits at least 8 months old were anaesthetized and shaved. An incision was made and the right carotid artery was exposed. Heparin was administered

intravenously at 10U/kg prior to surgery. Distal and proximal ends of a section of vessel were clamped to prevent blood flow through the vessel. End to end procedure was used for the vessel replacement surgery, the section of vessel was clamped to prevent blood flow and the vessel was cut between the clamps. The graft was sutured end to end directly the cut ends of the vessel using interrupted 6-0 prolene sutures. In all cases blood flow through the graft was confirmed by flushing the graft by tweezers and observation of graft re-expansion. A total of 8 rabbits were treated (5 bimimetic microstructure, 3 control).

7.2.6 Histology

Rabbits were sacrificed at 3 months after graft implantation. Grafts were cut out with portions of the distal and proximal vessel. The tissue was trimmed and a segment was cut from either end that included the anastomosis and approximately 1mm of the graft and or tissue on each end. The remaining portion of the graft was cut into rings approximately 1mm in length. Samples for histology were fixed in 4% paraformaldehyde overnight and embedded in paraffin. Serial sections were stained with hematoxylin and eosin for general microstructure, modified Masson trichrome stain for extracellular matrix, and immunostained with anti α-smooth muscle actin (Sigma, A5228) to identify smooth muscle cells. SEM images were taken with a scanning electron microscope (SEM, Hitachi TM-1000). Samples were not sputter coated.

7.2.7 X-ray photoelectron spectroscopy (XPS)

Samples were fabricated from solutions doped with PEG, PEG-NH2, and gelatin as described above. Three groups were analyzed using XPS: (1) Complete EDC heparinization reaction (2) Control EDC reaction without heparin added (3) Control washed with water only. XPS

measurements were carried out on the Kratos AXIS Ultra DLD XPS system equipped with a hemispherical energy analyzer and a monochromatic Al Kα source.

7.3 Results

7.3.1 Graft morphology

Tubular vascular grafts with similar dimensions to the explanted rabbit carotid artery were assembled using the fabrication methods described above and displayed in Figure 7.2A-C. Biomimetic grafts maintained a straight-wavy biomimetic nanofiber microstructure within the tubular grafts (Figure 7.2D). For control grafts, all fibers remained straight (Figure 7.2E). Biomimetic grafts appeared to have thicker walls and greater porosity when compared to control grafts.

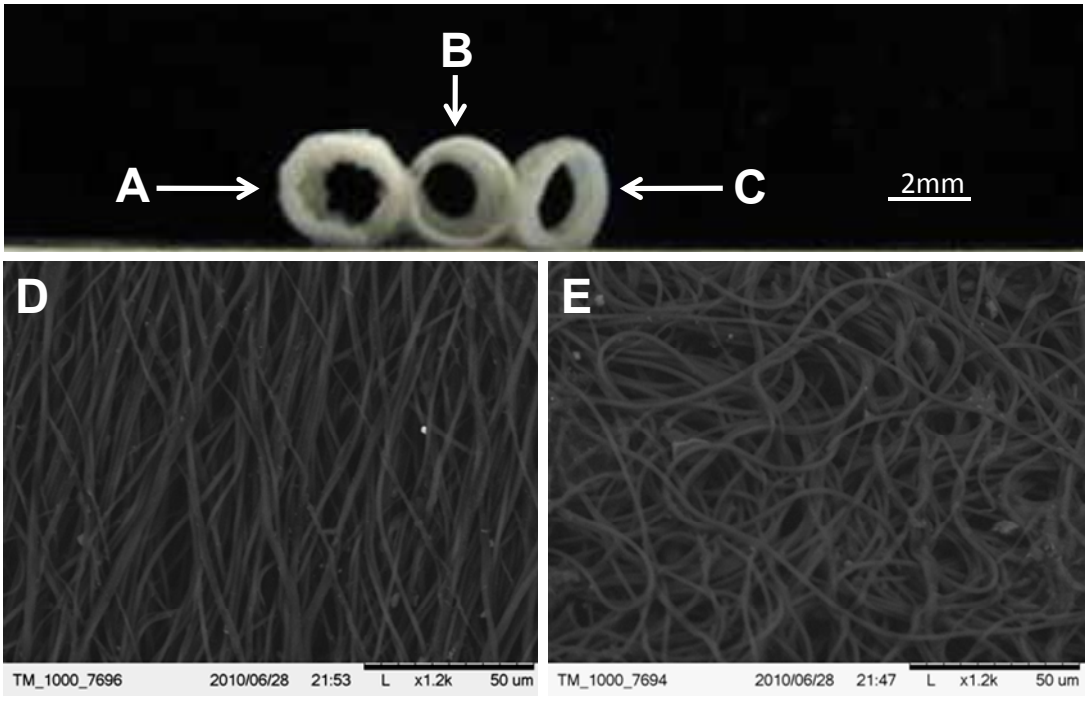

Figure 7.2: Gross morphology of rings cut from (A) tubular nanofiber graft with biomimetic microstructure, (B) tubular nanofiber graft with control microstructure, and (C) rabbit carotid artery explant. SEM images of nanofibrous microstructure of (D) tubular nanofiber graft with biomimetic microstructure (E) tubular nanofiber graft with control microstructure

7.3.2 Grafts mechanical properties

Biomimetic and control grafts were cut into ring sections and circumferentially strained by pins inserted into the lumen of the rings. Biomimetic grafts displayed a J-shaped mechanical profile characteristic of natural vascular tissue, while control grafts did not (Figure 7.3A). Graft mechanical properties could be optimized by varying (1) the ratio of PU to nylon fibers, (2)the total amount of nanofibers, and (3)fiber sheet width reduction (D in Figure 6.3).

7.3.2.1 Optimizing grafts mechanical properties

Because fiber deposition is steady state with our collecting device, the ratio of PU to nylon fibers could be modified by changing the collection times for each polymer type.

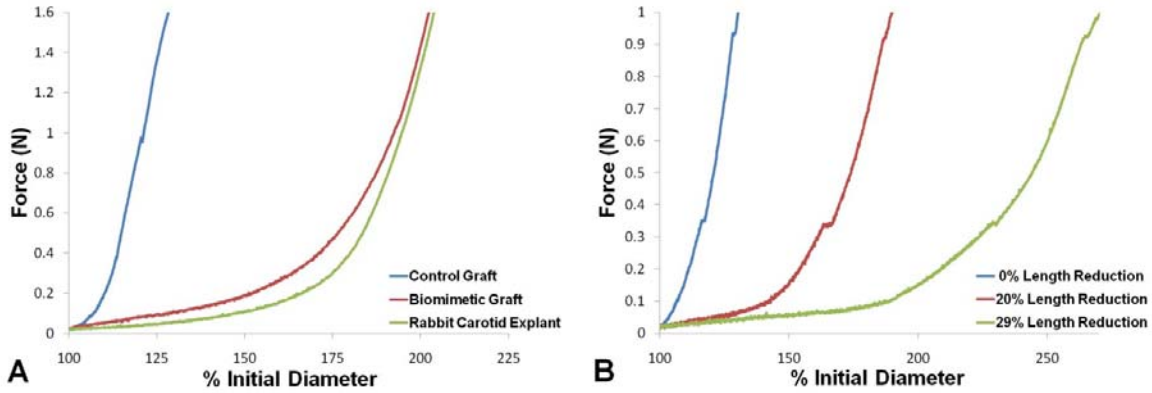

Figure 7.3: Force vs. increase in diameter of ring samples strained by a tensile testing machine: (A) Mechanical profiles of an optimized biomimetic nanofiber graft, control nanofiber graft, and rabbit carotid artery explants. (B) Length reductions of 0%, 20%, and 29% during fabrication caused different degrees of nylon fiber "wavyness" and thus required greater level of strain to reach the mechanical profile transition point.

The overall strength of tubular grafts can be increased by increasing the total amount of nanofibers in the structure. All grafts presented contained both PU and nylon nanofibers were electrospun for 45 total minutes each. The amount of fibers of each type appeared to be similar. These values were selected in an attempt to optimize grafts to mimic the circumferential mechanical profile of the rabbit carotid artery. Many grafts were evaluated

and screened in selecting these two parameters (data not shown).

The location of the transition point in the J-shaped mechanical profile, which represents the value of strain at which the strength of the graft rapidly increases, could be predictably moved by modifying the fiber sheet width reduction distance (D in Figure 6.3). Fiber sheet width reductions after nylon nanofiber deposition resulted in buckling of the nylon fibers and caused them to adopt a wavy orientation. As the width reduction increased, the "wavyness" of the nylon fibers increased, resulting in a shift of the mechanical profile transition point to higher values of strain. Grafts with several different values of D (Figure 6.3) were evaluated in an attempt to optimize grafts to mimic the circumferential mechanical profile of the rabbit carotid artery. A graft that closely matched the mechanical properties of a rabbit carotid artery explants was fabricated using a protocol where nylon fibers in these sheets buckled to conform to a 20% reduction in length (Figure 7.3A). The circumferential strength of optimized grafts was tested under cyclic loading conditions in order to evaluate the fatigue strength of the grafts. A ring sample was strained to approximately 200% initial diameter for 100 hundred cycles while immersed in PBS at 37ºC to simulate physiological conditions. The maximum force reached for each cycle remained unchanged throughout the duration of the test, indicating that grafts are able to withstand cyclic strains without permanent deformation or reduction in strength. Optimized grafts were evaluated in vivo in a rabbit carotid artery model.

7.3.3 Heparin attachment

Heparin attachment to nanofiber scaffolds was analyzed using XPS (Figure 7.4). Nanofibers grafts electrospun from solutions blended with PEG, PEG-NH2, and gelatin were analyzed. Heparin attachment was confirmed by peaks in an XPS spectrum at around and 164eV for

S2p and 228eV for S2s. These two peaks correspond to the $–OSO_3$ and $–NSO_3$ moieties in heparin. Three groups were used: (1) Sampled heparinized with EDC reaction, (2) control samples where EDC reaction was performed without the presence of heparin, and (3) control washed in distilled water. For all three groups, group 3 had negligible peaks at 164eV for S2p and 228eV for S2s. Group 2 had a small peak at 164eV for S2p and 228eV for S2s and group 1 had pronounced peaks at 164eV and 228eV. Within group1, grafts containing gelatin and PEG-NH2 with free amine functional groups available for covalent heparin binding had more pronounced peaks than grafts containing PEG without free amine groups. Results indicate that heparin is present in all grafts subject to the heparinization surface functionalization reaction. A small portion of the S2p and S2s signals detected appears to be due to the EDC reaction, which would indicate that some of the MES buffer remained within the scaffolds. It also appeared that a portion of the heparin incorporated into the scaffolds was due to physical absorption as indicated by the S2p and S2s peaks in grafts blend with PEG that contained no functional groups capable to covalently attaching to heparin in the EDC reaction.

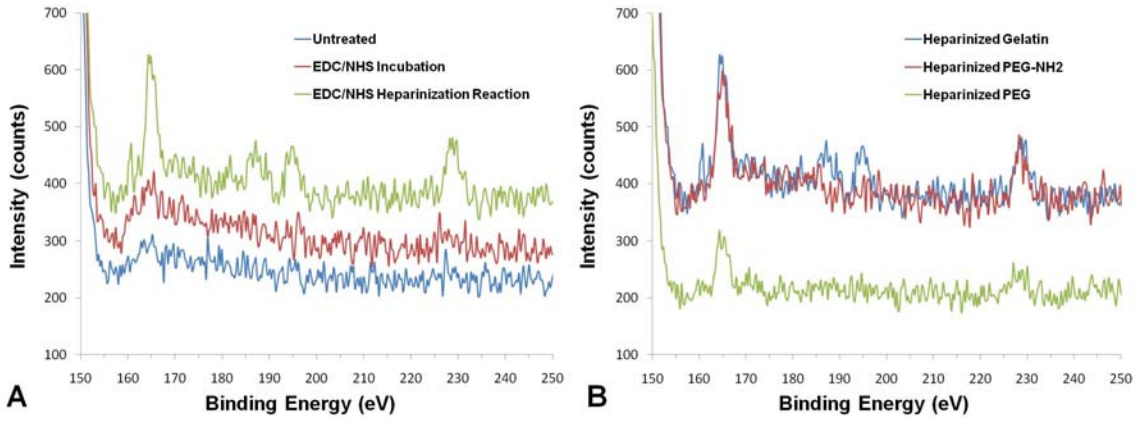

Figure 7.4: XPS analysis of grafts blended with gelatin, PEG-NH2, or PEG surface functionalized with heparin via EDC crosslinking reaction. (A) Comparison of spectra for gelatin blended grafts that were heparinized with EDC crosslinking reaction, underwent EDC crosslinking reaction without the presence of heparin, or left untreated. (B) Comparison of spectra for gelatin, PEG-NH2, and PEG grafts that were heparinized with EDC crosslinking reaction.

7.3.4 In vivo testing

A preliminary in vivo study was conducted to evaluate the potential of such grafts as vascular replacement grafts. Eight grafts were implanted into the carotid artery of rabbits (5 biomimetic & 3 control) (Figure 7.5A). Grafts preformed very well during surgical implantation. No stretching or tearing was evident during rigorous surgical manipulation, sutures held tight without tearing, and blood leakage though the grafts was not apparent. Blood flow though the grafts after implantation was confirmed. Grafts were removed after 3 months in vivo. Grafts remained similar in appearance to pre-implantation from the outside and in ring cross sections. Explanted biomimetic and control grafts are shown in (Figure 7.5B-E).

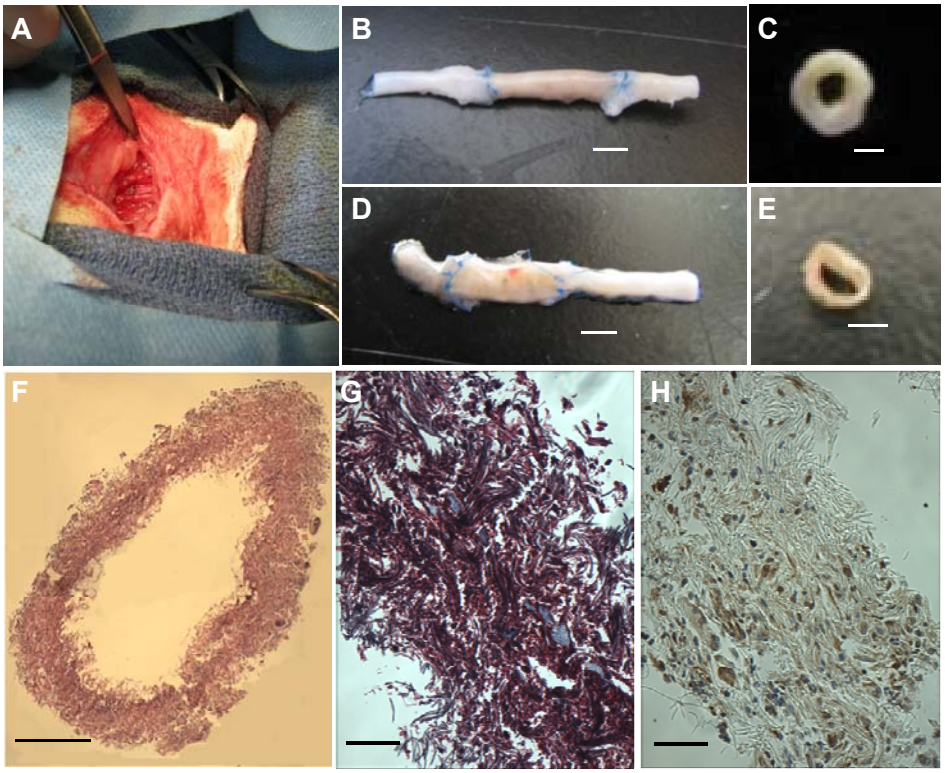

Figure 7.5: Pictures of: (A) Implanted graft. (B) Biomimetic and (D) control grafts removed after 3 months in vivo. Ring segments cut from explanted (C) biomimetic and (E) controls grafts. Sections taken from explanted biomimetic grafts stained with (F) H&E, (G) modified Masson's, and (H) anti-smooth muscle actin. Scale bars are 2mm (B&D), 1mm (C&E), 500um (F), and 50um (G&H)

Histology confirmed that biomimetic grafts maintained their 'wavy' microstructure, while control grafts contained all straight fibers. Infiltration of cells as well as ECM deposition within the grafts was also confirmed (Figure 7.5F-H). Modified Masson trichrome stain for extracellular matrix identified collagen disposition (light blue, Figure 7.5G) within the grafts and immunostaining for α-actin smooth muscle antibodies positively identified smooth muscle cell infiltration (brown, Figure 7.5H) deep within the microstructure of the grafts. Histology confirmed that grafts remained open at their center. A ring was cut from the center of the biomimetic and control grafts and mechanically tested to confirm whether optimized mechanical properties could be maintained throughout long term in vivo implantation. Results of this test confirmed that biomimetic graft did maintain a J-shaped mechanical profile, while control grafts did not (Figure 7.6).

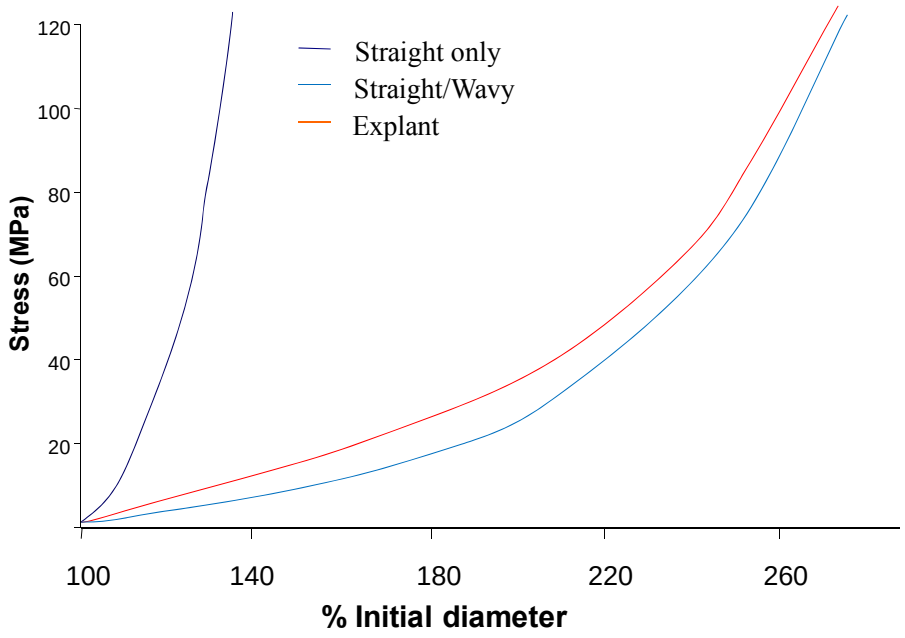

Figure 7.6: Force vs. % initial diameter plotted for ring samples of native rabbit carotid artery and biomimetic and control grafts explanted after 3 months in vivo.

7.4 Discussion

The goal of this study was to investigate the feasibility of designing a highly compliant vascular graft using a two component hybrid electrospun nanofiber material with biomimetic microstructure. Previous we developed hybrid nanofiber structures with a relatively elastic component in a straight aligned orientation and a relatively stiff component in a 'waved' aligned orientation. These composite nanofiber grafts adopted a two phase 'J-shaped' mechanical profile that is similar to that observed in several natural tissues. It was demonstrated that biomimetic mechanical properties corresponded to the precisely designed microstructure of the hybrid sheets.

There is an obvious need for a better vascular graft because current options for small diameter vessel replacement demonstrate unacceptably low patency rates [2]. Vascular graft design is a complex process because of several modes of failure that led to several sets of requirements. It is generally accepted that vascular grafts may fail due any of three mechanisms: (1) Thrombosis due to activation of the coagulation cascade by the graft. (2) Restenosis brought about by compliance mismatch or inflammatory response, and (3) infection. Therefore, a vascular graft must be made with non-thrombogenic properties, promote rapid and complete endothelialization, match the mechanical properties of natural vessels, be biocompatible, and be implanted under sterile conditions. A major difficulty in vascular graft design is that several of these properties are not related to one another, and therefore it is hard to design a single material that fits all of those needs. It was our goal to show that the mechanical properties of a vascular graft can be optimized for a wide variety of different materials by using precise microstructural arrangement. Thus, materials with excellent bioactivity and non-thrombogenicy that are non-compliant may be used to design a

compliant vascular graft. The ratio of mechanical strength of elastin digested blood vessel tissue vs. collagen digested tissue is around 30:1 (Figure 6.1). It can be hypothesized that a hybrid nanofibrous vascular graft where the ratio of the strength of the elastic straight fiber component and the stiff wavy fiber component is around 30:1 would mimic natural vessel behavior. We would hypothesize that any two materials with an elastic modulus ratio from around 10:1 to 100:1 could be arranged in a composite with an overall 30:1 ratio by modifying the total number and diameter of the nanofiber of each type. We expect that compliant vascular grafts may be fabricated from a very wide range of polymer materials using this method because many polymers can be easily electrospun into nanofibers.

In this study we used polyurethane as a relatively elastic material and nylon as a relatively stiff material. These materials are not known to be especially non-thrombogenic or bioactive, and in addition, the polyether based polyurethane may not be ideal for long term implantation due to potential for stress cracking [15]. However these materials were selected based on availability, cost, and very slow biodegradability properties, as model materials with which to test the mechanical performance of biomimetic fibrous grafts. Our goal was to show that two materials with such mechanical properties could be used to fabricate a durable vascular graft with highly tunable compliance that could withstand surgical implantation and retain its structural and mechanical properties long term in vivo.

It was demonstrated that tubular vascular grafts could be fabricated with geometry and mechanical properties that were remarkably similar to that of natural blood vessels. The mechanical profile of these grafts could be predictably tuned by modifying the precise orientation of nanofiber microstructure. Durable grafts were able to withstand surgical implantation, and blood flow though the grafts was confirmed without leakage. Grafts

removed after 3 months in vivo demonstrated smooth muscle cell infiltration and collagen production deep within the graft walls. Nanofiber microstructure and biomimetic mechanical properties appeared to be maintained in after long term in vivo implantation. It was our hope to show that the mechanical properties of an electrospun hybrid biomimetic vascular graft could be optimized by modulating microstructure, that such a graft would be durable enough for surgical implantation, and that mechanical properties would not change during long term in vivo implantation. Microstructure and mechanical properties appeared to be unaffected by long term implantation. Overall the results of this study demonstrate the potential of this technology for the design of a compliant vascular graft.

7.5 Conclusions

A method of fabricating hybrid nanofiber sheets with biomimetic microstructure and mechanical properties was previously designed. It was our hypothesis that a compliant vascular graft could be fabricated with wavy and straight nanofiber morphology to best mimic the mechanical properties of natural blood vessels. Evaluation of grafts in vivo demonstrated that these grafts were durable enough for surgical implantation and were able to retain their desirable mechanical properties during long term in vivo implantation. The results of this preliminary study demonstrates the potential of this technology in vascular graft fabrication. The versatility of this technology in allowing for highly compliant graft fabrication from materials with a wide range of mechanical properties highlights its potential in small diameter vascular graft applications.

7.6 References

[1] Mitchell SL, Niklason LE. Requirements for growing tissue-engineered vascular grafts. Cardiovasc Pathol 2003;12:59-64.

[2] Tai NR, Salacinski HJ, Edwards A, Hamilton G, Seifalian AM. Compliance properties of conduits used in vascular reconstruction. Br J Surg 2000;87:1516-24.

[3] L'Heureux N, Dusserre N, Marini A, Garrido S, de la Fuente L, McAllister T. Technology insight: the evolution of tissue-engineered vascular grafts--from research to clinical practice. Nat Clin Pract Cardiovasc Med 2007;4:389-95.

[4] Miyawaki F, How TV, Annis D. Effect of compliance mismatch on flow disturbances in a model of an arterial graft replacement. Med Biol Eng Comput 1990;28:457-64.

[5] Rittgers SE, Karayannacos PE, Guy JF, Nerem RM, Shaw GM, Hostetler JR, Vasko JS. Velocity distribution and intimal proliferation in autologous vein grafts in dogs. Circ Res 1978;42:792-801.

[6] Stewart SF, Lyman DJ. Effects of a vascular graft/natural artery compliance mismatch on pulsatile flow. J Biomech 1992;25:297-310.

[7] Sarkar S, Salacinski HJ, Hamilton G, Seifalian AM. The mechanical properties of infrainguinal vascular bypass grafts: their role in influencing patency. Eur J Vasc Endovasc Surg 2006;31:627-36.

[8] Walden R, L'Italien GJ, Megerman J, Abbott WM. Matched elastic properties and successful arterial grafting. Arch Surg 1980;115:1166-9.

[9] Perktold K, Leuprecht A, Prosi M, Berk T, Czerny M, Trubel W, Schima H. Fluid dynamics, wall mechanics, and oxygen transfer in peripheral bypass anastomoses. Ann Biomed Eng 2002;30:447-60.

[10] Roach MR, Burton AC. The reason for the shape of the distensibility curves of arteries. Can J Biochem Physiol 1957;35:681-90.

[11] O'Connell MK, Murthy S, Phan S, Xu C, Buchanan J, Spilker R, Dalman R, Zarins C, Denk W, Taylor C. The three-dimensional micro- and nanostructure of the aortic medial lamellar unit measured using 3D confocal and electron microscopy imaging. Matrix Biol 2008;27:171-81.

[12] Gupta BS, Kasyanov VA. Biomechanics of human common carotid artery and design of novel hybrid textile compliant vascular grafts. J Biomed Mater Res 1997;34:341-9.

[13] Beachley V, Wen X, Synthetic vascular tissue and method of forming same. Application #12/468,979 US. 2009.

[14] Beachley, V. and X. Wen, Fabrication of three dimensional aligned nanofiber array, US-7828539, 2010. Clemson University (Clemson, SC, US).

[15] Microspec Corporation, Materials:Tecoflex. http://www.microspecorporation.com/materials.php?id=8 (visited 4/7/11)

CHAPTER 8

8. ENGINEERING SKELETAL MUSCLE TISSUE WITH MYOBLAST CELL SEEDED ALIGNED NANOFIBER SHEETS

8.1 Introduction

Failure of adult skeletal muscle tissue to regenerate often occurs after traumatic injury, tumor ablation, congenital disorders, and other myopathies [1]. Currently, the standard treatment for radical muscle tissue loss is transfer from donor sites. However, this practice often results in significant donor site morbidity and loss of function [1]. Recently, tissue engineering approaches have been developed that show much promise in generating functional skeletal muscle tissues for transplantation that may replace conventional donor site transplantation. In addition to transplantation, engineering skeletal muscle tissues provide useful models for the study of skeletal muscle development and drug screening that may replace the use of animals [2].

Traditional tissue engineering approaches to skeletal muscle involve seeding myoblasts onto biodegradable, biocompatible scaffolds, followed by differentiation induction before in vivo implantation. Since native muscle tissue is characterized by aligned, multi-nucleated myotubes that are ideal for producing uniaxial contractile forces, many approaches have focused on generating these aligned myotubes in vitro. Successful approaches include seeding cells onto aligned electrospun nanofibers [3-5] and seeding cells onto micropatterned surfaces [6]. Skeletal muscle cell progenitor cell lines, such as C2C12 myoblasts and explanted skeletal muscle cells cultured on aligned electrospun nanofibers exhibited significantly greater alignment and myotube formation compared to cells cultured on randomly aligned fibers [3, 7]. Myotube contractility also appeared to be increased on aligned nanofibers as indicated by correctly arranged sarcomeric contractile machinery [7].

In order to utilize the advantages of aligned nanofibers in skeletal muscle tissue engineering, scaffolds must be designed in a way that is practical for functional muscle transplantation procedures. One promising approach is cell sheet engineering. The potential applications of cell sheet substrates for tissue engineering include thin sheet applications as well as other applications where thicker substrates are fabricated from stacks of cell sheets [8]. Aligned electrospun nanofibers were used to fabricate aligned cell sheets with uniaxial cell alignment useful in skeletal muscle engineering [9]. Because cell sheets do not include a biomaterial component they are not limited by biocompatibility issues and hindrance to cell-cell contact and mass transport that may be associated with scaffolds. However, disadvantages of this approach include relatively long cultures times required for sheet formation, mechanical and structural weakness, and difficulty in manipulating individual sheets. Tight adhesions are required for layer-by-layer stacking of cell sheets, and their tendency to fold and contract make this difficult. We developed an alternative approach to aligned cell sheet tissue engineering that retains some of the advantages of cell sheets, while also addressing some of its weakness. It was our hypothesis that free suspended ultra thin nanofiber sheets could be used to culture confluent aligned skeletal muscle cell sheets. The nanofiber component improves the mechanical properties of the substrate, and because these scaffolds are inherently fixed at their edges they are much easier to manipulate for three dimensional structure assemblies. However, a very low fiber density allows for retention of cell-cell contacts and mass transport advantages associated with conventional cell sheet tissue engineering.

8.2 Materials and Methods

8.2.1 Electrospinning

Polycaprolactone (PCL, Mn~80,000, Sigma, St. Louis, MO) was dissolved in dichloromethane and dimethylformamide (3:1) (DCM:DMF, Sigma) at a concentration of 17% wt/v. Polymer solution was feed by syringe pump (Medfusion 2010i; Smiths Medial Inc., Carlsbad, CA, USA) at a rate of 0.025 ml/min through a 21 G blunt tipped needle. A voltage of 9 KV was applied to the needle tip with a high voltage power supply (ES40P-10W, Gamma High Voltage Research, Ormond Beach, FL, USA). Nanofibers were collected using a custom built collecting device designed in our lab [10]. The device utilized electrostatic forces to deposit aligned nanofibers across the air gap between two parallel plates as described by Li et al [11]. However static parallel plates were replaced by conductive mobile tracks, which continuously distribute and assemble the aligned fiber arrays into mats with controllable fiber density. The needle tip was held at 10cm above this device during electrospinning, while the parallel mobile tracks pulled electrostatically aligned electrospun fiber arrays into a secondary collection area at a vertical speed of 21 mm/s. Ultra thin aligned fiber mats were assembled on a rectangular rack simultaneous to fiber collection and fiber density varied with collection times from 5 to 30 minutes. Ultra-thin aligned PCL nanofiber sheets were fixed to thin 25mm inner diameter stainless steel rings (Bokers, Minneapolis, MN) with medical silicon (NuSil) for in vitro cell culture. Aligned nanofiber mats with variable density were fabricated by modifying the collection time.

8.2.2 Cell culture

C2C12 myoblasts were cultured in T-75 flasks to near confluence in DMEM media with 10% fetal bovine serum (FBS). Aligned nanofiber scaffolds were sterilized in 6 well plates in 75% ethanol for 30 minutes, washed twice with PBS, and covered with media. Cells were trypsonized and resuspended in media at approximately 1 million cells per ml. Approximately 0.5ml of cell suspension was dripped evenly over each scaffold. Cells were dripped directly onto the tissue culture plate surface for controls that contained no scaffolds. Scaffolds were incubated in DMEM media supplemented with FBS for 5 days. After 5 days some scaffolds were incubated in DMEM with 10% horse serum (HS) to induce differentiation into myobtubes. Media was changed every 48 hours.

Nanofiber/fibrin gel composite thin films were fabricated using a procedure similar to one previous developed in our laboratory [12]. However, our new modified method, shown in Figure 8.1, allowed for direct cell incorporation during film fabrication. Fibrinogen (Bovine, MP Biomedicals 154165) was dissolved in PBS at a concentration of 15mg/ml and vacuum filtered with grade 417 filter paper to remove particulate, and a 0.22μm filter for sterilization. Thrombin (Bovine, MP Biomedicals 154163) was dissolved in DMEM culture media and sterile filtered with a 0.45μm syringe filter. Myoblast cells were suspended in fibrin and thrombin solutions at concentrations of approximately 500,000 cells/ml. An aligned nanofiber sheet was immersed in each solution and removed to form a thin liquid film. The fibrinogen and thrombin liquid films were then combined and allowed to polymerize into a fibrin gel film. Some fibrin scaffolds were incubated in media supplemented with tranexamic acid (trans-4-aminomethyl-cyclohexane-1-carboxylic acid, t-AMCA) at a concentration of 160ug/ml to inhibit fibrinolysis [13].

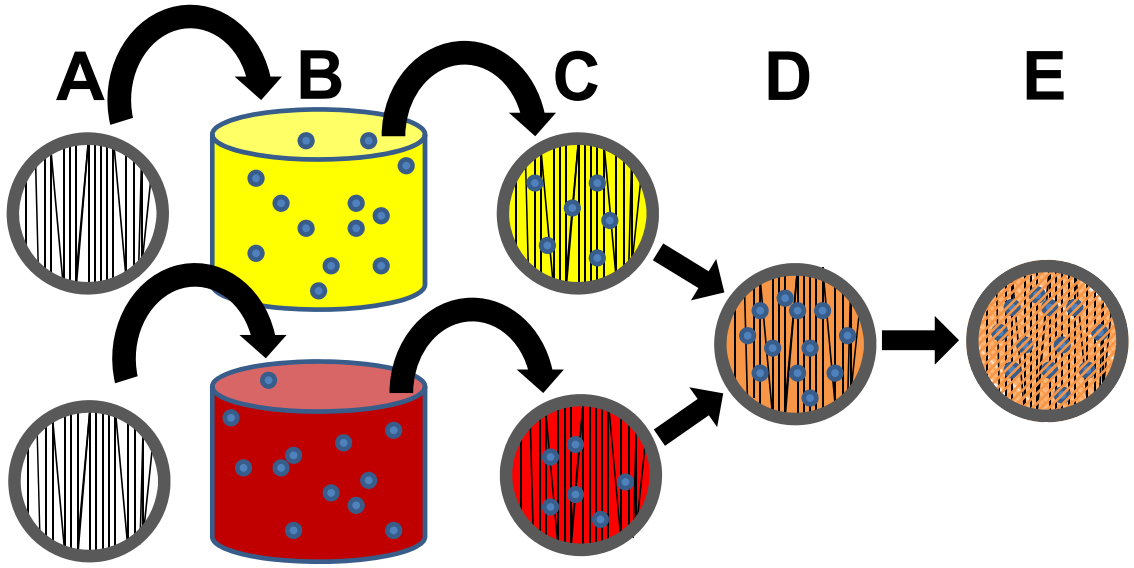

Figure 8: Aligned nanofiber-fibrin film composite fabrication. (A) Mounted nanofiber arrays are immersed in (B) fibrinogen (yellow) and thrombin (red) solutions containing suspended cells (blue). (C) Removal from the liquid results in the formation of a thin uniform liquid film over the nanofiber array. (D) Fibrinogen and thrombin films are sandwiched together to and allowed to mix. (E) Polymerization reaction results in crosslinked fibrin film with embedded nanofibers and cells.

8.2.3 Three-dimensional structure fabrication

Two dimensional aligned nanofiber/cell sheets were used to assemble 3-dimensional tissue engineering scaffolds. Two different methods where developed to demonstrate the potential of these structures as assembly blocks for engineering 3D tissues. Several layers were stacked layer-by-layer to form thick discs from the single layer sheets (Figure 8.2F). Up to 15 single layer nanofiber/cell sheets were stacked on top of one another on a supporting ring with a 15mm inner diameter. Four posts extending vertically from the face of the ring served to hold the layers in place. A second ring with holes cut to match the post locations was placed on top of the construct to sandwich the nanofiber/cell sheets together and secure them. Constructs were cultured for 5 days to allow cell layers to adhere to one another.

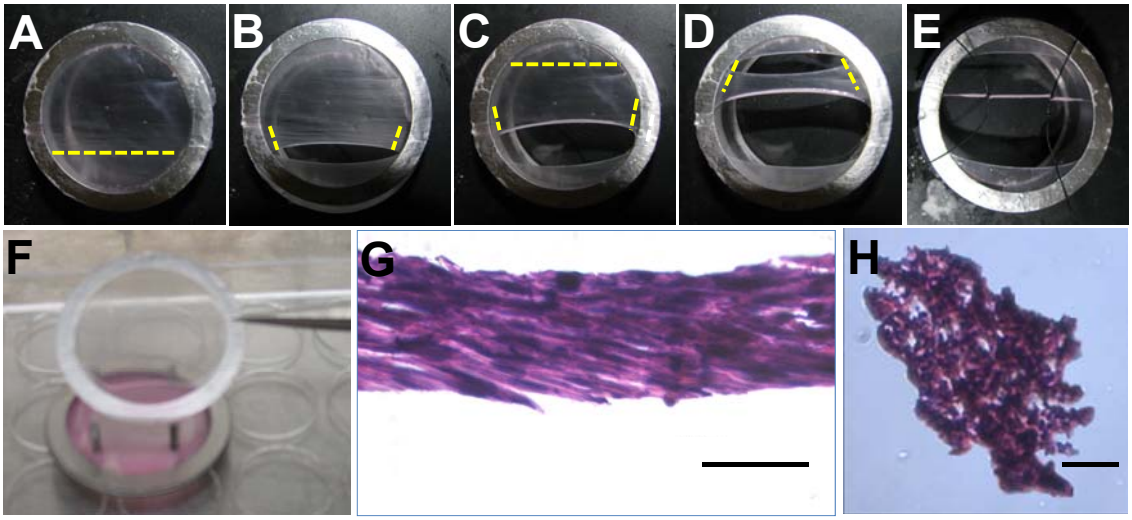

Figure 8.2: Aligned nanofiber-cell sheets were cut (yellow dotted line) in a pattern shown in A-D to promote self assembly into a tubular structure and bound together using sutures (E). A crosssection of this scaffold stained with H&E is shown in H. Aligned nanofiber-cell sheets were stacked on a secondary support ring (F) to form thick multilayered tissue constructs. The cross section of a 6 layered tissue construct (G) demonstrates cell alignment. Scale bar is 50µm.

Three dimensional aligned nanofiber/cell structures were also fabricated from the nanofiber/cell sheets using a novel technique. When ultra thin aligned myoblast/nanofiber sheets were cut according to the method shown in Figure 8.2A-E, they demonstrated a natural tendency to self assemble into bundled structures. Surface tension from the media covering the sheet and mechanical tensions within the nanofiber resulted in an oval shaped hole when sheets were cut along the direction parallel to nanofiber/cellular alignment (Figure 8.2A). The sheet was then cut in the direction perpendicular of nanofiber/cell alignment starting at the ends of this hole resulting in spontaneous folding of a portion of the sheet over itself (Figure 8.2B-D). After most of the sheet had been cut away, a thin tubular structure attached at both ends to its metal ring support remained. Tubular scaffolds were tied off on each end with 6-0 sutures and cut from their ring supports (Figure 8.2E). Larger scaffolds were fabricated by bundling up to 8 filaments together.

Thick nanofiber/fibrin gel composites containing cells were fabricated by layer-by-layer stacking as well. One fibrin composite film was fabricated, placed on a glass cover slip and allowed 2 minutes to polymerize. The following layer was added immediately after fibrinogen and thrombin combination to promote adhesion between layers. Fibrin layers were cut away from their steel support rings after polymerization. In contrast to layer-by-layer fabrication methods utilized for cell-nanofiber stacks, no support ring was necessary because layers adhered well to each other due to fibrin polymerization.

8.2.3 In vivo implantation

Mice were anesthetized and an incision was made along the spine to expose the paravertebral muscle. An incision was made along the paravertebral muscle of approximately 15mm in length and 2mm in depth. Nanofiber bundles with or without cells were placed in the incision and sutured at both ends so that they remained taut. The muscular and skin incisions were then closed. Mice were sacrificed and the grafts were removed with surrounding tissue for histological evaluation. Explanted grafts were embedded in OCT compound and cyrosectioned at 5-30um.

8.2.4 Histology/Immunohistochemistry

Cells were fixed in 4% paraformaldahyde for 45minutes or 2.5% glutaraldehyde overnight. Fixed specimens were stained with AlexaFluor 488 Phalloidin (Invitrogen) for the actin filament inside the cells, 4′-6-Diamidino-2-phenylindole (DAPI, Invitrogen) for the cell nuclei, and immunostained with anti-skeletal myosin heavy chain antibody (Sigma, M4276) for differentiated myotubes. Explants were immediately embedded in OCT compound, cyrosectioned, fixed in 4% parafomaldahyde for 1 minute, washed in PBS and stained using

hematoxylin and eosin (H&E).

8.2.5 Microscopy/Image processing

Fluorescent and microscope images were taken using a Nikon Eclipse TE2000-S microscope with an EXFO X-cite 120 fluorescence illumination system, and a Q-Imaging Micropublisher 3.3 RTV camera with Q-Capture software and a Leica confocal microscope (TCS SP5 AOBS). Scanning electron microscrope (SEM) images were taken at 1,000 to 6,000 times magnification using an Hitachi TM-1000 SEM. ImagePro Plus 4.0 (Media Cybernetics, L.P.) was used to analyze SEM images of nanofibers and florescent images of cells to measure fiber diameter, alignment and density, and cellular alignment, density, and myotube dimensions respectively.

8.2.6 Statistical Analysis

Kruskal–Wallis test was used as an initial test for differences within a sample set. For sample sets with a Kruskal–Wallis p-value (ρ) < 0.05 the Mann–Whitney test was used to evaluate differences between groups using $\rho < 0.05$. All statistical analysis was done using SPSS software.

8.3 Results

8.3.1 Nanofiber sheets

8.3.1.1Fiber density

PCL nanofibers scaffolds were made up of free suspended aligned fiber arrays with an average fiber diameter of around 750nm. The average standard deviation of the fiber angle was 4º +/- 0.5 ºand the degree of fiber alignment was not affected by fiber density. Aligned nanofiber scaffolds with variable fiber densities were fabricated and seeded with C2C12 cells

to investigate the cell response to scaffolds of different fiber densities. Cells were seeded on scaffolds with aligned fiber densities of 0.1, 0.25, 0.35, 0.5, 0.85, and 1.1 fibers per μm length (measured in the direction perpendicular to fiber alignment) and fixed at 1, 3 & 7 days. Several parameters were evaluated quantitatively. Percent cell confluence was evaluated as the ratio of the area of actin staining to the overall area, and cellular alignment was evaluated as the standard deviation of the angular direction of the long axis of the actin cytoskeleton. Representative images and graphs of percent confluence and cell alignment for all groups are shown in Figure 8.3.

It was found that cells aligned well in the direction of the nanofiber substrates. The standard deviation of the direction of cell elongation was between 2-8º for various fiber densities and days in culture. Statistically significant differences in cell alignment for different fiber densities were not present, but there was a marked increase in cell alignment as fiber density increased.

Aligned cells were able to proliferate and form nearly confluent monolayers on aligned nanofiber sheets. After three days in culture, a systematic increase in the percentage of area occupied by cells was apparent as fiber density was increased from 0.1 fibers/μm to 0.5 fibers/μm. At 3 and 7 days the average percentage area coverage for all groups where fiber density was 0.5 fibers/μm or greater was above 95%. It was apparent from images taken on a confocal microscope that myotubes were present on both sides of the nanofiber sheets despite single side seeding (Figure 8.4). This would indicate that cells were able to migrate through the nanofiber sheets. It is estimated that an aligned nanofiber sheets with 0.5 fibers/μm had a porosity of more than 60%. Statistically significant differences in percent area coverage ($\rho < 0.05$) were present for 1.1 fibers/μm versus all groups except for 0.85

fibers/μm (ρ =.827).

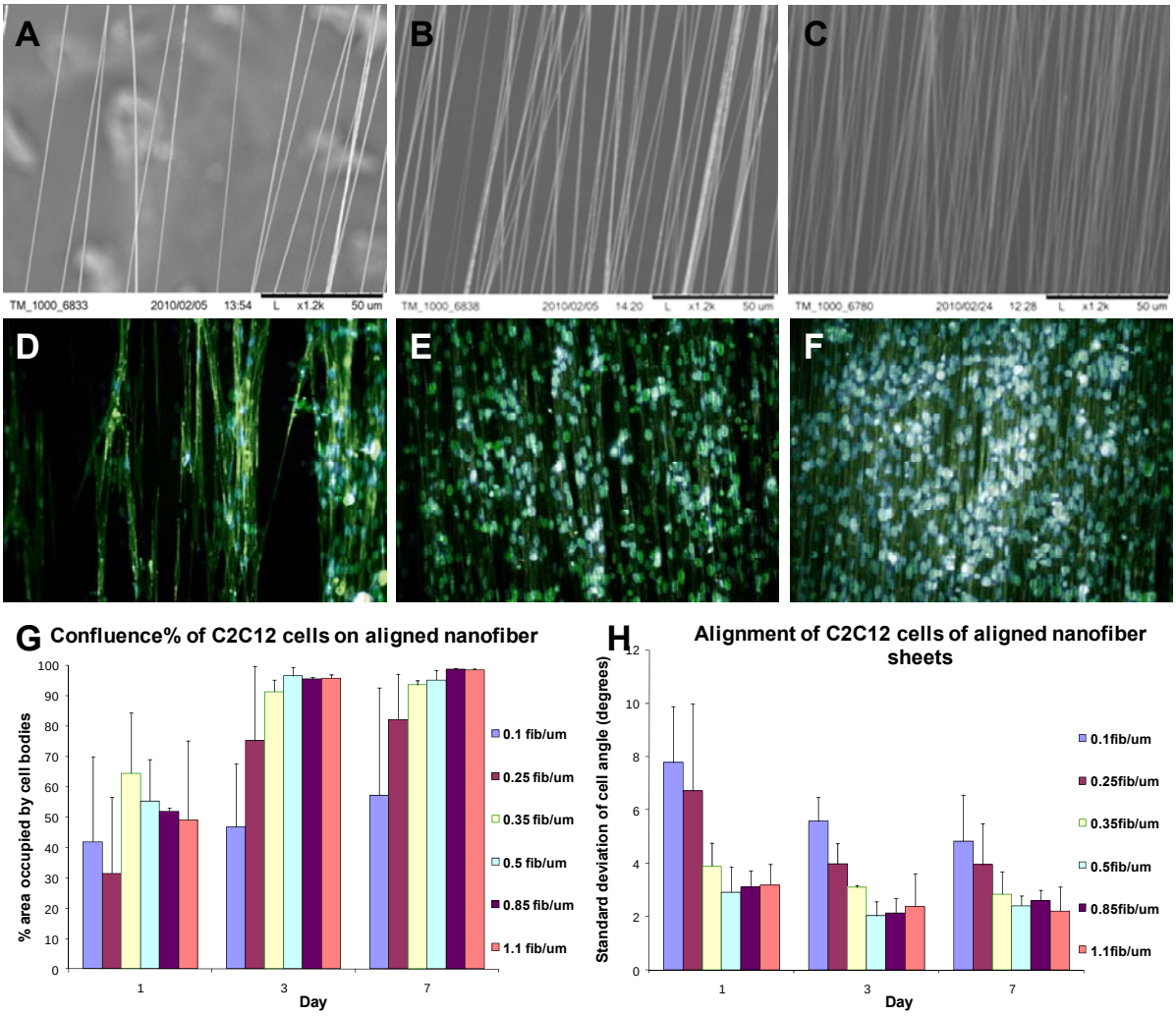

Figure 8.3: SEM images of aligned PCL nanofiber sheets with fiber densities of (A) 0.1 fibers/um, (B) 0.35 fibers/um, and (C) 0.85 fibers/um. C2C12 cells cultured on these fiber sheets are shown in fluorescent images in (D-F) respectively. Quantitative measurements of (G) % confluence and and cell alignment (H) are graphed for fiber densities from 0.1 – 1.1 fibers/um.

8.3.1.2 Myotube formation on nanofiber sheets

Myotube formation by C2C12 cells on aligned PCL nanofiber sheets versus tissue culture plate (TCP) was evaluated. Cells were seeded and allowed to proliferate to confluence for 5 days in proliferation media (DMEM supplemented with FBS). After 5 days some samples were incubated in differentiation media (DMEM supplemented with horse serum, HS).

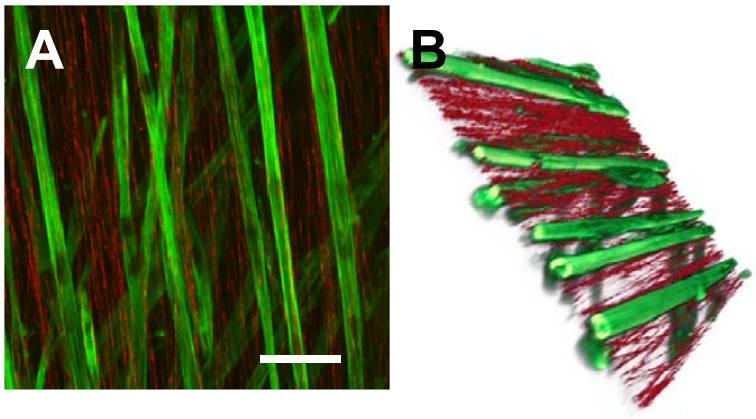

Figure 8.4: Myotube formation on aligned nanofiber sheets: (A) top view of fluorescent image & (B) 3D reconstruction.

C2C12 myotube formation was evaluated for four groups where different substrates and medias were used: (1) Nanofiber sheets/differentiation media (HS), (2)nanofiber sheets/proliferation media (FBS), (3)TCP/HS, and (4)TCP/FBS. Myotube formation was evaluated by: (1) Number of myotubes per unit area (2) myotube length, and (3) myotube alignment. Quantitative results and representative fluorescent images are displayed in Figure 8.5. Myotube formation was analyzed from 1 to 21 days after culture media was switched. Both average myotube density and average myotube length were considerably greater for TCP when compared to nanofiber substrates. However, C2C12 cells seeded on TCP formed confluent sheets that eventually detached from the substrate surface. Cells incubated in differentiation media on TCP peeled off after 5-7 days and cells remaining in proliferation media peeled off of TCP surfaces after 16-20 days in culture. All samples cultured on PCL nanofiber grafts remained adhered for the duration of the experiment. In addition, all samples cultured on nanofibers for in vivo implantation remained adhered for cultures times up to 7 weeks. Local myotube alignment on TCP was quite good, but clusters of aligned myotubes were very randomly aligned over large areas. As expected, myotubes grown on aligned

nanofibers were much better aligned than those cultured on TCP. However, myotube alignment on nanofiber scaffolds showed a considerable systematic decrease from days 1-7 after which alignment values leveled off or decreased. In conjunction with the decrease in alignment, myotube density and average length showed tends of systematic increase from days 1-7 followed by leveling off after day 7. Analysis of all parameters revealed little difference between cells cultured in proliferation medium and differentiation medium.

8.3.2 Fibrin gel nanofiber composites

A thin fibrin film with embedded aligned nanofibers was formed due to polymerization of fibrinogen and thrombin liquid film combination. Cells were observed embedded throughout the composite films in a uniform distribution. Cells began to align in the direction of the nanofibers after only one hour of incubation. After one day, cells were observed to align and elongate along the embedded nanofibers. Cell proliferation resulted in aligned cell sheets at nearly full confluence by day 7. Fluorescent images of cell morphology at various time points are shown in Figure 8.6. Fibrin gel degradation in culture media supplemented with t-AMCA was investigated for films incubated with and without cells. Fibrin gel fibrils could be observed within the films using fluorescent confocal microscopy in samples fixed in glutaraldehyde. In films without cells, fibrin gel matrix was observed in all time points from 1-7 days. However, it appeared that the fibrin may have degraded with time as the thickness and organization of the matrix appeared to decrease between 5 hours to 7 days incubation. Images of films incubated with cells appeared to degrade much faster. A substantial fibrin matrix was observed at 1 hr after incubation. After 1 day in culture, fibrin matrix could still be identified, but large areas that contained no fibrin matrix were present. On days 3 and 7, fibrin matrix could not be identified in fluorescent images. Identification was difficult

because of large areas covered by cells, but holes containing no cells or fibrin matrix were present. Images taken at various time points are shown in (Figure 8.6).

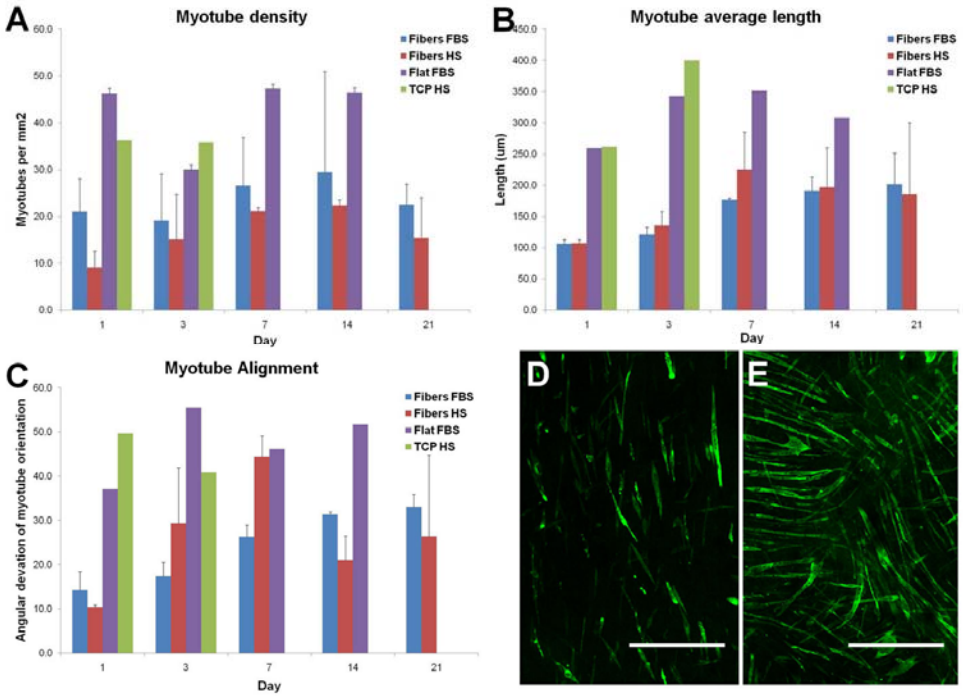

Figure 8.5: Myotube (A) density, (B) average length, and (C) alignment for C2C12 cell cultured on aligned PCL nanofibers in proliferation & differentiation and cultured on TCP in FBS & horse serum for 1-21 days. Representative fluorescent images of C2C12 cells cultured in FBS for 14 days on (D) nanofibers and (E) TCP stained for skeletal myosin heavy chain. Scale bar=500µm.

8.3.3 Three-dimensional structure fabrication

Mulitlayer cell-nanofiber constructs up to 15 layers were fabricated using layer-by-layer assembly. Scaffold layers appeared to be well adhered to one another as confirmed by manipulation of the scaffolds and observation of crossectional histological images. The cross section of a six layer scaffold is shown in Figure 8.2G. Fibers and cells appeared to remain well aligned thought the thickness of the constructs and cell survival was demonstrated throughout its thickness.

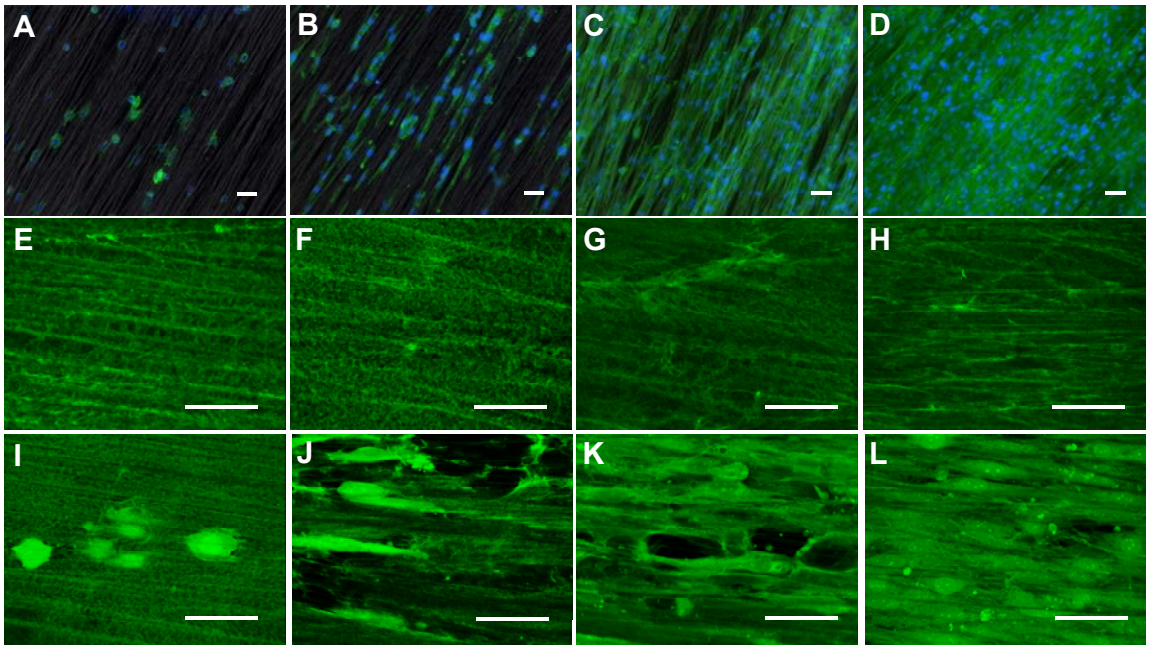

Figure 8.6: Fluorescent images of aligned nanofiber-fibrin film composites with (A-D & I-L) and without (E-H) embedded C2C12 myoblast cells. Images A-D are stained green for actin filament and blue for nuclei. PCL nanofibers, fibrin gel microstructure, and cell bodies are fluoresced due to glutaraldehyde fixation in images E-L.

Cell nanofiber 3D bundles assembled from single aligned nanofiber-cell sheets had an oval shaped cross section with a diameter of around 150μm. The overall lengths of these constructs were up to 20mm. The cross section of such a construct is shown in Figure 8.2H.

Multilayer fibrin composite scaffolds also demonstrated cell survival throughout their thickness. Scaffold layers appeared to be well adhered to each other as confirmed by manipulation of the scaffolds and observation of crossectional histological images.

8.3.4 In vivo

Bundled scaffolds were successfully implanted inside the paravertebral muscle of a mouse (Figure 8.7A). Scaffolds remained taut at all time points due to sutures holding the ends in tension. Scaffolds were removed with the surrounding tissue, sectioned and analyzed after 1 to 14 days. A cross section of one of these samples removed after 5 days is shown in Figure

8.7B. It is apparent the implanted cells were able to retain a well aligned microstructure during in vivo implantation.

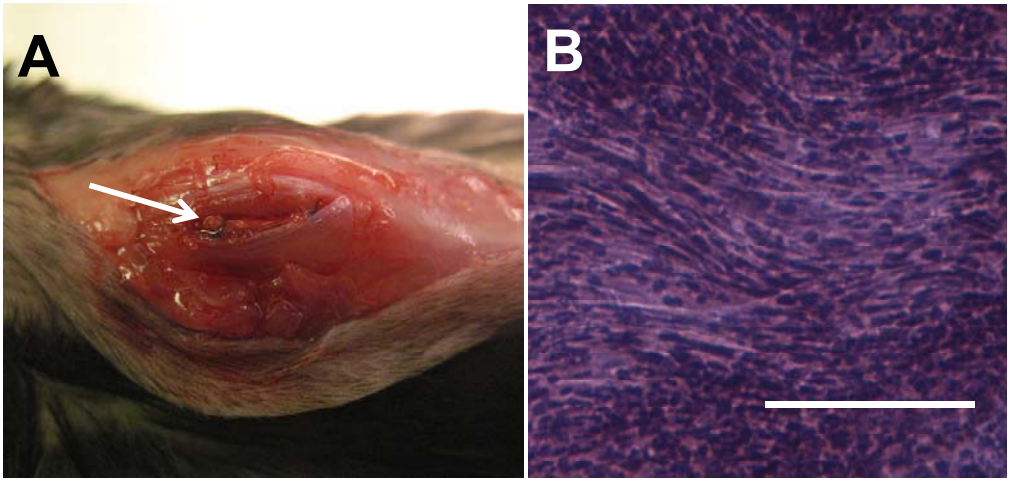

Figure 8.7: (A) Tubular aligned nanofiber-cell constructs were implanted in the paravertebral muscle on the back of a mouse. (B) The aligned microstructure of grafts is visualized after removal with sectioning and H&E staining.

8.4 Discussion

Favorable cell response to aligned nanofibrous substrates demonstrates the potential of aligned nanofibers in the regeneration of damaged or degenerated aligned tissues. However, most investigations of cell interactions with aligned nanofibrous are conducted on relatively thick, densely packed aligned nanofiber mats, or on aligned nanofibers that are attached to stiff flat substrates. Constructs containing aligned nanofibers that are practical for functional tissue engineering applications must be developed to expand the versatility of this technology.

We previously developed a method to fabricate free suspended ultra thin aligned nanofiber sheets with precisely controlled fiber packing density and we hypothesized that these structures could have advantages as tissue engineering scaffolds. Ultra thin nanofiber sheets were able to support practically confluent cell sheets that demonstrated uniaxial

alignment. Cell sheets with greater than 95% confluence were grown on aligned PCL nanofiber sheets with fiber densities as low as 0.5 fibers per microns or 60% porosity. Myotube formation on the bottom side of nanofiber sheets that were not seeded with cells indicates that cells were able to migrate though the scaffolds. We hypothesize that because of low fiber densities, these scaffold will share advantages of traditional cell sheet technology such as a lack of hindrance to cell-cell contacts and mass transport. In addition, these scaffolds may be superior to cell sheets for structure assembly due to their improved mechanical properties and the fact that these scaffolds are inherently fixed at their edges, and thus easier to handle and manipulate.

Single aligned nanofiber cell sheets were evaluated for potential in skeletal muscle tissue engineering. Scaffold seeded with C2C12 cells were able to support the formation of well aligned myotubes, although a marked decrease in myotube alignment was observed with increasing time in culture. We hypothesis that the effect of the nanofibrous topography on cells is reduced as cell density increases. Cells may have reduced contact to the fibers due to crowding, or may even grow on top of one another. Myotube density and average length were both lower on aligned PCL scaffolds compared to TCP. However, cell layers spontaneously detached from TCP after 5-20 days. In contrast, cell layers did not detach from nanofiber scaffolds in long term culture up to 7 weeks. We hypothesize that decreased myotube density and average length demonstrated on aligned nanofiber scaffolds was due either to a lower bioactivity in PCL compared to TCP or to restrictions on cell proliferation and migration that may have been caused by the microstructure or mechanical properties of the substrates. Fibrin gel-nanofiber thin film composites offered an alternative method of aligned cell sheet fabrication. This method allowed one step cell incorporation directly during

fabrication. These composites materials may be ideal for tissue engineering applications because they allow ample space for vascular ingrowth. This technique is very promising, but fibrin may not be an ideal material for the matrix component due to rapid degradation that was observed.

The potential of aligned nanofiber cell sheets and matrix-nanofiber composites as building blocks for functional tissue engineering scaffolds was demonstrated with the fabrication of several structures. Thicker structures were fabricated by layer-by-layer stacking of both types of scaffolds. Stacking procedures were effective and easily performed because scaffolds were fixed to stiff steel rings on their edges. Three-dimensional fiber bundle structures were formed by simply cutting the sheets according to a pattern. These bundle structures demonstrate a microstructure that is similar to natural aligned tissues and are very promising in applications involving regeneration of such tissues.

8.5 Conclusions

Ultra thin aligned nanofiber sheets were fabricated using technologies that we previously developed. It was found that practically confluent aligned cell monolayers could be grown on such nanofiber sheets with porosities as high as 60%. A high cell to material ratio imparts the potential to fabricate three-dimensional structures from aligned cell sheets that minimally interfere with cell migration, cell-cell contacts, and mass transport. In addition, these scaffolds are versatile for assembly into three-dimensional structures because they are fixed at their edges, and thus easy to handle and manipulate. Sheets were stacked layer-by-layer and assembled in to three-dimensional bundles with high cell density. The potential of aligned nanofiber-cell sheets for regeneration of aligned tissues such as skeletal muscle was demonstrated.

8.6 References

[1] Bach AD, Beier JP, Stern-Staeter J, Horch RE. Skeletal muscle tissue engineering. J Cell Mol Med 2004;8(4):413-22.

[2] Yamamoto Y, Ito A, Fujita H, Nagamori E, Kawabe Y, Kamihira M. Functional evaluation of artificial skeletal muscle tissue constructs fabricated by a magnetic force-based tissue engineering technique. Tissue Eng Part A 2011;17:107-14.

[3] Choi JS, Lee SJ, Christ GJ, Atala A, Yoo JJ. The influence of electrospun aligned poly(epsilon-caprolactone)/collagen nanofiber meshes on the formation of self-aligned skeletal muscle myotubes. Biomaterials 2008;29(19):2899-2906.

[4] Huber A, Pickett A, Shakesheff KM. Reconstruction of spatially orientated myotubes in vitro using electrospun, parallel microfibre arrays. Euro Cells & Materials 2007;14:56-63.

[5] Neumann, T., S.D. Hauschka, and J.E. Sanders, Tissue engineering of skeletal muscle using polymer fiber arrays. Tissue Eng, 2003. 9(5): p. 995-1003.

[6] Lam MT, Huang YC, Birla RK, Takayama S. Microfeature guided skeletal muscle tissue engineering for highly organized 3-dimensional free-standing constructs. Biomaterials 2009;30(6):1150-5.

[7] Aviss KJ, Gough JE, Downes S. ALIGNED ELECTROSPUN POLYMER FIBRES FOR SKELETAL MUSCLE REGENERATION. European Cells & Materials 2010;19:193-204.

[8] Yang J, Yamato M, Kohno C, Nishimoto A, Sekine H, Fukai F, Okano T. Cell sheet engineering: recreating tissues without biodegradable scaffolds. Biomaterials 2005;26(33):6415-22.

[9] Dang JM, Leong KW. Myogenic Induction of Aligned Mesenchymal Stem Cell Sheets by Culture on Thermally Responsive Electrospun Nanofibers. Adv Mater Deerfield 2007; 19(19):2775-9.

[10] Beachley V, Wen X, Fabrication of three dimensional aligned nanofiber array, US-7828539 2010, Clemson University (Clemson, SC, US) US.

[11] Li D, Wang YL, Xia YN. Electrospinning of polymeric and ceramic nanofibers as uniaxially aligned arrays. Nano Letters 2003;3(8):1167-71.

[12] Beachley V, Wen X. Fabrication of nanofiber reinforced protein structures for tissue engineering. Materials Science & Engineering C 2009. 29(8):2448-53.

[13] Cholewinski E, Dietrich M, Fanagan TC, Schmitz-Rode T, Jockenhoevel S. Tranexamic acid--an alternative to aprotinin in fibrin-based cardiovascular tissue engineering. Tissue Eng Part A 2009;15(11): p. 3645-53.

CHAPTER 9

9. OVERALL CONCLUSIONS AND FUTURE DIRECTIONS

9.1 Conclusions

The major impact of this work is in the development of three specific technologies useful in fabrication of tissue engineering scaffolds for aligned tissue regeneration. These technologies included a technology of electrospinning nanofiber collection and assembly using mobile tracks, a technology of aligned nanofiber/protein matrix thin film fabrication, and a technology of fabricating multicomponent hybrid nanofiber arrays with biomimetic microstructure and mechanical properties. Preliminary studies demonstrated the potential of several tissue engineering structures assembled using these technologies. Detailed conclusions are summarized below by chapter.

Chapter 3: This experiment demonstrated that continuous individual nanofibers with nanoscale diameters could be collected across parallel plates at lengths of 35-50cm. This confirmed that nanofibers at lengths up to or exceeding the expected requirements of most tissue engineering applications could be fabricated using the parallel plate method. As expected, it was discovered that several electrospinning parameters such as, voltage and polymer solution concentration had effects on fiber properties such as, maximum fiber length, fiber diameter, and fiber uniformity. The most notable finding was that longer fibers could be collected by increasing the size of the plates used.

Chapter 4: A novel technology was developed that utilized parallel mobile tracks to collect and distribute loose aligned nanofiber arrays. This method of nanofiber collection is unique

in that a uniform electric field can be maintained. This is possible because fibers are removed from the collection area, thus alleviating repulsive charge accumulation. The uniform electric field allowed for steady state indefinitely continuous delivery of loose nanofiber arrays. Mobile track collection also allowed for an indefinite amount of time for individual fibers to dry or cool before assembly into a structure, thus eliminating complications due to fiber-to-fiber adhesions. Fixation of aligned nanofiber arrays from the violent highly charged electrospinning jet prior to structure assembly allows post processing of nanofiber arrays into complex structures with precise nanofiber density and placement. Evidence demonstrated that this technology may allow for precise fabrication of complex nanofiber structures difficult to assemble using current methods. It is hypothesized that steady state fiber collection makes this technology very practical for industrial scale up.

Chapter 5: A technology was developed to fabricate thin nanofiber/protein matrix composites. When a nanofiber array was immersed and removed from a liquid, surface tension forces resulted in a thin liquid film that could be congealed into a thin gel. Gels fabricated by this method where quite uniform. Dried films had an average thickness of 2-3 um with a standard deviation of just 10%. Results of mechanical testing showed that embedded nanofibers at a volume fraction as low as 3%v/v significantly increased the strength of protein gels. Composites combined the strengths of each material as a tissue engineering scaffold for aligned tissue regeneration, while addressing their individual weaknesses.

Chapter 6: Two component hybrid nanofiber sheets with precisely arranged biomimetic microstructure were fabricated. These sheets were composed of a relatively elastic fiber component in a straight orientation and a relatively stiff fiber component in a 'waved' orientation. Under tensile strain these hybrid sheets adopted a 'J-shaped' mechanical profile, similar to natural tissues such as blood vessels, with a relatively elastic region at low strain that transition into a much stiffer region at a critical value of strain. It was confirmed the transition to the stiff region corresponded to the degree of strain when the 'waved' fiber component became taut. It was further demonstrated that this transition point could be predictably moved by changing the orientation of the nanofibers in the material. These materials were tested under cyclic loading conditions to confirm that the microstructure was not altered during normal loading and that the material would be suitable for tissue engineering applications were such loading was present. Evidence demonstrated that this material was extremely promising for tissue engineering applications, such as in vascular grafts, where mechanical property matching is of importance.

Chapter 7: It was demonstrated that tubular vascular grafts with biomimetic straight-wavy nanofibers could be fabricated to match the mechanical properties of natural blood vessels. Graft mechanical behavior could be predictably modulated by precisely changing the graft microstructure. Optimized vascular grafts demonstrated remarkable similarity in geometry and mechanical properties when compared to rabbit carotid artery explants. The durability of grafts was sufficient to withstand surgical implantation and blood flow through the grafts without leakage was confirmed. Grafts retained favorable mechanical properties after long term in vivo implantation and smooth muscle cells were observed infiltrating deep inside the

volume of the grafts. Results of this study demonstrated the potential of biomimetic nanofiber structures in the design of compliant vascular grafts.

Chapter 8. Skeletal muscle tissue engineering grafts were fabricated by seeding C2C12 myoblasts onto aligned nanofiber sheets. Cells were able to align and form confluent sheets on nanofiber sheets with fiber densities above 0.5fibers/um. C2C12 cells differentiated into myotubes on free suspended aligned PCL nanofiber sheets, but appeared to inhibit myotube formation when compared to tissue culture plate. Confluent aligned skeletal muscle sheets were fabricated in a single step as cell/nanofiber/fibrin gel composite thin films. Three dimensional skeletal muscle grafts were constructed by stacking layer-by-layer aligned cell sheets. Individual sheets appeared to fuse into a single construct. Cell sheets were observed to self assemble into three dimensional bundled structures when cut in a precise method. It was hypothesized that this behavior was due to surface tension forces and tensions within the thin sheets. Skeletal muscle tissue constructs were evaluated in vivo in a skeletal muscle defect model. Histology demonstrated integration of the constructs with natural muscle tissue. Aligned cellular constructs demonstrated potential in skeletal muscle regeneration as well as other tissue engineering applications.

9.2 Challenges

Several tissue engineering scaffolds with promising results were fabricated using the novel nanofiber fabrication technologies presented in this dissertation. However, several challenges remain in the way of developing better functional tissue engineering scaffolds. Some of these challenges are arranged by chapter and listed below.

Chapter 5: Aligned nanofiber/protein composite films were fabricated with PCL nanofibers and gelatin or fibrin protein matrices. These composite demonstrated the potential of the technology and showed promise as tissue engineering scaffolds, but have limitations. The gelatins film fabricated are water soluble and thus have limited use in tissue engineering applications without modification. Crosslinked gelatin films remain intact under in vitro conditions, but crosslinking procedures may lower the biocompatibility of the structure and a new technology is needed to increase the crosslinking of ECM without compromising the biocompatibility. Fibrin films demonstrated the ability for direct cell incorporation, but may degrade too quickly for many tissue engineering applications. Better matrix materials must be designed or identified to maximize the potential of this technology.

Chapter 7: Vascular grafts with biomimetic straight-wavy nanofibers demonstrated mechanical properties that were remarkably similar to natural vessels and proved suitable for surgical implantation. The major challenges faced in this technology are to establish a anti-thrombogenic surface but allow for fast endotheilization.

Chapter 8: Aligned skeletal muscle cells were successfully grown to confluence on free suspended cell sheets and assembled into thicker sheets and cylindrical structures. While C2C12 cells proliferated and aligned well on nanofiber sheets, they did not form myotubes as well as controls on flat tissue culture plate. There is a need to further improve the adhesiveness of the nanofibers to improve myotube formation.

Thicker stacked construct fabrication offer one major challenge. For thicker constructs (greater than a few hundred um) to be viable, a method of nutrient transport will

need to be developed and incorporated.

9.3 Future goals

The ultimate goals of this project are to develop novel technologies for use in advanced functional tissue engineering applications. Immediate goals will be to expand upon the technologies developed here to open the door to more tissue engineering applications. In the long run, more advanced technologies can be further derived from this work. Future plans and goals are organized by chapter and summarized below.

Chapter 4: We hope to further advance the loose nanofiber array fabrication technology for in-situ surface modification of fabricated nanofibers, in-situ 3D structure and graft fabrication and cell incorporation during the fabrication process.

Chapter 5: We hope to design or select several hydrogel materials to combine with aligned nanofibers to make slow degrading thin film composite structures. Selection criteria for these materials will include degradation properties, cell permeability, and bioactivity. Only hydrogels that are compatible with direct cell incorporation fabrication procedures will be considered. Therefore, hydrogels must be a viscous liquid at 37ºC with a crosslinking method that is conducive to cell survival. Composite design will be investigated according to specific tissue engineering applications such as myocardium patch, skin graft, and so on.

Chapter 6: We hope to develop a cell-seeded vascular graft biofabricator by combining the wavy-straight nanofiber spinning and cell spraying during the tube fabrication process. The other direction is to functionalization of lumen surface for endothelial precursor cell

recruitment from circulating blood for fast enthdothelization.

Chapter 7: We hope to improve the structural properties of our vascular grafts by investigating modification to our design. It is our goal to optimize both circumferential and axial mechanical properties by modifying the orientation of fibers in the grafts. We also hope to investigate several designs for a composite structure where the nanofiber portion of the grafts is stabilized by a matrix material. Composite grafts will be designed in such a way that the matrix material provides support, but the nanofibers component still dominates the overall mechanical properties.

We will try to incorporate the most effective biofunctional molecules for preventing thrombosis and promoting endothelialization by bulk incorporation and surface functionalization techniques.

Chapter 8: We hope to investigate myotube formation of free suspended aligned nanofiber arrays further. Myotube formation appeared to be decreased on aligned PCL sheets compared to flat tissue culture plate. One possible reason is the amount of adhesive molecules available for myoblast adhesion, growth, and differentiation. We will compare the myotube formation with different types of functional surfaces. We also hope to develop new methods to stack aligned nanofiber/cell sheets into thicker structures by developing better ways to stabilize and adhere layers together during fabrication. Further development of this technology will involve combining multiple cell types into layered structures.